NASA TECHNICAL TRANSLATION NASA TT F-15,841

EXTERNAL SOUND FIELD EFFECT ON A TURBULENT BOUNDARY LAYER

P. Gougat

Translation of "Influence d'un champ acoustique extérieur sur une couche limite turbulente". Centre National de la Recherche Scientifique, Lab. d'Aérothermique. Meudon, France, Rept. 70-8. Sept. 1970, 103 pages.

(NASA-TT-F-15841) EXTERNAL SOUND FIELD EFFECT ON A TURBULENT BOUNDARY LAYER (Scientific Translation Service) 113 p HC $8.75 CSCL 20D

N74-31764

Unclas

G3/12 47779

NATIONAL AERONAUTICS AND SPACE ADMINISTRATION
WASHINGTON, D. C. 20546 SEPTEMBER 1974

STANDARD TITLE PAGE

1. Report No.	2. Government Accession No.	3. Recipient's Catalog No.
NASA TT F-15,841		

4. Title and Subtitle	5. Report Date
EXTERNAL SOUND FIELD EFFECT ON A TURBULENT BOUNDARY LAYER	September 1974
	6. Performing Organization Code

7. Author(s)	8. Performing Organization Report No.
P. Gougat	10. Work Unit No.
	11. Contract or Grant No. NASw-2483

9. Performing Organization Name and Address	13. Type of Report and Period Covered
SCITRAN Box 5456 Santa Barbara, CA 93108	Translation

12. Sponsoring Agency Name and Address	14. Sponsoring Agency Code
National Aeronautics and Space Administration Washington, D.C. 20546	

15. Supplementary Notes

Translation of "Influence d'un champ acoustique extérieur sur une couche limite turbulente". Centre National de la Recherche Scientifique, Lab. d'Aérothermique. Meudon, France, Rept. 70-8. Sept. 1970, 103 pages. N71-18572

16. Abstract

The response of a boundary layer to harmonic oscillations is analyzed. The study is restricted to the influence of an acoustic field on heat exchange in a turbulent boundary layer on a flat plate. Wind tunnel tests have been performed using a hot-wire anemometer linked to a Wheatstone bridge. It is shown that an ultrasonic field is not appropriate and that, with the wind tunnel used, measurements were not possible for low frequencies.

17. Key Words (Selected by Author(s))	18. Distribution Statement
	Unclassified - Unlimited

19. Security Classif. (of this report)	20. Security Classif. (of this page)	21. No. of Pages	22. Price
Unclassified	Unclassified	111	

PRECEDING PAGE BLANK NOT FILMED

A N N O T A T I O N

Within the framework of a contract with the Directorate of Research and Test Methods, the Aerothermal Laboratory has undertaken to study a boundary layer subjected to a harmonic perturbation.

The effects that these perturbations can produce on the transition phenomena are large but in an established turbulent regime, these effects are smaller and not well understood.

A part of this study is presented in this report and concerns the experimental study of the effect of an external acoustic field upon the boundary layer on a flat plate. Various experimental methods were used.

On the one hand, dynamic studies have led to the development at the Laboratory of measuring techniques based on hot filament anemometry. On the other hand, thermal studies have led to the study of platinum film sensors.

At the same time, of course, it was necessary to perfect the production, the control and the analysis of acoustical perturbations, in the usual sonic as well as the ultrasonic range.

It is to be noted that the discussion concerning platinum film does not appear in this report, but in report 70-7.

Edmond A.BRUN

NOMENCLATURE

a	- vibration amplitude
c	- acoustic sound velocity
c_p	- specific heat
C_f	- drag coefficient
d	- wire or cylinder diameter
f	- frequency
G	- amplifier gain
I	- current intensity
ℓ	- wire length
L	- acoustic level
M	- time constant
$\mathcal{N}$	- Nusselt number
P	- electric power
$\mathcal{P}$	- Prandtl number
Q	- electric resistance
R_s	- acoustic impedance
$R_{u'v}$	- correlation coefficient
$\mathcal{R}$	- Reynolds number
t	- time
T	- temperature
u	- velocity component along Ox
u_∞	- free flow velocity
u_f	- drag velocity
u_n	- projection of the velocity vector on the normal to the hot filament
u'	- longitudinal velocity fluctuation
v	- vibration velocity
v'	- transverse velocity fluctuation
V	- electric potential

x	- abscissa measured from the leading edge and along the principal flow direction
y	- ordinate measured along the normal from the plate
z	- breadth coordinate
δ_{ac}	- acoustic perturbation thickness
δ_2	- momentum thickness
ε	- unbalanced electric potential
Θ	- reduced temperature
λ	- coefficient of air conductivity'
ν	- kinematic viscosity
ρ	- density
τ_p	- shear stress at the wall
φ_p	- local heat flux
Φ_p	- average heat flux
ω	- angular velocity

TABLE OF CONTENTS

		Page
ANNOTATION		iii
NOMENCLATURE		iv
TABLE OF CONTENTS		vi
Chapter 1	- INTRODUCTION	1
Chapter 2	- REVIEW OF ACOUSTICS	3
Chapter 3	- EARLIER STUDIES	7
3.1.	- General Remarks	7
3.2.	- Dynamic Studies	8
	3.2.1. - Exact solution for the flat plate	8
	3.2.2. - Solution of the dynamic problem for a cylinder	9
	3.2.3. - Classification of dynamic studies	10
3.3.	- Thermal Studies	11
Chapter 4	- EXPERIMENTAL SET UP	13
4.1.	- Wind Tunnel	13
4.2.	- Acoustic Generator	16
	4.2.1. - Ultrasonic domain	16
	4.2.2. - Sonic domain	17
4.3.	- Acoustic Field Measurements	17
Chapter 5	- HOT WIRE ANEMOMETRY	20
5.1.	- General Remarks	20
5.2.	- Hot Filament Probe Calibration	22
5.3.	- Servocontrol Study	25
5.4.	- Linearization	31
5.5.	- Effects of Wire Angle	34
5.6.	- Construction	36
	5.6.1. - Straight-wire anemometer	32
	5.6.2. - Two-wire anemometer	38

Page

Chapter 6 - FLUXMETER PROBE 43

6.1. - Introduction 43

6.2. - Heat Flux Measurements 43

6.3. - Conclusions 43

Chapter 7 - RESULTS 45

7.1. - Utilization of the Hot Wind Anemometer 45

7.2. - Visualization 46

7.3. - Tests in the Ultrasonic Domain 47

7.4. - Tests at Low Frequency 48

7.4.1. Parameters of the study 48

7.4.2. Effects of the frequency on the acoustic wave 50

7.4.3. Effect of acoustic level 51

7.4.4. Effect of velocity in the main flow 51

7.4.5. Effect of the measurement location along the abscissa 52

7.5. - Tests at Intermediate Frequencies 53

7.5.1. No title 53

7.5.2. Control of the friction coefficient 54

7.5.3. Variation of the heat flux 56

Chapter 8 - CONCLUSIONS 58

REFERENCES 59

EXTERNAL SOUND FIELD EFFECT ON A TURBULENT BOUNDARY LAYER

Pierre Gougat

Assistant - Researcher /1*

Chapter 1

INTRODUCTION

The experimental study of the effect of an acoustic field upon the phenomena of heat exchange in a boundary layer on a flat plate follows a line of research requiring various experimental techniques. The purpose of these investigations is to study the response of a boundary layer to harmonic perturbations.

Such a study can lead us to concern ourselves with the effects of a perturbation on the boundary layer. We are referring to transition when an artificial triggering mechanism is involved. A very different study concerns the effects of a perturbation on a turbulent boundary layer whose regime is well established.

The different forms the perturbations can take are worth defining at the outset:

---

* Numbers in margin indicate pagination in original foreign text.

- it can be a wall perturbation produced by a harmonic wall roughness;

- it can be an acoustic phenomenon produced in the free flow external to the boundary layer;

- finally, it can be a harmonic vibration of the wall whose oscillation is a time-dependent sine function and varies with position in the direction of the flow.

We wish to point out that the above-enumerated perturbations have as an objective the modification of the boundary layer structure in the immediate neighborhood of the wall so as to produce mixing of the fluid and to increase the heat transfer coefficient. As such, these studies present points of comparison with studies concerning injection near walls.

Chapter 2

REVIEW OF ACOUSTICS

Let us study the case of a linear medium infinite in the Oy direction, and let us assume that the point 0 is the source of a sinusoidal excitation / 2

$$a = a_m \sin \omega t$$

As time proceeds, the oscillations propagate by the formation of a periodic wave.

The solution to the wave equation is written:

$$a = a_m \sin \omega \left(t - \frac{y}{c}\right)$$

$$a = a_m \sin 2\pi \left(\frac{t}{T} - \frac{y}{\lambda}\right)$$

This is the solution for the propagation of a sinusoidal longitudinal wave of period T, of velocity C and wavelength $\lambda = c\,T$, traveling in the direction of the Oy-axis and in a fluid medium of density ρ and of compressibility coefficient χ. The velocity is given by the relation

$$c = \sqrt{\frac{1}{\chi \rho}}$$

The vibrational velocity v and acoustic pressure p is associated with the amplitude

$$v = \frac{\partial a}{\partial t} = a_m \omega \cos \omega \left(t - \frac{y}{c}\right)$$

$$p = -\frac{1}{\chi} \frac{\partial a}{\partial y} = \frac{a_m \omega}{\chi c} \cos \omega \left(t - \frac{y}{c}\right)$$

We will assume this wave is a plane wave, and that it propagates in an elastic medium where energy dissipation during propagation is negligible. / 3

Let us compute the energy transported by this wave across a section of the fluid; it consists of the following terms:

- potential energy per unit volume:

$$e_p = \frac{1}{2} \rho c^2 \left(\frac{\partial a}{\partial y}\right)^2$$

- kinetic energy per unit volume

$$e_c = \frac{1}{2} \rho \left(\frac{\partial a}{\partial t}\right)^2$$

The total energy is then:

$$e_t = e_p + e_c = \rho \omega^2 a_m^2 \cos^2 \omega \left(t - \frac{y}{c}\right)$$

The energy contained in a cylinder of cross sectional area S and height λ is equal to:

$$E = S \int_0^{\lambda} e_t(y)\, dy = \rho \omega^2 a_m^2 S \frac{\lambda}{2}$$

The acoustic intensity or the acoustic energy per unit time and unit surface is written

$$I = \frac{E}{S T} = \frac{1}{2} \rho c \omega^2 a_m^2$$
$$= \frac{1}{2} R_a a_m^2 \omega^2$$

with $R_a = \rho c$ (acoustic impedance).

For air $R_a = 400\ kg/m^2.s.$

The acoustic pressure p has an effective value P such that:

$$P^2 = \frac{1}{2}\frac{\zeta^2 \omega^2}{\chi^2 c^2} \quad ,$$

$$P^2 = \frac{1}{2}\rho^2 c^2 a_m^2 \omega^2 \quad ,$$

$$P^2 = \frac{1}{2} R_s^2 a_m^2 \omega^2 \quad .$$

The acoustic pressure and intensity are related by / 4

$$P^2 = R_s I$$

It is customary to characterize an acoustic phenomenon by the ratio of its intensity I to a reference intensity I_o. By convention, we choose $I_o = 10^{-12}$ W/m^2 which corresponds to $P_o = 2.10^{-5}$ N/m^2. This value of the reference intensity corresponds to the audible threshhold of the human ear at a frequency of 1000 Hz.

A logarithmic scale is used and the acoustic level, called the decibel, is the number

$$L = 10 \log \frac{I}{I_o} \quad , \quad \text{or} \quad 20 \log \frac{P}{P_o} \quad .$$

Thus, to hold a constant acoustic level amounts to maintaining a constant velocity amplitude. Under these conditions, the wavelength varies with frequency.

There is some value in establishing a relation between the vibrational velocity and the acoustic level.

The value of the peak vibrational velocity is $a_m \omega$ and its effective value is $a_m \omega / \sqrt{2}$:

$$\frac{a_m \omega}{\sqrt{2}} = \chi_c P \quad ,$$

$$\frac{a_m \omega}{\sqrt{2}} = \frac{P}{\rho c} \quad , \quad \text{with} \quad \rho c \simeq 400 \text{ kg/m}^2 \text{ s} \quad .$$

/5

On the other hand:

$$L = 20 \log \frac{P}{P_o} \quad ,$$

$$\frac{P}{P_o} = 10^{L/20} \quad ,$$

$$P = 2.10^{(L/20)-5} \quad ,$$

$$\frac{a_m \omega}{\sqrt{2}} = 0,5.10^{(L/20)-7} \quad .$$

As an example,

$$L = 120 \text{ dB} \longrightarrow 0,05 \text{ m/s} \quad ,$$
$$L = 140 \text{ dB} \longrightarrow 0,5 \text{ m/s} \quad ,$$
$$L = 160 \text{ dB} \longrightarrow 5 \text{ m/s} \quad .$$

Chapter 3

EARLIER STUDIES

3.1. General Remarks

The effect of an acoustic field upon the phenomena of heat transfer has very often been studied, because this subject is of very great practical importance. In fact, the desire to increase the efficiency of a heat exchanger can lead one to finding methods of this type. However, one should not expect the total energy balance to be positive because, in this energy balance, the power necessary to produce these perturbations must be accounted for.

It is only in the case of boilers that earlier studies have produced interesting results. However, we are considering here overall results, and it seems that the acoustic field has an effect, not only on the heat exchange coefficient between the hot gas and the wall of the tubes, but also on the efficiency of the exothermal reaction of combustion.

These studies can nevertheless be of interest in the case where the acoustic field or the vibrations do not have to be produced externally, that is, if the acoustic field or the vibrations are produced by the phenomenon itself. This is the case for all flow where an acoustic field exists within the fluid. This is also the case, for example, for the instabilities in a rocket engine combustion chamber.

It should be stated, however, that one must not consider that the acoustic field produced at the wall will necessarily have analogous effects. In fact, a fluctuation in the relative velocity of the wall relative to the fluid is not the only parameter, but one must take account of the wavelength or at least

of the ratio of the wavelength to the characteristic dimension of the wall.

/7

In this spirit, the case of a cylinder subjected to vibration whose direction of propagation is perpendicular or parallel to the cylinder axis has been particularly studied. The number of studies concerning flat plates is very small.

3.2. Dynamic Studies

3.2.1. Exact solution in the case of a flat plate.

The case of heat transfer from a heated wall placed in a vibration field has led different authors to undertake a careful study of the dynamic field in the neighborhood of the body.

The exact solution of the dynamic problem can be obtained for a very special case. This is the case of a flat plate excited by harmonic oscillations parallel to the plate.

The equation of motion then reduces to

$$\frac{\partial u}{\partial t} = \nu \frac{\partial^2 u}{\partial y^2}$$

with the boundary conditions on the plate,

$$u(0,t) = u_0 \cos(\omega t) \quad .$$

We see here the analogy with the thermal problem of temperature fluctuations at a wall of a semi-infinite medium. This partial differential equation is transformed to an ordinary differential equation by taking the similitude as the variable

$$\eta = \frac{y}{\sqrt{\frac{2\nu}{\omega}}} \quad .$$

The solution is written

$$u(y,t) = u_0 e^{-\eta} \cos(\omega t - \eta)$$

This review is in fact of no practical interest to this study: it allows us, nevertheless, to bring out a characteristic thickness

$$\delta_{ac} = \sqrt{\frac{\nu}{\omega}}$$

which is the thickness of the acoustic perturbation.

3.2.2. Solution of the dynamic problem for a cylinder

In the case where the convection term $u\,(\partial u/\partial x)$ of the momentum equation can be neglected compared to the term $\partial u/\partial t$, the solution of the equations of the stationary boundary layer is obtained by an approximation method proposed by Schlichting [1]. This method is the same as the method one applies in the case of a body being moved from rest.

Assume that the potential flow velocity has the form

$$u(x,t) = u_0(x)\, e^{j\omega t}$$

The solution consists in expanding the current function in a power series in powers of increasing time:

- the first term describes the oscillatory motion;
- the second term leads us to consider the existence of stationary velocity that does not go to zero far from the wall.

We thus establish, outside the boundary layer, the existence of the flow velocity:

$$u(x) = -\frac{3}{4}\,\frac{u_0}{\omega}\,\frac{du_0}{dx}$$

This flow, which we have named acoustic current and which is due to viscosity forces is, in fact, independent of the coefficient of viscosity. /9

The boundary layer in the neighborhood of the cylinder consists of an average stream of four closed vortices. These vortices are induced by sonic vibrations (see Figure 1). Its thickness δ_i is of the order of δ_{ac} and does not depend on the amplitude of the oscillation.

The magnitude of the external flow depends on $u_o^2/\omega d$, that is, on $(a^2\omega^2)/(\omega d)$ or $(a^2\omega)/d$.

It is a characteristic velocity with which an acoustic field Reynolds number can be formed:

$$\mathcal{R}_s = \frac{\frac{u_o^2}{\omega d} d}{\nu} = \frac{a^2\omega}{\nu} = \left(\frac{a}{\delta_{ac}}\right)^2 .$$

The external stationary flow depends on this Reynolds number. According to Stuart [2], for high values of $\mathcal{R}_s$, a second boundary layer develops. Its thickness δ_e would be an increasing function of the ratio d/a:

$$\frac{\delta_e}{\delta_{ac}} = f\left(\frac{d}{a}\right) .$$

3.2.3. Classification of dynamic studies

Let us close this dynamic study by a classification due to Richardson [3].

Let us enumerate the different parameters of such a study:

$$\frac{a}{d}\ ,\quad \frac{\delta_{ac}}{d}\ ,\quad \mathcal{R}_s = \left(\frac{a}{\delta_{ac}}\right)^2 .$$

Another Reynolds number can be defined starting with the oscillation velocity $a\omega$ or, more precisely, with its effective value $(a\omega)/\sqrt{2}$:

$$\mathcal{R}_{osc} = \frac{\frac{a\omega}{\sqrt{2}}\, d}{\nu} .$$

The significance of these parameters can be seen more clearly on one graph (Figure 2). /10

For high values of a/d the flow appears as it would for a stationary flow.

For small values of δ_{ac}/d it is possible to apply the laminar boundary layer equations and the solution method proposed by Schlichting.

In contrast, for $\delta_{ac}/d > 1/10$ the complete Navier-Stokes equations would have to be used.

On this figure, we have shown straight lines corresponding to constant values of the Reynolds numbers $\mathcal{R}_s$ and $\mathcal{R}_{osc}$.

3.3. Thermal Studies

If we neglect the effect of free convection, the velocity field is independent of the temperature field, but, as mentioned above, any thermal study requires a detailed knowledge of the dynamic field.

Different cases can occur depending on the thickness of the thermal boundary layer relative to δ_i, the internal dynamic boundary layer thickness, and relative to δ_e, the external dynamic boundary layer if it exists, that is, if the Reynolds number $\mathcal{R}_s$ is sufficiently large.

We see here the problem in all its complexity.

To take up the case of the cylinder in more detail does not seem to be necessary.

We will only mention here a publication by Feiler and Yeager [4] concerning the case of a heated plate subjected to transverse waves of frequencies in the range between 34 and 680 Hz.

The pre-turbulence in the channel is 10%. The study was performed for Reynolds numbers ranging between 1.5×10^4 and 10^5. The authors showed that there was a 65% increase in the heat transfer coefficient. We may add that the photographs taken with an ultra-high speed camera showed the existence of a reverse flow near the wall during a portion of the period. /11

Chapter 4

EXPERIMENTAL SET UP /12

4.1. Wind Tunnel

The study was conducted in two wind tunnels of the Eiffel type.

The first wind tunnel, SS-1, was used to perfect the hot wire anemometer and for the measurements of the velocity profile and of temperature.

The second wind tunnel, SS-2, was equipped with an acoustic generator. It is in this wind tunnel that the final measurements were made.

The first hot filament tests showed that the large drifts are a function of time. Various users of hot wires had already pointed out that filament aging was due to dust deposition. We have, therefore, equipped both wind tunnels with anti-dust filters.

We have chosen filters made from folded paper. The assembly consists of interchangeable stacked dihedra. The type of paper and the number of dihedra have been chosen in terms of the required efficiency, the air flow rate, and the acceptable charge loss after a given operating time.

The large number of dihedral forms necessary leads to an entrance surface considerably larger than the normal entrance surface of the test section. For each wind tunnel, it was thus necessary to provide a good aerodynamic connection between the dihedra and the entrance collector.

This was achieved by a convergent nozzle section for the / 13
case of the SS-2 wind tunnel. The wind tunnel dimensions and flow rates are shown in Figure 3. For the SS-1 wind tunnel, a flow rate of 30,000 m^3/h is required and it was no longer possible to consider flow stagnation along a vertical wall. We have therefore adopted a different method: a stacking of dihedra on five of the six faces of a cubic frame directly connected to the entrance collector of the wind tunnel. The diagram is shown in Figure 3.

The smooth plate used is the one that was used as a reference plate in an earlier study concerned with measuring the fraction coefficient and the heat exchange coefficient of a rough plate.

The study is performed on a smooth plate with no pressure gradient. This requires a choice of the plate incidence such that the pressure gradient is negligible. This adjustment is obtained by comparing the static pressures at two points in the free flow. These points are located at equal distances from the plate and the test section wall.

These static pressures are measured within 0.1 mm of water. We have regained as final adjustment the incidence which leads to a deviation in Δp on the order of 0.5 mm of water which corresponds to a relative variation in $\Delta p/(1/2\ \rho\ u^2)$ of 1%.

The plate also serves as a lid on a frame divided into compartments. The leading edge is integral with the chassis and has an elliptic profile whose ratio of the major to minor axis is 10.

Under the incidence conditions mentioned above the transition occurs before that predicted [5]:

- beginning of transition: $x = 90$ mm $\rightarrow \mathcal{R}_x = 1{,}8.10^5$;

- end of transition: $x = 300$ mm $\rightarrow \mathcal{R}_x = 6.10^5$.

The results of measurements in the laminar regime are shown in Figure 4.

These results agree well with those obtained by Brunello [6] in the same wind tunnel but with slightly different generator conditions. In fact, the installation of an anti-dust filter has modified the preturbulence. This can have an effect on the transition conditions.

Nevertheless, we should note that the measurements with a hot wire agree well with those obtained with a Pitot tube except in the region near the wall. However, the hot wire enables measurements to be made near the wall (0.1 mm) providing that careful attention is paid to the play in the probe displacement system. In particular, an optical measurement must be made of the separation distance between the probe and its image on the plane of the plate. The compartments of the chassis are fed by circulating hot water. The adjustment of the flow rate in each compartment allows, after a fairly long settling time, a uniform temperature on the plate surface to be reached. This temperature is measured by means of thermocouples soldered in rivets that are integral with the plate. We obtain a temperature that is uniform within ± 0.5°.

4.2. Acoustic Generator

4.2.1. Ultrasonic domain

The preliminary tests had as their objectives the determination of the frequency and amplitude domain that we could obtain so as to have a measurable effect on the heat transfer.

The first attempts have been in the ultrasonic domain where the wavelengths are small relative to the characteristic dimensions of the plate. The industrial production of ultra-sound in air of high acoustic power are obtained by means of sirens or whistles. But these sound sources produce sounds that are of complex structure with a high proportion of harmonics. Additionally, in most commercially available systems, the air stream required for the production of ultra-sound perturbs the principal flow and it is thus the secondary air flow that acts on the boundary layer and not the acoustic phenomena itself.

Another technique consists of using electromechanical resonance transmitters. A metal bar experiences a reduction /15
in its length when subjected to a uniform magnetic field parallel to its length produced by a uniform current. If an alternating current of frequency f is superposed on the uniform current, then the contraction of the metal bar oscillates between two values. However, this is subject to the condition that the frequency f is equal to the resonant frequency of the metal bar. Such a magnetostriction transmitter, made from drawn duraluminum bar, was used in our experiments. Its resonant frequency was 23 KHz.

Another method consisted in making tests with a commercially available ultrasonic device called Ionophone. The principle of

the Ionophone is close to that of the singing arc or electric arc connected to a resonant circuit which is the source of ionic emission that maintains air vibrations. In the case of the Ionophone, a crystal capable of emitting high temperature ions is heated by a high frequency current whose amplitude is modulated to acoustic frequency. The ionic emission undergoes periodic variations. There follow fluctuations in pressure in the cavity connected to the horn.

4.2.2. Sonic domain

To transmit high acoustic power in air we were led to reduce the frequency and to use electrodynamic loud speakers. The mobile spool of the loud speaker was attached to a membrane made from a thin sheet of ebonite. It is not possible to operate the assembly under conditions of resonance. For acoustic frequencies the velocities of the membrane would remain small. To improve the power of such a device the membrane is attached to a "compression chamber" which is a space of small volume connected to the atmosphere by a small orifice whose cross section is smaller than that of the membrane. We thereby artificially increase the velocity amplitude fluctuations.

But such an orifice has the inconveniences of a source of small dimensions. To avoid the transmission of spherical waves, /16 an exponential horn is attached to it with the objective of producing plane waves.

4.3. Acoustic Field Measurements

The characteristics of an acoustic field are its frequency and its wave amplitude a_m. We prefer, in fact, to replace the wave amplitude by its vibrational velocity $a_m\omega$ or its acoustic pressure $\rho c\, a_m \omega$.

Direct measurements of the vibrational velocity are difficult because it can only be done with a hot wire. Therefore, there arises the problem of the response of the hot wire to harmonic perturbation.

It is easier and more common to measure pressure. In addition, in the case of an established stationary wave between an acoustic generator and a flat plate, the plane of the plate is an anti-node of pressure. The measurement of this pressure can be accomplished with a microphone embedded in the wall.

We have used condenser microphones whose range covers the total range of frequencies used in this study (20 Hz-50 kHz). These microphones can measure pressure levels ranging from 15 to 150 decibels.

The microphone consists of a metallic diaphragm and a fixed armature that constitute the electrodes of a condenser. The charge of this condenser is obtained by a continuous voltage bias. In the presence of an acoustic field, the pressure fluctuations involve a displacement of the diaphragm which causes a variation in the capacitance. The alternating component of the voltage at the condenser terminals is thus directly related to the pressure fluctuations.

The air volume between the diaphragm and the armature connects to the exterior by means of a capillary tube. This tube is designed to equalize the static pressure between the two faces of the diaphragm. The frequency characteristics are not sensitive to ambiant temperature variations so long as this /17
temperature is less than 100°C.

For these conditions, we have neglected changes in microphone response as a function of ambiant temperature or static pressure in the test section in the presence of flow.

The use of the microphones as sensors embedded in the wall or as pressure sensors displaced into the space between the acoustic generator and the plane of the plate requires a review of the definitions of the response of a microphone in free field or under pressure.

The free field response is the ratio of the output voltage to the acoustic pressure that would exist in a free field (plane wave) at the location of the microphone.

The pressure response is the ratio of the output voltage to the effective pressure applied on the diaphragm. At high frequency, wave diffraction on the microphone produces an appreciable change in the resultant pressure acting on the diaphragm. This effect depends on the ratio of the wavelength to the microphone diameter.

The first microphones used had a diameter of 12 mm. But the precise measurements carried out for frequencies in the range between 1000 and 10,000 Hz have required the use of microphones having a 6 mm diameter. Under the worst conditions the ratio of wavelength to diameter is equal to 5.

We have therefore assumed that the pressure response is equal to the free field response, especially because the measurements with non-embedded microphones had as their objective only to characterize the acoustic field.

Chapter 5

HOT WIRE ANEMOMETRY / 18

5.1. General Remarks

The study was begun at a time when complete hot wire anemometric chains were not commercially available. This led us to build an electronic device that would meet our needs:

- measurements of average velocities
- measurements of longitudinal and vertical velocity components
- measurements of turbulent stresses

We will briefly summarize the operating principle of a hot wire. A wire of small diameter (5 microns) constitutes one branch of a Wheatstone bridge in equilibrium. The resistance of the wire is constant; therefore it follows that the filament temperature is constant.

The heat exchange between the wire and the fluid takes place mainly by convection, radiation being negligible. However, we point out that in the vicinity of a wall the exchange mechanism is more complex because there is then an effect due simultaneously to conduction and to the modification of the convection phenomena due to the presence of the wall.

A dimensional analysis of the heat exchange between the wire and the fluid shows that the Nusselt number depends:

- on the Reynolds number relative to the filament diameter,
- on the Prandtl number of the fluid,
- on the Grasshof number

$$G = \frac{g \rho^2 d^3 \beta (T_{wire} - T_{gas})}{\mu^2} .$$

We note that for the case of interest here, that is, for the wire operating at constant resistance, the effect of Grasshof number disappears. /19

A number of formulas have been proposed by different authors depending on whether or not the effects of free convection are taken into account. Let us mention the hypothesis of King:

$$\mathcal{N} = A + B \sqrt{\mathcal{R}} .$$

A complete study by Collis and Williams [7] allows the definition of three different regimes depending on the value of the Reynolds number relative to the wire diameter (Figure 5):

- $\mathcal{R} < 0{,}02$ (dominant effect due to free convection)
- $0{,}02 < \mathcal{R} < 44$
- $\mathcal{R} > 44$ (appearance of the alternating vortices downstream of the wire)

It is the second case that is of interest to us here because, for a wire 5 microns in diameter, the limits mentioned above correspond to a velocity range between 0.06 m/sec and 132 m/sec.

Under these conditions, the formula we will retain here is written:

$$\mathcal{N} = A + B \mathcal{R}^n . \quad \text{(Figure 6)} \qquad (1)$$

with n = 0.45, A = 0.24 and B = 0.56.

In fact, it is not possible to rely on these empirical formulae to accurately measure velocity profiles. It is essential to perform a direct calibration of each probe.

5.2. Hot Filament Probe Calibration

The probes are calibrated directly under experimental conditions. The test section of the wind tunnel has a fairly large cross section to allow simultaneous measurements with a double Pitot tube and a hot wire. /20

The probe and the Pitot tube are placed in the same section and separated by approximately ten centimeters and in a manner to avoid all interaction between both sensors.

We have, on the other hand, verified the reproducibility of the measurements by exchanging the positions of the Pilot tube and the hot wire. This was done to bring out the eventual effect on a perturbation whose distribution would not be uniform in the section under consideration (preturbulence).

This calibration is always performed at ambiant temperature and only the variations of this temperature can have a non-negligible effect on the accuracy of the measurements.

The electronic device for the control of the constant resistance wire provides a voltage proportional to the current flowing in the wire. This current is related to the flow velocity of the fluid.

This voltage is measured by means of a digital voltmeter, To eliminate the effects of fluctuations, it is necessary to apply a time constant of integration of the type produced by a resistance-capacitance circuit.

The dynamic pressure produced by the Pitot tube is measured by means of an accurate differential pressure gauge. Pressure fluctuations are eliminated by the volumetric capacity of the manometer which acts as an integrator.

The profile of the calibration curves for three different wires have been reproduced on Figure 7.

It nevertheless should be pointed out that the use of such calibration curves is not recommended because several parameters modify this calibration:

- R_a (resistance of the probe to ambiant temperature)
- α (temperature coefficient)
- T_a (ambient temperature)

Thus, the calibration can be modified not only by going from one probe to another, but also for a given probe as a function of ambient temperature variations. /21

A different presentation of the calibration curve will allow us to reduce the number of parameters.

In effect, the empirical formulae of King\ or of Collins\ lead us to use a logarithmic presentation of the Nusselt number as a function of the Reynolds number.

The Nusselt number is directly related to the measured voltage:

$$\mathcal{N} = \frac{\alpha d}{\lambda},$$

$$\mathcal{N} = \frac{Q d}{\Delta T \lambda},$$

$$\mathcal{N} = \frac{R I^2 d}{\Delta T \lambda},$$

$$\mathcal{N} = \frac{V^2 d}{R \lambda \Delta T}.$$

For a given wire, maintained at a resistance R corresponding to a constant temperature deviation from ambient temperature, the Nusselt number is directly proportional to the square of the measured voltage.

The empirical relation (1) becomes

$$V^2 = a + b\,U^n \qquad (2)$$

The coefficient a corresponds to the ordinate at the origin of the straight line representing the function V^2 of the variable U^n. The experimental determination of the coefficient a is often difficult and it is common practice to replace its value by the voltage corresponding to a null velocity. Let V_o be this voltage. Note that we always have $V_o^2 > a$ because of the effects of free convection. On the other hand, it should be noted that V_o can be measured very accurately. In these conditions, the representation that we have chosen consists of showing in the ordinate the voltage difference on a logarithmic scale $V^2 - V_o^2$ and in the abscissa the velocity U (Figure 8).

Equation (2) can be transformed to /22

$$V^2 - V_o^2 = B\,U^n \qquad (3)$$

This introduction of calibration can be put to use for the direct measurement of the velocity profile where the absolute velocity is of no interest.

To simplify the data reduction we have decided to make use of all experimentally determined profiles in the following manner.

Let V correspond to the voltage at an ordinate point y where the velocity is U and let V_∞ be the voltage corresponding

to the velocity u_∞ far away.

Equation (3) allows one to write

$$\frac{V^2 - V_o^2}{V_\infty^2 - V_o^2} = \left(\frac{u}{u_\infty}\right)^n$$

or

$$\frac{u}{u_\infty} = \left(\frac{V^2 - V_o^2}{V_\infty^2 - V_o^2}\right)^{1/n} \qquad (4)$$

Thus, the profile $u/u_\infty(y)$ can be obtained directly by a determination of the calibration coefficient n and the measurement of the voltages V_o, V_∞ and the voltages V(y).

Comment: The method has the enormous advantage of freeing the measurements of ambiant temperature variations. It is only necessary to ensure that the temperature does not vary during the test. This is done by one voltage measurement V_o before and after the test. This calibration method will be used for linearization. But, this does not exclude direct velocity measurements taking account of the coefficient n.

5.3. Servocontrol Study

The wire is mounted in one of the branches of a Wheatstone /23
bridge (Figure 9). The unbalanced voltage of the bridge is fed into a differential amplifier as error voltage. This large gain amplifier with low thermal drift delivers an output voltage proportional to the input error voltage. This control voltage modifies the feedback to the bridge current.

The large pass band (30 kHz) of the amplifier ensures at all times the bridge equilibrium when the wire is subjected to velocity fluctuations.

The operating principle of this feedback control requires some explanation. We will here give the results of a preliminary study of the response of the apparatus to transient signals. A more complete study of this penomena would require a study of the conduction phenomena in wires.

We will compute an approximate value for the time constant of the apparatus for the case of a resistance of constant value. Figure 10 shows a functional schematic.

For a filament subjected to a non-null velocity, the steady state equations are written:

$$(R_o + R_1)\, I_1 = (R_o + R)\, I_2 \quad , \tag{5}$$

$$I - I_o = G\, e \quad , \tag{6}$$

$$e = R_o\, (I_2 - I_1) \quad , \tag{7}$$

$$I = I_1 + I_2 \quad . \tag{8}$$

From these equations the value of the resistance R can be derived:

$$R = R_1 - \frac{2(R_o + R_1)}{G\, R_o + 1 - \frac{I_o}{I}} \quad . \tag{9}$$

/ 24

We can choose the value of the reference current I_o; in particular if $I_o/I < 1$, there results

$$R = R_1 - 2\,\frac{R_o + R_1}{G\, R_o + 1} \quad . \tag{10}$$

In that case, if the flow velocity u varies rapidly and if we assume that the feedback amplifier does not introduce any appreciable phase shift, the above equations remain valid for the

transient regime. The probe resistance would then be rigorously constant and the time constant of the apparatus would be zero.

It is nevertheless clear that this limiting case does not correspond to the real behavior of a wire placed in a flow because we have taken into account the average wire resistance. In fact, the local convection phenomena at the wire surface should be studied, and the conduction terms in the wire cannot be neglected.

If the rest current I_o is no longer neglected, Equations (5) through (9) remain valid. By differentiating each of these equations, we obtain the following corresponding transient equations

$$\Delta I \, (R_o + R_1) \frac{I_o}{I_2} = - 2 \, G \, R_o \, I_2 \, \Delta R \quad , \tag{11}$$

$$(R_o + R_1) \, \Delta I = (I_2 \, \Delta R + R + R_1 + 2 \, R_o) \, \Delta I_2 \quad . \tag{12}$$

Moreover, we can write the equation that characterizes the most general operation of a wire subjected to flow of velocity u and heated by a current I_2:

$$(1 + j \, M \, \omega) \, \Delta R = \frac{\partial R}{\partial I_2} \, \Delta I_2 + \frac{\partial R}{\partial U} \, \Delta U \quad . \tag{13}$$

The quantity M would be the real time constant of a wire heated by a current of constant intensity.

Different authors [8] have proposed calculations for the time constant M: /25

$$M = \frac{m \, c}{2 \, R \, I_2} \, \frac{\frac{\partial R}{\partial I_2}}{\frac{\partial R}{\partial T}} \quad . \tag{14}$$

The approximate law of King

$$R I_2^2 = (A + B\sqrt{U}) (T - T_a)$$

gives

$$\frac{\partial R}{\partial I_2} = 2 \frac{R - R_a}{R_a} \frac{R}{I_2} \quad .$$

On the other hand, the relation

$$R = R_a \left[1 + \chi_1 (T - T_a) \right]$$

leads to

$$\frac{\partial R}{\partial T} = \chi_1 R_a \quad .$$

Equation (10) becomes

$$M = \frac{m c}{\chi_1 R_a} \frac{R - R_a}{R_a I_2^2} \quad . \qquad (15)$$

For the wire that we use, Equation (15) gives a numerical value of M equal to 0.4×10^{-3} sec.

Starting from Equations (11), (12) and (13), we can compute the response $(\Delta I/\Delta U)_r$ for a real case and compare it to the response $(\Delta I/\Delta U)_p$ for an ideal case where the thermal inertia of the wire is zero.

These calculations lead us to the following results:

$$\frac{\left(\frac{\Delta I}{\Delta U}\right)_r}{\left(\frac{\Delta I}{\Delta U}\right)_p} = \frac{1}{1 + \frac{I_o}{G R_o I} \frac{R_a (R_o + R_1)}{R (R - R_a)} j M \omega} \quad . \qquad (16)$$

/26

The new time constant grows with I_o and decreases with:

- the feedback amplifier gain
- the overheating coefficient $(R - R_a)/R_a$,
- the operating current I,
- the operating resistance R.

For practical application $G = 200$, $I_o = 50.10^{-3}$ A, $I = 250.10^{-3}$ A; and the time constant becomes $M/2.10^3$, or $0,2.10^{-6}$ s.

This study of the response of a hot filament to velocity fluctuations only serves to justify the use of a constant resistance rather than constant current intensity. The adjustment of the frequency response of the system requires, in fact, an experimental test. The adjustment of this time constant is often performed by the square signal method by superposing on the signal a voltage fluctuation with a square profile. We have, in fact, chosen a different method which consists of simulating a velocity fluctuation by attaching a resistor in parallel with the probe resistance. This assembly is achieved with a relay and to understand the operation it is necessary to graph the hot wire characteristics. The measurement was done for a hot wire probe. In Figure 11 we show the probe resistance as a function of the heating current for different flow velocities. On this figure, we can clearly see both operating modes of the hot wire.

- Constant current intensity operation: when velocity increases, the probe cools and its resistance decreases; the heating current intensity is constant; therefore, the voltage at the filament terminals varies as a function of the velocity.

- Constant resistance operation: this is the case we have kept when the velocity increases, the heating current of the probe is increased by the control system in a manner to keep the

resistance of the probe constant.

It is starting from this illustration of the wire operation that we can explain how we proceeded to the adjustment of the frequency response of the servocontrol. /27

By means of a "chopper" relay, we have attached a resistance R_2 in parallel to the filament of resistance R (Figure 12). The servocontrol modifies the current in the resistance R. Because of this variation in the current, the resistance R changes to a new resistance R'. Note that this variation R' - R is due to the fact that the servocontrol operates so that the parallel resistances R' and R_2 have an equivalent resistance R of the probe alone. Between R, R' and R_2 there is a relation:

$$\frac{R' R_2}{R' + R_2} = R$$

so that

$$R' = \frac{R R_2}{R_2 - R}$$

We can thus characterize each element by its operating point on Figure 13.

- When the relay is open, the operating point of the probe is the point A.

- When the relay is closed, the assembly made up of the probe and the resistance R_2 has an operating point B and as far as the servocontrol is concerned, everything is as if the probe maintained a resistance R and that the velocity goes from a value U to a value U + ΔU. In fact, it should not be forgotten that the probe experiences the velocity U and that its

operating point C remains on the characteristic curve U = const.

This method then allows for a simulation of the velocity fluctuation and the observation of the servocontrol response on an oscilloscope (Figure 14) shows the perturbations due to the presence of the resistance R_2.

The adjustment of the frequency response of the control amplifier allows the improvement of the servocontrol response to a velocity fluctuation.

This method seems to be about the same as the square signal method but it differs by the fact that we are here really taking account of the wire response. Indeed, the ideal calibration would consist of directly applying a sinusoidal velocity with the actual magnitude. But, as we will note in the study that follows, this is neither easy to accomplish nor interpret. /28

5.4. Linearization

In the study of hot wire calibration, we have presented the results in the form

$$V^2 - V_o^2 = B\,U^n \quad .$$

This formula can be used by means of a direct calculation of the velocities U as a function of the voltages V. It is also possible to apply this formula in the case of fluctuations providing that a linearization about an operating point is made. But this assumes that the fluctuation level is small relative to the average value.

We have in fact achieved a linearization of the signal over the entire range of measurements by staying as close as possible to the above relation.

The linearization is obtained by a nonlinear electronic diode device [9]. A chain of diodes is a series of diodes that becomes succeedingly more conductive as a function of the variations in the input voltage.

This allows one to obtain an output voltage that is a polygon approximation to a continuous function and an increasing function of the input voltage. This is particularly suited for a power law. The first tests were conducted by assuming the hypothesis of King to be valid, that is, by assuming n = 1/2 in Equation (1). These diode chains were therefore adjusted so as to obtain a power law of degree 2, that is, an output voltage proportional to the square of the input voltage. /29

Thus, starting from the voltage V, the first quadratic chain gives V^2. The voltage V_o^2 is eliminated by subtraction.

The resultant voltage $V^2 - V_o^2$ is then amplified (gain k) and then fed into a second quadratic chain. The output is then

$$V_s = k\,(V^2 - V_o^2)^2 \quad .$$

As a function of Equation (3) we can then write

$$V_s = k\,(B\,u^{1/2})^2 = k\,B^2\,u \quad .$$

The output signal is proportional to the velocity U. Adjustment of the gain k yields the desired proportionality constant.

In fact, the use of such a method is only approximated and a good linearization requires that the second diode chain be adjusted to exact exponent of Equation (1). Thus, for each calibration, we can modify the adjustment of this second diode chain. The purpose of the first diode chain is to produce a

voltage proportional to the power produced by the wire.

This linearization has not only been done for the average velocity measurements but mainly for velocity fluctuations. It was nevertheless necessary to determine the dynamic response of the system. A sinusoidal voltage v is superposed on a continuous voltage V which corresponds to a given operating point.

Let us label the input values by e and the output values by s in the linearization chain system.

The linearization then consists of achieving an approximation to the equation

$$(V_e^2 - V_o^2)^2 = k\, B^2\, U$$

by the equation /30

$$V_s = k\,(V_e^2 - V_o^2)^2 \quad .$$

Dynamically, this is written

$$\overline{V_s} + v_s = k\left[(\overline{V_e} + v_e)^2 - V_o^2\right]^2 \quad ,$$

or, to a first order approximation

$$\overline{V_s} = k\,(\overline{V_e^2} - V_o^2)^2$$

and

$$v_s = 4\,k\,\overline{V_e}\,(\overline{V_e^2} - V_o^2)\,v_e \quad .$$

We characterize the fluctuations v_s and v_e by their effective values $\sqrt{\overline{v_s^2}}$ and $\sqrt{\overline{v_e^2}}$.

There follows:

$$\frac{\sqrt{\overline{v_s^2}}}{\overline{V_s}} = \frac{4\,\overline{V_e^2}}{\overline{V_e^2} - V_o^2}\,\frac{\sqrt{\overline{v_e^2}}}{\overline{V_e}} \quad . \qquad (17)$$

This dynamic calibration has been done for four pairs of the voltage values V_o and V_e. The results are shown on Figure 15. Equation (17) shows that the ratio $4\,V_e^2/(V_e^2 - V_o^2)$ is always greater than 4. This means that whatever the operating conditions, a fluctuation $\sqrt{\overline{v_e^2}}/V_e$ of 10% results in a fluctuation $\sqrt{\overline{v_s^2}}/V_s$ at least equal to 40% at the output of the linearizer. This output fluctuation gives directly the real magnitude of the ratio $\sqrt{\overline{u^2}}/U$. We note on Figure 15 that it is not possible to make measurements of output fluctuations that exceed 50%, because we are then outside the linearity conditions. In addition, note that it concerns a calibration from a sinusoidal voltage. In the case of velocity fluctuations, it would also be necessary to take account of the wire response limits and of the limitations of linearizer response to a complex signal. /31

5.5. Effects of Wire Angle

Older studies have shown that the velocity that must be taken into account for wire cooling is in fact the normal velocity component, that is, the projection of the velocity vector on the normal to the wire.

This simple hypothesis was subsequently replaced by the suggestion that the effective velocity U_{eff} be related to the velocity U by the equation

$$U_{eff}^2 = U^2 (\cos^2\varphi + k^2 \sin^2\varphi) \qquad (18)$$

where φ is the angle between the normal to the wire and the average flow direction.

The coefficient k depends on the ratio of the length to diameter ℓ/d of the filament [10].

For 1/d=200, the coefficient k would equal 0.2.

We have conducted tests with different wires with the objective of bringing out the eventual correction factor to be applied to the response of an inclined filament. The filament is mounted on an adjustable probe and we have sought to represent the results from measurements with such an arrangement in a concise manner.

For a zero φ angle, the output voltage from the anemometer is shown on Figure 16 as a function of the velocity U by the upper curve. For a non-zero φ angle, the curve would be displaced downward. The simplified hypothesis $U_{eff} = U_{cos}$ translates into the fact that the voltage $\bar{v}_{\varphi,U}$ corresponds to a filament subjected to a velocity U, whose normal is inclined by an angle φ in relation to the direction of the velocity vector, and is equal to the voltage $\bar{v}_{\varphi=0,U\cos\varphi}$ corresponding to a wire subjected to a velocity of magnitude U cos φ and which is normal to the direction of the velocity vector.

The approximation $U_{eff} = U \cos\varphi$ can, therefore, be described by the ratio $\bar{v}_{\varphi,U}/\bar{v}_{\varphi=0,U\cos\varphi}$.

The results of these tests are shown on Figure 17.

We note that the ratio considered remains near unit for angles less than 50° so long as the ratio of 1/d is at least equal to 200. These results are in good agreement with Equation (18) which can be transformed to

$$\frac{U_{eff}}{U \cos\varphi} = \sqrt{1 + k^2 \, tg^2\varphi}$$

Using our notation, this equation can be written

$$\frac{V_{\varphi,U}}{V_{\varphi=0,U\cos\varphi}} = \sqrt{1 + k^2 \operatorname{tg}^2\varphi}$$

As an example, let us mention, that for $u_\infty = 30$ m/s, $\ell/d = 200$, $\varphi = 60°$ and $k = 0.2$, the above equation gives a ratio of 1.06 whereas the experimental results give us 1.04. We have chosen probe characteristics such that we do not have to apply correction factors.

5.6. Construction

5.6.1. Straight wire anemometer

The hot filament is positioned perpendicularly to the direction of the average velocity. We therefore conjecture that the filament is sensitive only to the average velocity $\bar{u}$ and to its longitudinal fluctuation u'.

The filament, mounted on one branch of a Wheatstone bridge, is connected to a transistorized control amplifier. This high gain (200) low background noise (50 μV) differential amplifier feeds the bridge with a current as high as 400 mA. The output signal is taken from the terminals of a resistor in series with the bridge. The output current which is proportional to the current flowing through the filament is then fed into the linearization chain.

We have seen (paragraph 5.4) that it is of interest to linearize the signal. This linearization is obtained by means of an analog system which, starting with an input voltage V_e, produces an output voltage V_s proportional to the velocity by obeying the equation: /33

$$V_s = k\,(V_e^2 - V_o^2)^2$$

(see Figure 18 for synoptic diagram of this linearization chain).

We find in turn:

- the control amplifier
- the first diode chain
- the zero adjustment amplifier
- the gain adjustment amplifier
- the second diode chain.

The schematics of the principle of each element of this system has been detailed in Figure 21. The results of the linearization process are shown on Figure 19. The upper curve represents the average of the points obtained when the second diode is adjusted in such a manner as to furnish an output signal proportional to the square of the input signal. This diode chain has in fact been adjusted point by point in a manner to yield, not just a power law of exponent 2, but a power law of exponent n, where n is deduced for each wire of the calibration curve.

The points shown on Figure 19 therefore illustrate the quality of the linearization.

We note the flexibility of this system. So long as the exponent n need not be modified, the adjustment of this linearization chain requires only two operations:

- adjustment of the zero potentiometer so that the output voltage is zero for a zero velocity,

- adjustment of the gain potentiometer so that the output voltage is a maximum for a maximum value of the flow velocity.

A long and delicate operation is involved if we have to modify the adjustment of the second diode chain. However, we should point out that the exponent n depends on the wire diameter and not on its length [11]. But, the wires we are using are Wollaston wires. We strip them electrolytically of the outer silver coating that surrounds the inner platinum core. For a Wollaston wire spool, the platinum wire diameter is constant and it is only the cleaned surface that varies from one wire to another. /34

The measurement of the average squared value is obtained either with thermal voltmeter with thermocouples or with an electronic voltmeter giving a real effective value.

5.6.2. Two-wire anemometer

The measurement of the longitudinal component of the velocity fluctuation is obtained with a straight wire.

The measurement of the other two components requires a two-wire probe.

It is common practice to use probes with the wires in the form of a cross and to make the assumption that both wires are arranged symmetrically relative to the direction of the average velocity and that both wires have the same sensitivity to velocity fluctuations.

We have preferred to use a double-wire probe consisting of:

- a straight wire used as reference
- an inclined wire allowing the measurement of fluctuations.

The straight wire is perpendicular to the direction of the average velocity. It is directed along the Oy-axis and perpendicular to the plane of the plate. This wire is sensitive to the projection u_{n1} on its normal of the instantaneous velocity vector:

$$u_{n1} = \bar{u} + u' \quad .$$

The linearization chain associated with this wire is the same as the one we have described for the single wire anemometer. It delivers a voltage $v_{s1} = k_1 \cdot u_{n1}$.

The inclined wire is located in the plane xOy. It is inclined at an angle of approximately 45° relative to the flow direction Ox. This wire is sensitive to the projection u_{n2} on the normal of the instantaneous velocity vector. To a first approximation we have /35

$$u_{n2} = \bar{u} \cos\varphi + u' \cos\varphi + v' \sin\varphi \quad .$$

A linearization chain with variable gain k_2 is coupled to this second wire. The output voltage would be

$$v_{s2} = k_2 \cdot u_{n2} \quad .$$

The gain k_2 is in fact automatically adjusted so that the average value of the output signal is the same in both chains.

We ensure that

$$\overline{V_{s1}} = \overline{V_{s2}} \quad .$$

This adjustment is obtained by means of a photoresistance control system that compares the average voltage of the chain that connects to the straight wire to the voltage of the chain that connects to the inclined wire.

The chain that connects to the straight wire acts as a master chain.

The chain that connects to the inclined wire acts as a controlled chain.

The equality $\overline{V_{s1}} = \overline{V_{s2}}$ means that

$$k_1 \cdot \overline{u_{n1}} = k_2 \cdot \overline{u_{n2}} \quad ,$$

or

$$k_1 \cdot \bar{u} = k_2 \cdot \bar{u} \cos\varphi \quad ,$$

or again

$$k_1 = k_2 \cos\varphi \quad .$$

This operation amounts to a compensation for the sensitivity deficiency of the inclined wire on the linearization level. / 36

Under these conditions, the output voltage fluctuations of the two chains are proportional to u' and u' + v', respectively.

v' and u' are therefore isolated because of the difference of the signals from the two chains.

The mean quadratic values $\overline{u'^2}$ and $\overline{v'^2}$ are then obtained in the same way as for the apparatus with one wire.

The correlation coefficient between the two fluctuations, for example between u' and v', is given by the relationship

$$R_{u'v'} = \frac{\overline{u' v'}}{\sqrt{\overline{u'^2}}\sqrt{\overline{v'^2}}} \quad .$$

This coefficient is independent of a possible amplification of one of the fluctuations, i.e., the correlation coefficient between the fluctuations u' and k v' is the same as the correlation coefficient between the fluctuations u' and v'.

If the coefficient k is such that $\overline{u'^2} = \overline{(k\,v')^2}$, the correlation coefficient can be written as:

$$R_{u'v'} = R_{u',kv'} = \frac{\overline{(k\,v' + u')^2} - \overline{(k\,v' - u')^2}}{\overline{(k\,v' + u')^2} + \overline{(k\,v' - u')^2}} \quad .$$

or:

$$R_{u'v'} = \frac{1 - \dfrac{\overline{(k\,v' - u')^2}}{\overline{(k\,v' + u')^2}}}{1 + \dfrac{\overline{(k\,v' - u')^2}}{\overline{(k\,v' + u')^2}}} \quad .$$

We have the fluctuations u' and k v', where k is adjustable, so that

$$\sqrt{\overline{u'^2}} = \sqrt{\overline{(k\,v')^2}} \quad .$$

An inverting amplifier produces the voltage - u'.

Two summing units produced the instantaneous voltages /37
$k\ v' + u'$ and $k\ v' - u'$.

Two diode chains produced $(k\ v' + u')^2$ and $(k\ v' - u')^2$.

These voltages are applied to two coupled potentiometers. The correlation coefficient is obtained from a direct reading of the angular displacement of the slides of the potentiometers.

Figure 20 shows a synoptic diagram of the two-wire anemometer. The linearization chains for the inclined and the straight wire are connected to the control system by the photoresistor. The lower part of this figure is concerned with the measurements of fluctuations and the correlation coefficient. Figures 21, 22, 23, and 24 show schematically the principles of the various components of this electronic assembly [12].

The principle behind the linearization and the control system of both linearization chains are of sufficiently original character to have led us to apply for a patent [13].

Chapter 6

FLUXMETER PROBE

6.1 Introduction

The steady state heat flux measurements have led to the development of flux measuring pellets with a small time constant. It is especially for measurements in shock tubes that the thin filament fluxmeters have been developed.

Some experimentalists have also proposed using this type of sensor for the measurement of the local friction coefficient. In this case, the fluxmeter replaces the Preston tube or the wall balance. We have sought to use such sensors for the measurement of heat flux at the wall of a flat plate.

6.2. Heat Flux Measurements

For heat flux measurements in a shock tube, the probe receives a certain amount of heat. The resistance of the probe changes with variations in temperature. Measurement of this resistance allows an estimate of the heat transfer to be made between the fluid and the wall. We have tried to develop a heat flux measuring technique based on this principle.

A very thin platinum coating is placed on the area to be studied and located at a point sufficiently far from the leading edge of the plate so as to be in the fully developed turbulent region. In the neighborhood of the metal coating, a thermal boundary layer develops within a dynamic boundary layer.

The coating is maintained at a constant temperature by means of an electronic device identical to the one that is used in the hot wire anemometer.

6.3. Conclusions

/39

Two theoretical studies have been undertaken; the first one to calculate the effects of conduction in the support, the second one to calculate the three-dimensional characteristic of the conduction phenomena in air. These two effects are coupled and it is easier to use a probe after calibration.

This flux measuring probe is sensitive both to the variations in the local friction coefficient and to the heat flux variations if, upon checking by another method, the local friction coefficient is not appreciably modified during the experiment.

Chapter 7

RESULTS

7.1 Utilization of the Hot Wind Anemometer

The anemometer was perfected in the SS-1 wind tunnel. It is in this wind tunnel that Brunello [6] carried out measurements on smooth plates by means of a Pitot tube.

The velocity profiles were measured for various values of the abscissa in the turbulent region. We have chosen a free flow velocity of 40 m/sec so as to obtain an established turbulent regime. For this velocity, the wind tunnel vibrations are quite large but only under these conditions are direct comparisons with Brunello's results possible [6].

As an example, Figure 25 shows a velocity profile for an abscissa of 500 mm. Starting with the velocity profiles, we have calculated by numerical integration the momentum thickness δ_2 (Figure 26). Note here the excellent agreement between the results. The quality of Brunello's results is due to the fact that he calculated the momentum thickness from the average value of the various profiles.

By applying the equation for the total momentum, we can also compute the local friction coefficient

$$c_f = 2 \frac{d\delta_2}{dx} \quad .$$

For x = 500 mm, we find $c_f = 3{,}32.10^{-3}$. This result is very near to the value 3.5×10^{-3} which corresponds to the empirical formula

$$c_f = 0{,}0592 \mathcal{R}^{-0,2}$$

To this value of the friction coefficient, there corresponds a friction velocity /41

$$u_f = 1{,}63 \text{ m/s}$$

This calculation leads to the velocity profiles on semi-logarithmic graphs (Figure 27). We have drawn on this figure the straight line that represents the wall effect law. This law is fairly well established and we will use this property of the velocity profiles to justify the use of the flux probe pellets. We have seen (§6.3) that measuring the heat flux is possible with these pellets, provided that the local friction coefficient remains unchanged. This check is obtained by comparing the slope on the linear portion of the semi-logarithmic plot with and without acoustic perturbation.

7.2. Visualization

Before any measurements of the effects of the acoustic field could be made, we sought to develop an optical method to determine the frequency and amplitude region in which this effect would be large. The preliminary study was therefore carried out with an interference strioscope. Measurements of variations in the index of refraction was done by observation of the local variations in coloration or by studying the geometrical shape changes in the fringes (Figure 28).

The interferometer has a high response but is difficult to use in the immediate neighborhood of a wall.

On the other hand, it does not seem possible in our case to be able to make measurements from interferograms because the optical

path is such that it would mean an integration along the width of the test section: the wall boundary layer and the non-homogeneity along the breadth of the acoustic field and its effect in perturbing the measurements.

Only a local measurement can provide us with useful information and any optical method can only serve as a preliminary study. /42

Finally, it should be pointed out that it is only in free convection, where the phenomena of mixing by the acoustic field is large, that visualization is possible. In fact, such visualization falls outside the framework of our study.

7.3. Tests in the Ultrasonic Domain

The experimental set-up is shown on Figure 29.

Tests in the ultrasonic domain entail practically no change in the flux probe response. Likewise, the velocity profiles remain unchanged for free flow velocities within the range from 10 m/sec to 30 m/sec.

We recall that for these tests we have used two different ultrasonic sources:

- on the one hand, a magnetostriction transmitter

- on the other, a variable frequency generator of the Ionophone type.

The magnetostriction transmitter can only operate at one frequency. We gave up trying to change frequency because it meant changing the bar.

The Ionophone is more flexible in its use but the acoustic level on the plate does not exceed 110 decibels.

These tests do not lead to any results because the acoustic power output is too small. It is also necessary to consider the poor propagation of ultrasounds in air. We know, in effect, that, independently of the poor transmission between quartz and air, the attenuation is proportional to the square of the frequency.

7.4. Tests at Low Frequency (200 Hz < f < 1000 Hz) /43

7.4.1. Parameters of the study

In this frequency range, the tests still lead to a small but measurable effect.

The two acoustic parameters of the study are:

- f, the frequency of the acoustic wave,
- a_m, maximum amplitude.

In fact, we will replace the maximum amplitude by the vibrational velocity $a_m\omega$ which is directly related to the acoustic level L.

We add to the acoustic parameters the two principal parameters of the dynamic problem. The study was thus performed as a function of four parameters:

- f, the infrequency of the acoustic wave
- L, the acoustic level
- u_∞, the main flow velocity
- x, the position of the heat flux measurement along the abscissa measured from the leading edge.

The measurements were carried out by continuously varying the frequency, the other parameters remaining constant. In fact, it was required to achieve in the plane of the plate a constant acoustic level regardless of the frequency. The electronic assembly is shown in Figure 30. The voltage supplied to the acoustic generator is adjusted by a feedback voltage produced by the microphone. Numerous tests had to be conducted to obtain a suitable operation and a good quality control system. The continuous variation of the frequency is obtained by a mechanical control coming from a recording potentiometer upon which we ensure that the acoustic level remains at a constant value. The frequency sweep speed is adjustable but we have preferred to choose a very slow speed to ensure that the phenomena becomes established.

The electromechanical characteristics of the acoustic generator membrane is such that, for each acoustic level, system control is possible only within a given frequency band. The /44
higher the acoustic level, the narrower the frequency band.

In addition, during these tests we have taken an additional parameter into consideration. This parameter is the film temperature of the flux probe or, more precisely, the difference between this temperature and the ambiant temperature. In fact, this parameter does not come into the study, but we have noticed that this difference $T_p - T_\infty$ must be between 120° C and 160° C to obtain a good sensitivity of the measurement. For a difference $T_p - T_\infty$ less than 120°C, measurement reproducibility is very poor. For a difference $T_p - T_\infty$ higher than 160° C, the probe is no longer stable and platinum film deterioration begins to appear.

The effect of the acoustic field is characterized by the relative variation in the heat flux at the wall of the plate $(\Phi - \Phi_o)/\Phi_o$.

It should nevertheless be noted that, in the various measurements, the value of the flux Φ_o varies. But the use of a relative measurement allows for a direct comparison between the measurement with the acoustic field present and without.

7.4.2. Effects of the frequency on the acoustic wave

The behavior of the curves varies considerably depending on the given values of the velocity u_∞.

We provide curves that correspond to the velocities of 30 m/sec and of 10.8 m/sec as well as those corresponding to free convection.

For u_∞ = 30 m/sec (Figure 31) it is worth noting that the effects of the acoustic field changes sign as a function of the frequency. There exists a frequency band (350 Hz - 700 Hz) for which there is an increase in the heat flux. Outside this frequency band this effect is "negative".

For u_∞ = 10.8 m/sec (Figure 32), the effect is always negative for the frequency range used. /45

By contrast, in free convection (Figure 33), the effect is always positive and decreases very steadily with increasing frequency. This result is reasonably well explained because the classical notions of a boundary layer vanishes. To the free convection phenomena we superpose an oscillating field that can only increase the heat flux at the wall. When the frequency increases, the effect disappears because the onset of vortices in the neighborhood of the plate wall is no longer affected by rapid local pressure fluctuations even if their amplitude is not negligible.

7.4.3. Effect of acoustic level

We show (Figure 34) the results that correspond to a velocity u_∞ of 30 m/sec for two frequencies. But the behavior of the curves would be the same for the other values of the velocity or frequency.

In particular it should be pointed out that whatever the values of the various parameters, the acoustic field effect retains the same sign when the acoustic level varies.

For small acoustic levels the effect is zero because when that level increases, the effect changes in steadily increasing manner.

This result is logical because the acoustic level is related to the effective applied pressure fluctuation. In contrast, for a level of about 150 decibels the curve seems inexplicably to level off.

7.4.4. Effect of velocity in the main flow.

We have chosen some particular values of the velocity u as well as the abscissas X such that we could bring out the effect of the Reynolds number.

The six values chosen for the velocity have been complemented by other values so that the evolution of the phenomena could be better followed.

The measurements that correspond to a frequency of 500 Hz /46
(Figure 35) show that, for velocities between 6 m/sec and 18 m/sec, the effect of the acoustic field is negative. By contrast, for a

frequency of 1000 Hz (Figure 36), the curve no longer shows the same behavior.

7.4.5. Effect of the measurement location along the abscissa

We have experienced some difficulties in modifying the measurement location along the abscissa. In effect, the acoustic generator and its horn are integral with the wind tunnel. On the other hand, the mounting and adjustment of the plate in the experimental vein does not allow for longitudinal displacements. Finally, the calorimetric probe requires a flush mounting in the plate, thus causing damage to it.

We have, nevertheless, modified the measurement abscissa by attaching a new leading edge upstream of the old. Depending on the length of this new leading edge we have carried out measurements for X = 0.25 m, 0.30 m, 0.35 m, 0.40 m, and 0.416 m along the abscissa.

This design allows measurements to be made in the horn axis and to maintain an acoustic field with well established standing waves.

In fact, this series of measurements, the reference flux (Φ_o) varies from one abscissa to another but, for the same velocity, the effect $(\Phi-\Phi_o)/\Phi_o$ remains unchanged.

The variations of the effects as a function of the abscissa are of the same order of magnitude as the measurement uncertainty.

Under these conditions, the Reynolds number does not seem to be a characteristic of the measurement.

We have nevertheless added the values of the Reynolds number on Figures 35 and 36. But, it should be pointed out that two tests corresponding to the same Reynolds number will have the same effect only if they correspond to the same velocity.

7.5. Tests at Intermediate Frequencies /47

7.5.1. Between the ultrasonic and the low frequency range there exists an entire region of frequencies allowing a non-negligible power transmission to be made by maintaining a correct acoustic impedance.

Indeed, in the preceding tests, no mention was made with regard to the distances between the plate and the acoustic generator. In any case, for a frequency of 200 Hz, that is, for a wavelength of 1.5 m, it is not possible to set up a standing wave in the neighborhood of the plate.

We have therefore undertaken a new study in the range from 1000 Hz to 10,000 Hz the latter being the maximum acoustic generator frequency for a generator with a compression chamber.

The acoustic adjustment is henceforth obtained by fine adjustment of the plate height so that the acoustic level at the plate goes through a maximum. This adjustment is easy for a frequency range between 5000 and 10,000 Hz. In contrast, between 1000 Hz and 2000 Hz, we have encountered difficulties and it is only after 1700 Hz that it is possible to obtain the correct adjustment.

We have shown on Figure 49 the test results obtained at 1720 Hz:

- the curve 37 (1) shows the evolution of the acoustic level at the wall as a function of the distance between the plate and the acoustic generator;

- the curves 37 (2, 3 and 4) show the evolution of the acoustic level above the plate for three given positions on the plate.

We see the appearance of a distance of 5 cm, whereas the quarter of the wavelength is equal to 4.8 cm.

Note that as a function of these adjustments, the acoustic level does not seem to change much. However, let us not forget that we are dealing with a logarithmic scale where a deviation of 20 decibels corresponds to a ratio of 100 of the effective value of the vibrational velocity.

This adjustment can reach several centimeters for frequencies on the order of 2000 Hz. /48

For each measurement position, after this distance adjustment, we must verify that the longitudinal pressure gradient is still zero. Now, it happens that in certain cases these two adjustments are incompatible.

7.5.2. Control of the friction coefficient

Checking for the friction coefficient is obtained from the trace of the velocity profiles in semi-logarithmic coordinates (§7.1). The straight line portion of the curve represents an equation of the form

$$\frac{u}{u_\infty} = a \log y + b \quad . \tag{38}$$

Let us relate to the equation the classical form of the wall effect law equation

$$\frac{u}{u_f} = A \log \frac{y\, u_f}{\nu} + B \quad . \tag{39}$$

There results

$$\frac{u_f}{u_\infty} = \frac{a}{A} \quad . \tag{40}$$

For the velocity U_f to remain constant, it is, therefore, only necessary for the slope a of the semi-logarithmic profile to remain constant.

This check is shown on Figure 38. We observe that as long as the acoustic level is small, the wall effect law remains valid and the slope of the semi-logarithmic profile remains constant.

We have also provided curves showing the longitudinal (Figure 39) and transverse (Figure 40) fluctuations in the presence of an acoustic field. Figure 41 shows the evolution of the correlation coefficient between these two fluctuations. These results are correct as long as the acoustic level remains small. /49 As soon as this level exceeds 140 decibels, the measurements are no longer reliable because the values measured fall outside the linearity domain of the apparatus.

7.5.3. Variation of the heat flux

A correct acoustic adjustment allows important effects to be obtained:

- On Figure 42 we have shown the results corresponding to different frequencies and different velocities. The acoustic field effect reaches 16% for a frequency of 8000 Hz and a velocity of 10 m/sec. The curve corresponding to u_∞ = 60 m/sec has been obtained by decoupling the anti-dust filter so as to reduce charge losses.

- Figure 43 shows again the previous results to bring out the effect of the velocity on the free flow. The various curves of this figure have been drawn for constant values of the acoustic level, that is, for constant vibrational velocities. When the velocity u_∞ increases, the ratio of the vibrational velocity $a_m \omega/\sqrt{2}$ to the velocity u_∞ decreases. The acoustic field effect would, therefore, be an increasing function of this ratio.

Figure 44 shows the variation of the acoustic field effect as a function of the acoustic level. The curve is smooth but its slope is much higher than for the case of low frequency perturbations (Figure 34). Above 140 decibels, measurements are no longer reliable because the perturbation is such that the local friction coefficient is modified.

We note finally that, for a given measurement abscissa, an increase in the frequency has the same effect as a decrease in the velocity. It seemed worth the interest to show the results in dimensionless form. We have made a dimensionless number from the perturbation frequency and from the flow velocity with the measurement abscissa as a reference length. The effect of the acoustic field which normally depends on the four parameters x, L,

f and u_∞ seems in fact to be only a function of the wave number f x/u_∞. /50

We have shown on Figures 45 and 46 the variations in the acoustic field effect as a function of the frequency and the velocity, respectively, for tests corresponding to constant values of the wave number f x/u_∞. It would be interesting to ascertain if this property is conserved for variations along the abscissa.

Chapter 8

CONCLUSIONS

We have begun this study by a bibliographical review relating to cylinders subjected to vibrations. We have then noted that the various authors have attacked the thermal problem only after a detailed study of the dynamic field. /51

The accomplishment and the perfecting of a hot wire anemometer have allowed us to make measurements in the neighborhood of a wall. The choice of an external acoustic field entails a non-measurable effect on the velocities so long as the acoustic level remains low. This important result is at the foundation of the use of the fluxmetric pellet.

- This study has shown that it does not seem possible to obtain an effect from the ultrasonic perturbations.

- The dimensions of the experimental test section does not allow for the establishment of good acoustic quality for low frequencies. In this frequency domain, the results are difficult to interpret. However, we have chosen to retain these results because the reproducibility of these measurements is excellent.

- It is, therefore, only in the intermediate region that the results can be correctly interpreted. We have brought out some important effects. These effects are no doubt small compared to the effects mentioned in the case of cylinders in free convection. But, our study of forced convection has for an objective the production of small perturbations within the boundary layer.

The good results obtained in this frequency domain is due to the small adjustment of the distance between the plate and the sound source. This adjustment allowed an important value of the standing coefficient to be obtained.

REFERENCES

1. Schlichting, H. Boundary Layer Theory. Mc Graw-Hill Book Co. 1955.

2. Stuart, J. T. Double Boundary Layers in Oscillatory Viscous Flow. J. Fluid Mech., Vol. 24, No. 4, 1966, p. 673.

3. Richardson, P. D. Effect of Sound and Vibrations on Heat Transfer. Applied Mech. Reviews, Vol. 20, No. 3, March, 1967, p. 201.

4. Feiler, C. E. and E. B. Yeager. Effect of Large Amplitude Oscillations on Heat Transfer. NASA TR 142, 1962.

5. Schubauer, G. B. and N. K. Skamstadt. Laminar Boundary Layer Oscillations and Transition on a Flat Plate. J.A.S., Vol. 14, 1947, p. 69.

6. Brunello, G. Contribution to the Study of Forced Heat Convection on Rough Walls. P.S.T. du Ministère de l'Air, 1957, p. 332.

7. Collis, D. C. and M. J. Williams. Two Dimensional Convection from Heated Wires at Low Reynolds Numbers. J. Fluid Mech. Vol. 6, No. 3, October 1959, p. 357.

8. Gaviglio, J. Some Turbulence Measurement Problems Carried out with Hot Wire Anemometers Carrying Constant Current. P.S.T. du Ministère de l'Air, 1962, p. 385.

9. Hussenot, C. and J. Baudoin. Linearization within a Hot Wire Constant Temperature Anemometer using Diode Chains. C.R. de l'Académie des Sciences, Vol. 254, 1962, p. 2144.

10. Champagne, F. H. Turbulence Measurements with Inclined Hot Wires. J. Fluid Mech., Vol. 28, April, 1967, p. 1.

11. Comte-Bellot, G. Hot Wire Anemometers and Temperature and Velocity Fluctuation Measurements. Turbulence Seminar of the Polish Academy of Sciences, Jablonna, Oct. 2-12, 1961.

12. Galinaro, R. and P. Gougat. Hot Wire Anemometers with Constant Temperature. Report of Laboratoire d'Aérothermique du C.N.R.S., 66-11, 1966.

13. Galinaro, R., P. Gougat and B. de Gramont. Improvements made to the Hot Wire Device for Measuring Fluid Velocity. Patent document, C.N.R.S. 1460 008-1966.

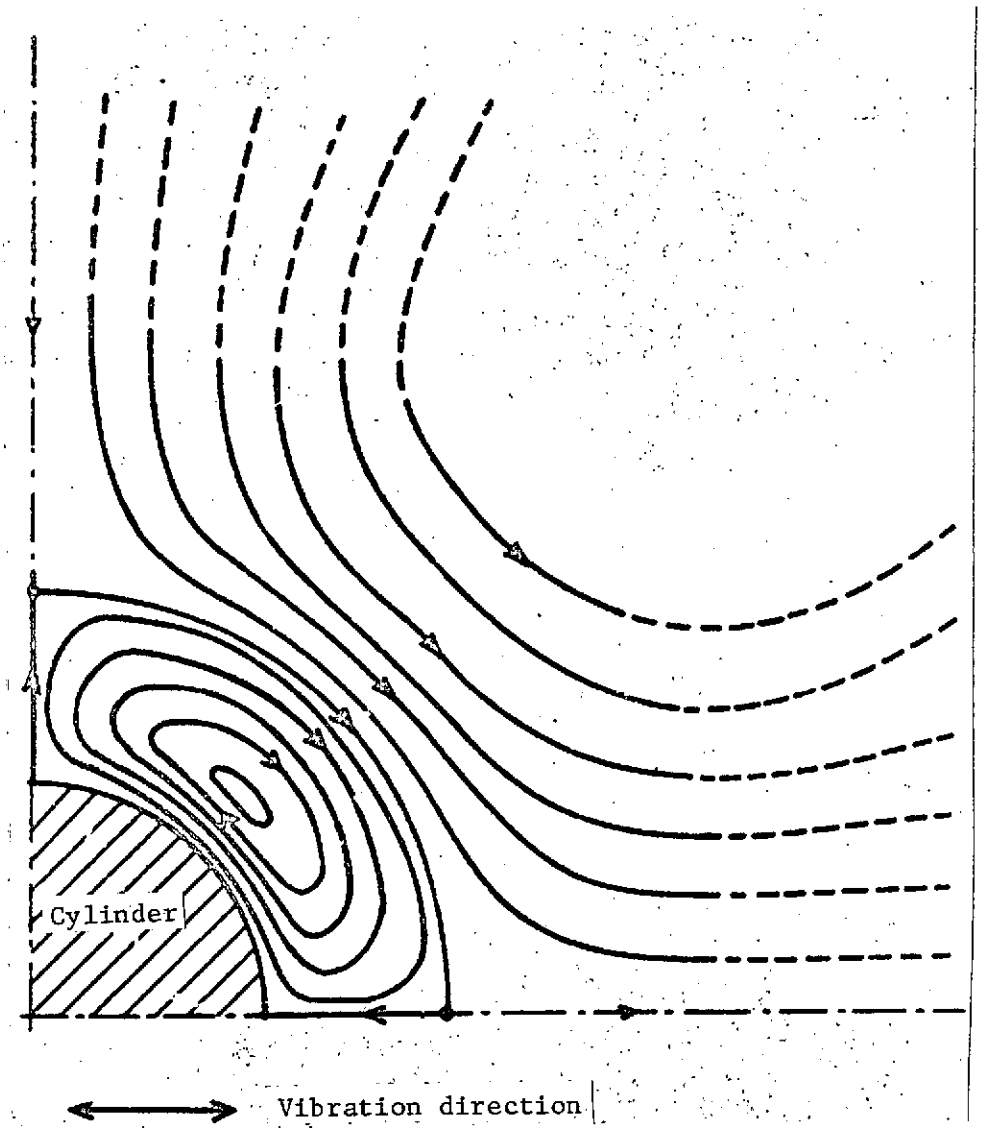

Figure 1. Stream lines in the neighborhood of a vibrating cylinder

/54

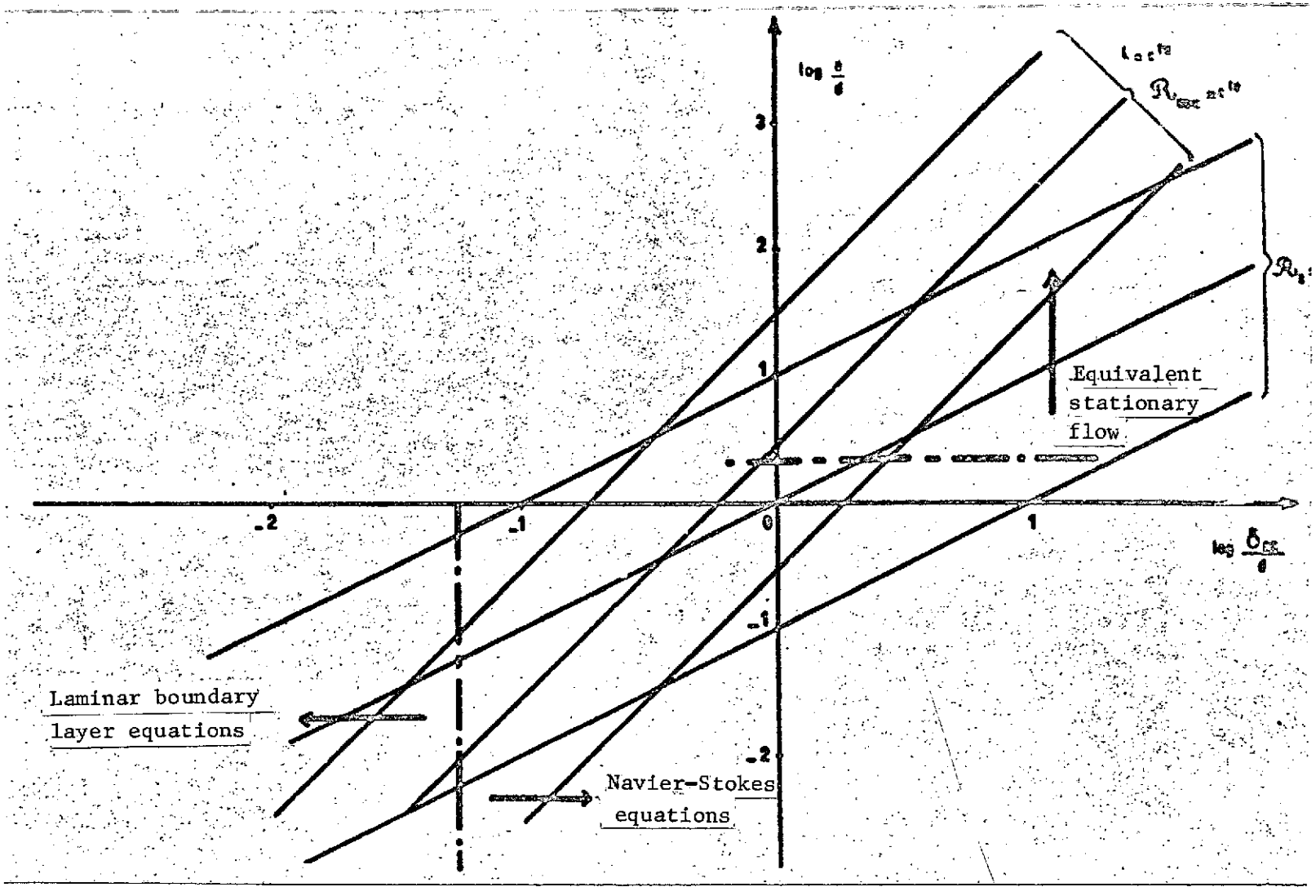

Figure 2. Classification of dynamic studies for a vibrating cylinder [3].

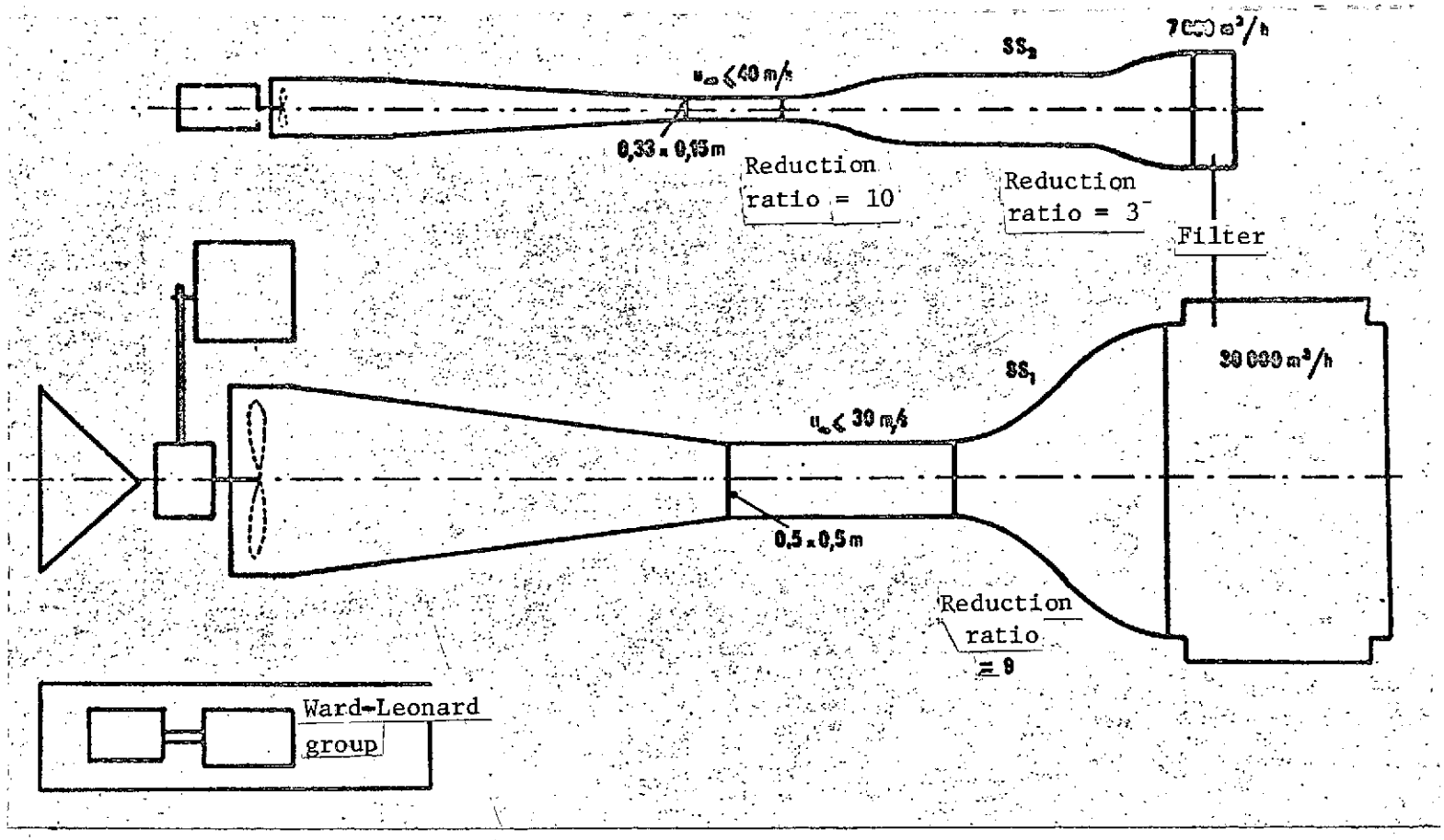

Figure 3. Wind tunnel configurations

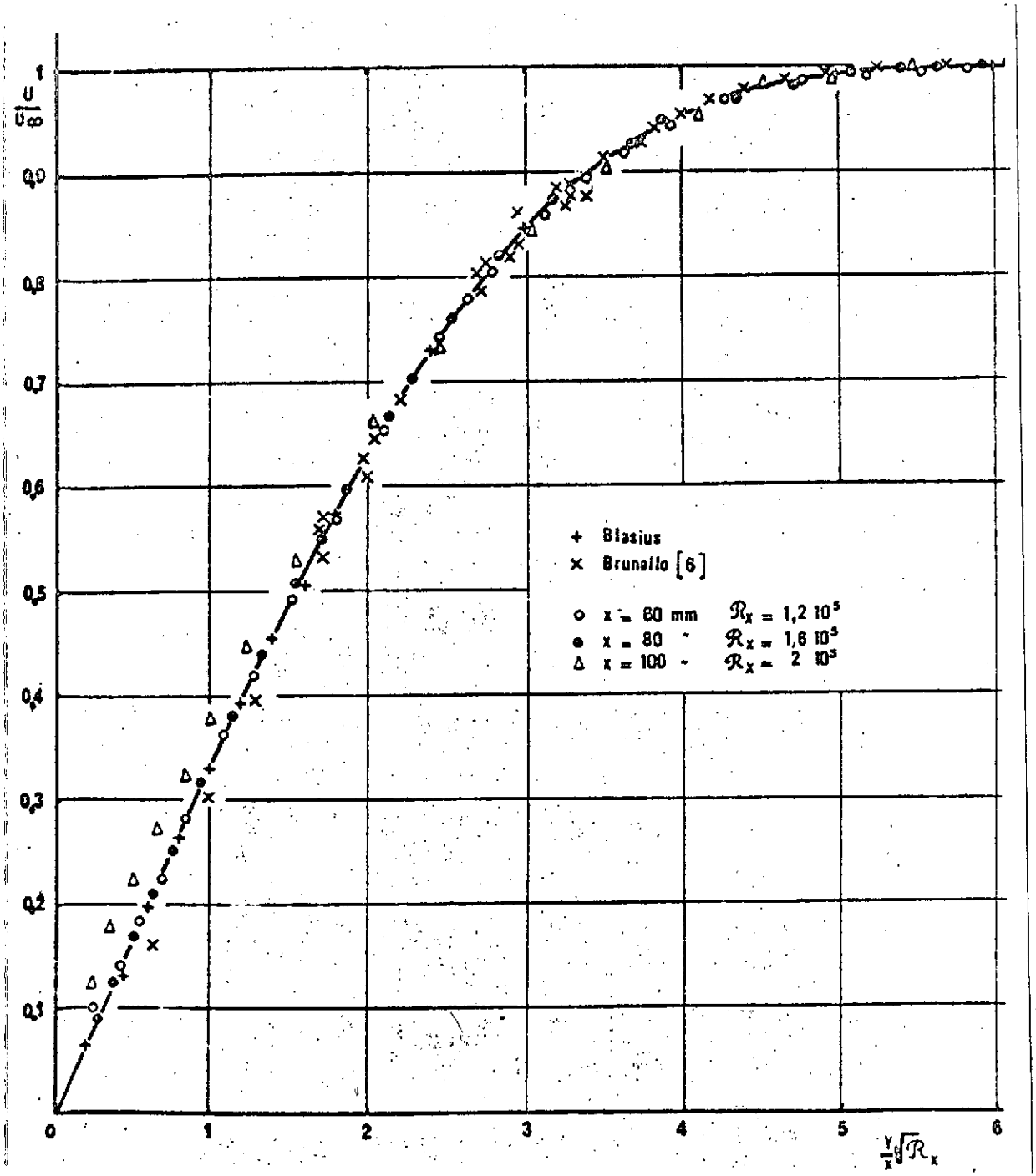

/57

Figure 4. Velocity profile in the laminar region

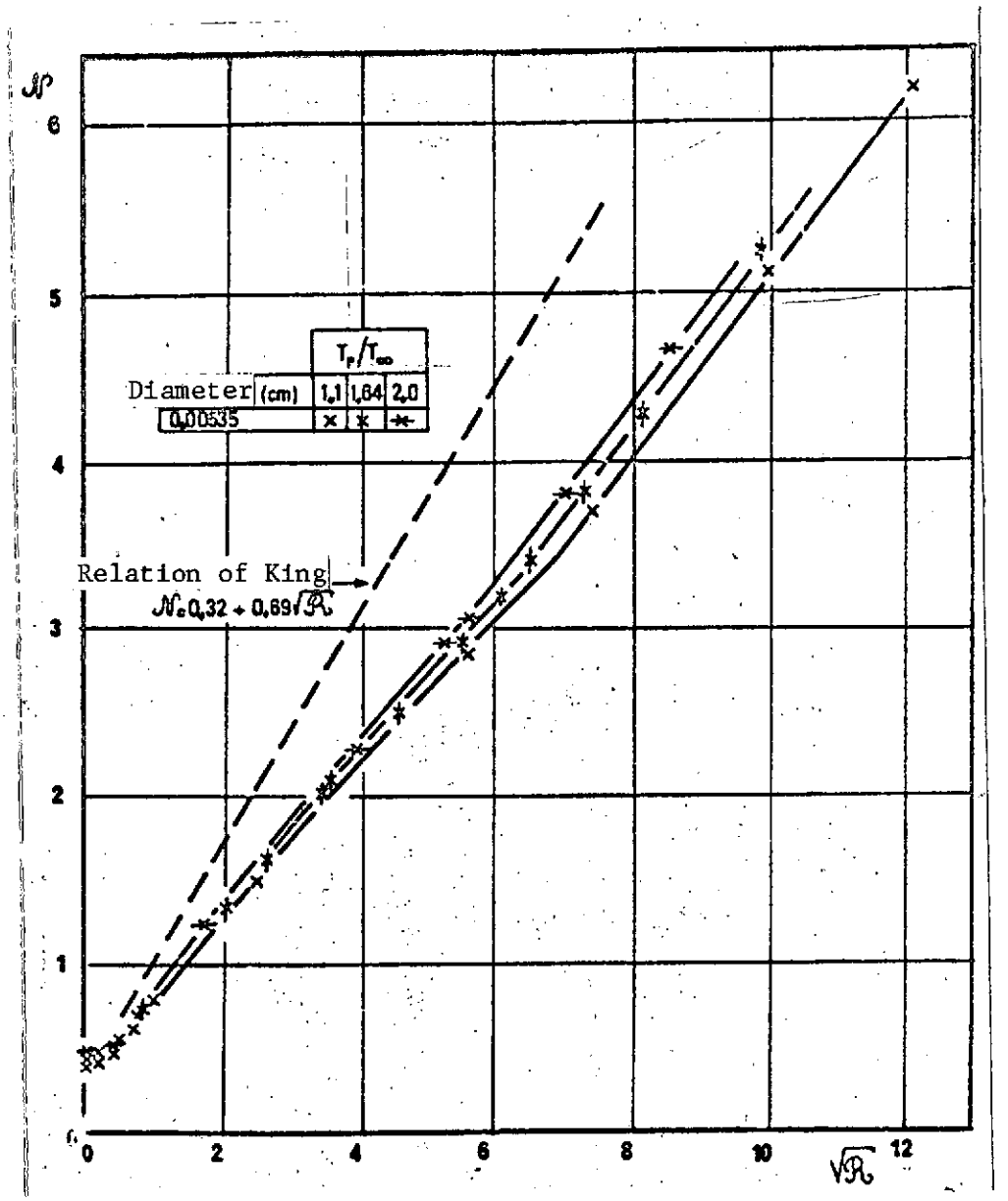

Figure 5. Results of D. C. Collis and M. J. Williams [7]

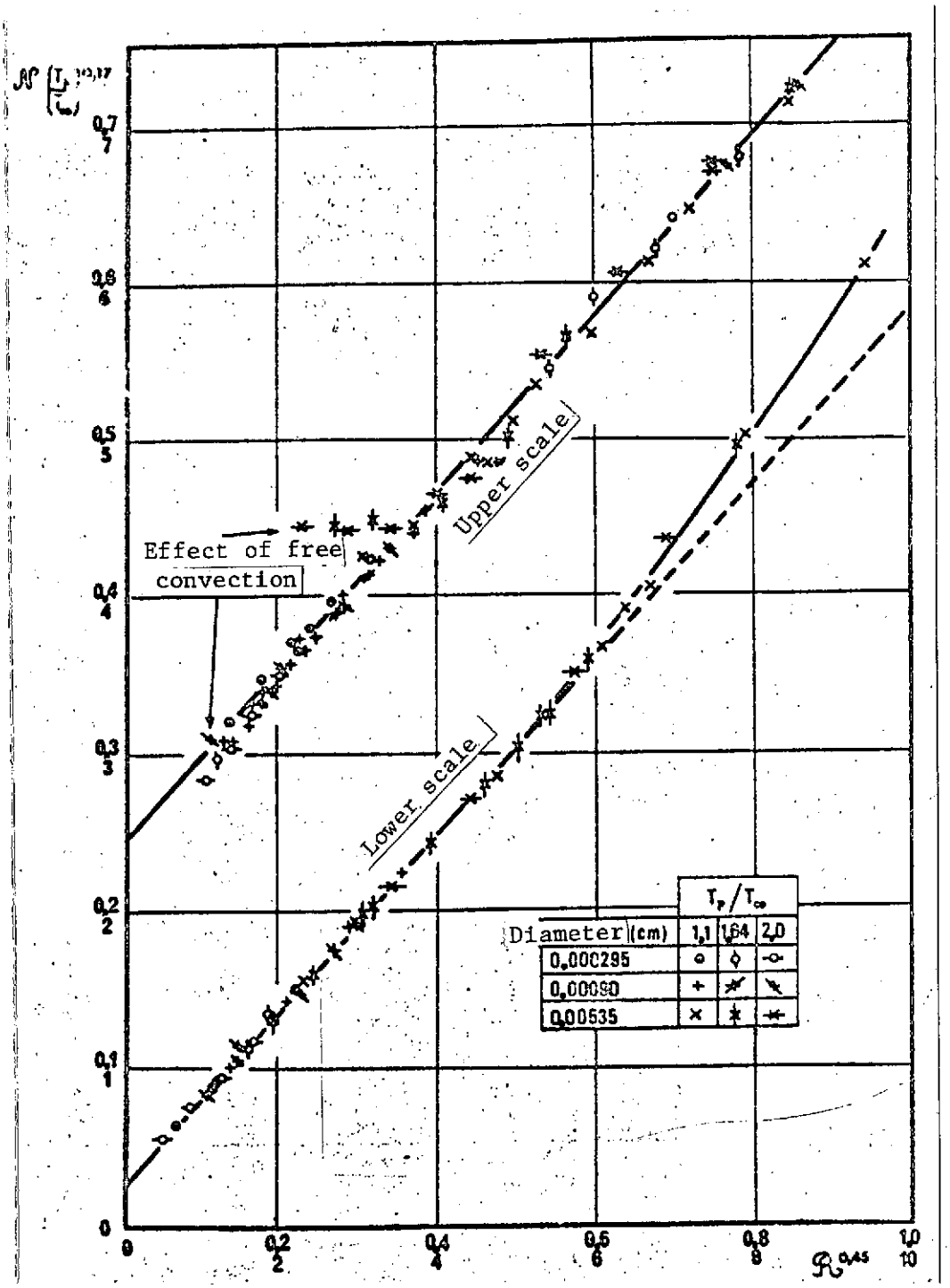

Figure 6. Results of D. C. Collis and M. J. Williams [7]

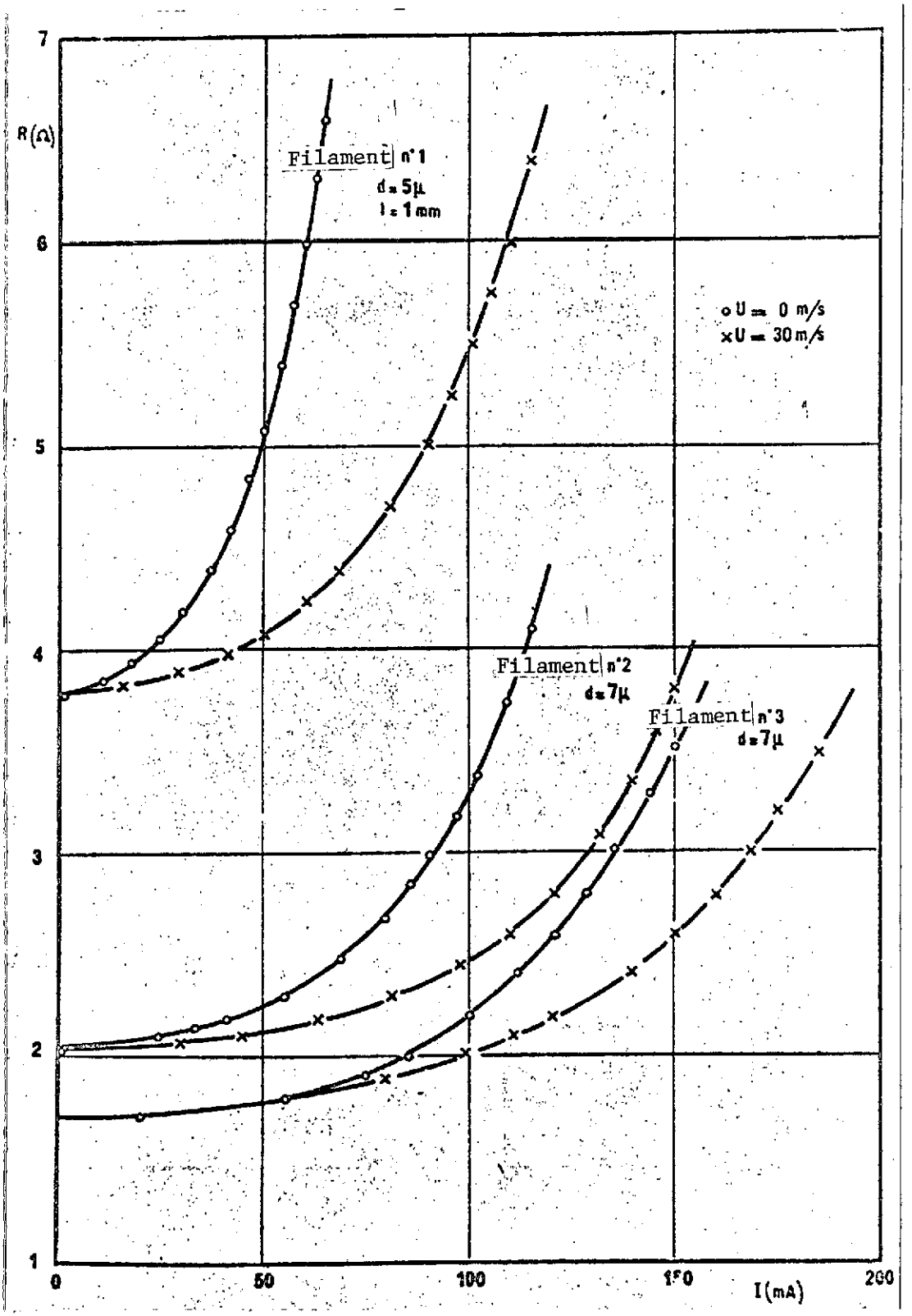

Figure 7. Hot wire calibration curves

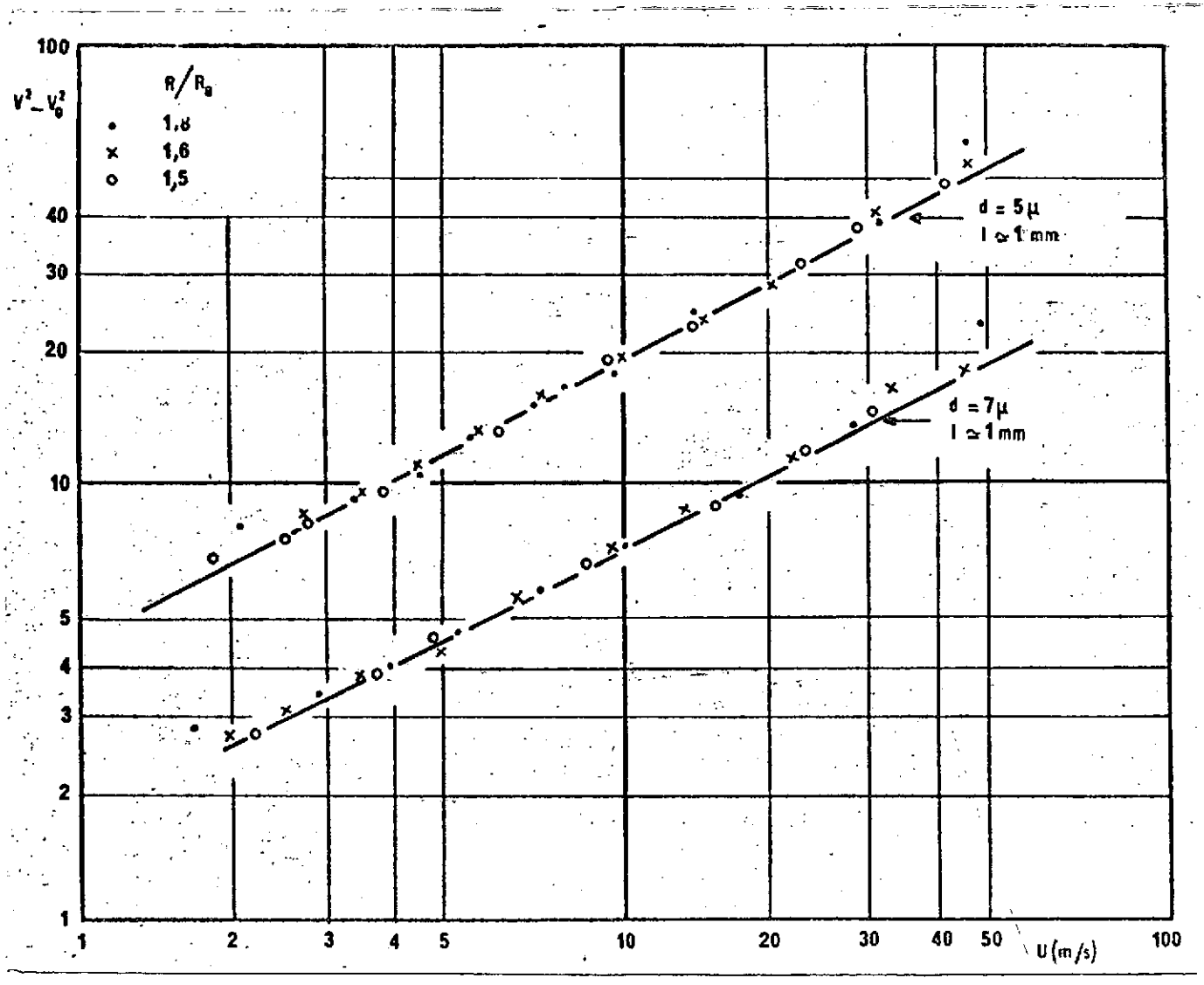

Figure 8. Hot wire calibration curves

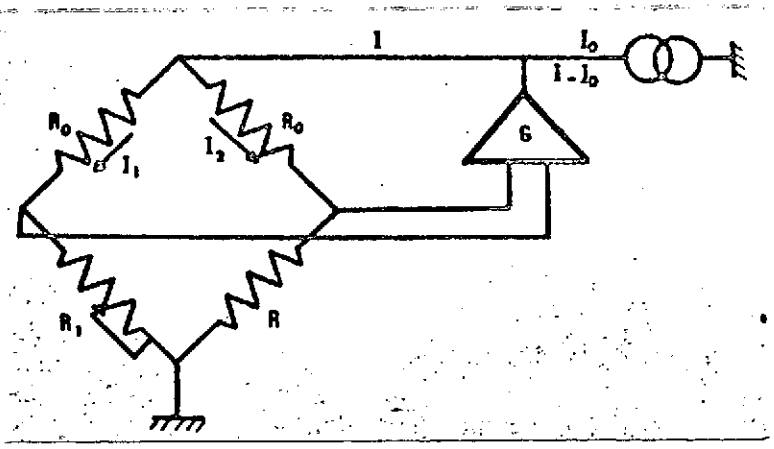

Figure 9. Wheatstone bridge

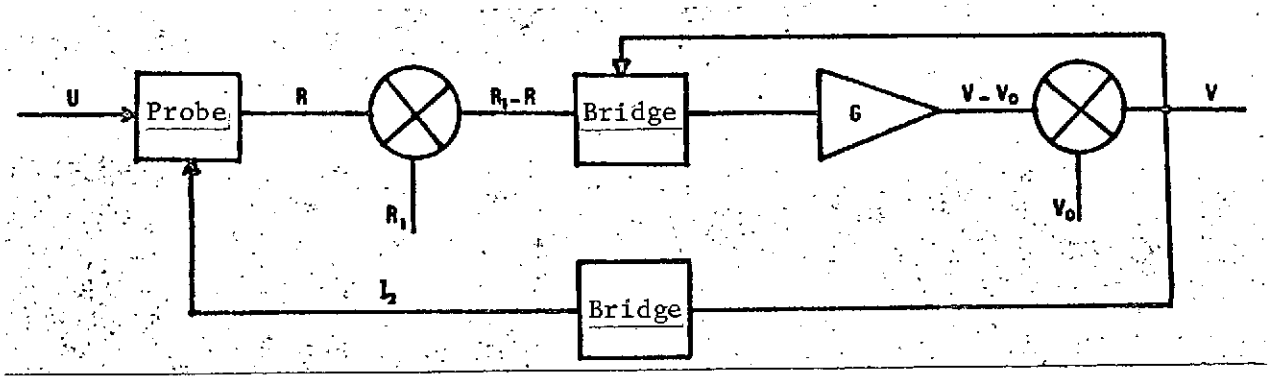

Figure 10. Functional servocontrol schematic

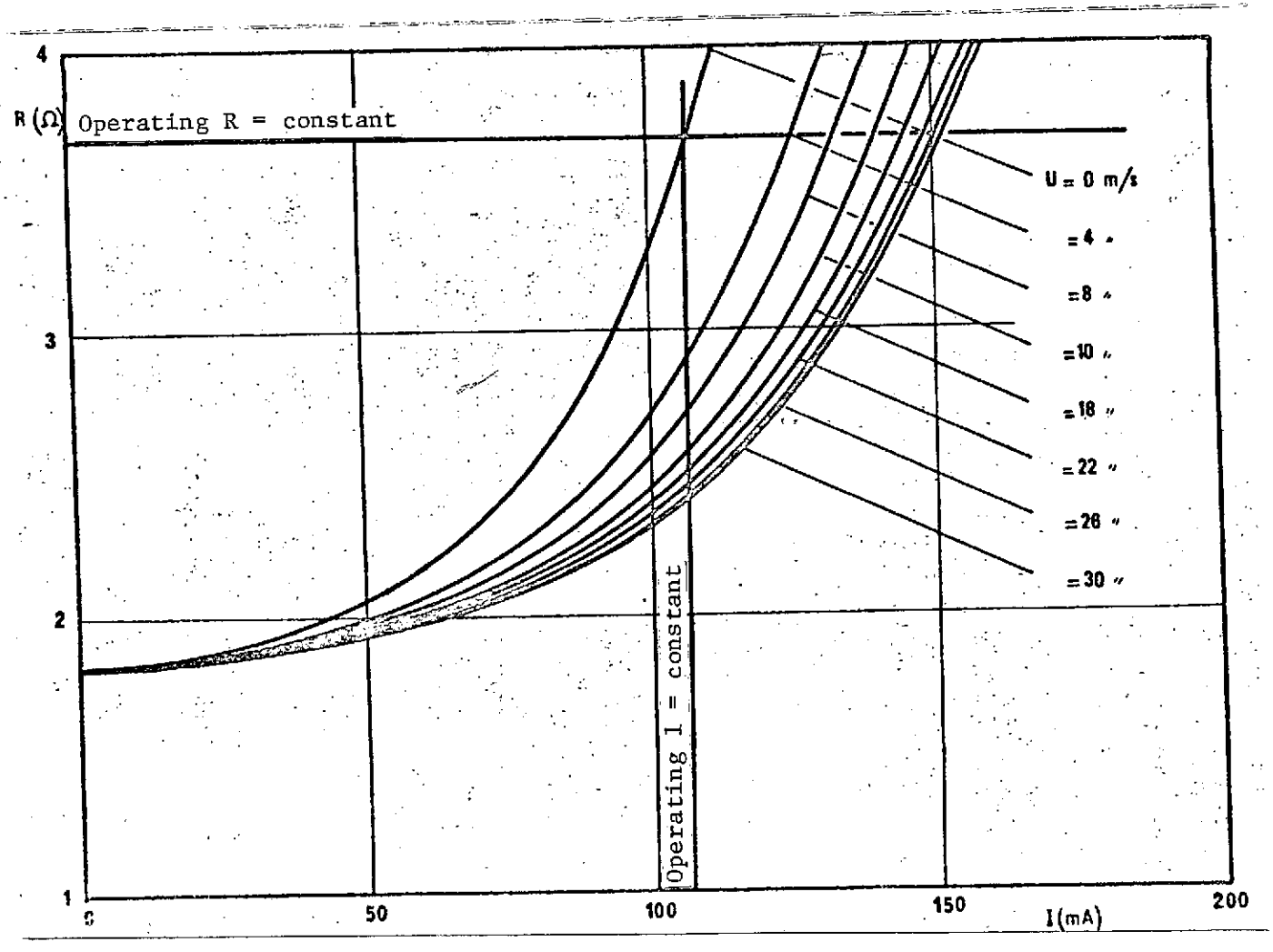

Figure 11. Hot wire operating ranges

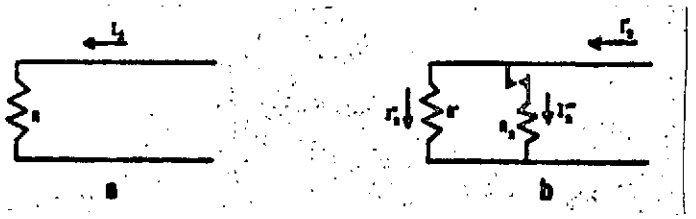

Figure 12. -Velocity fluctuation simulation

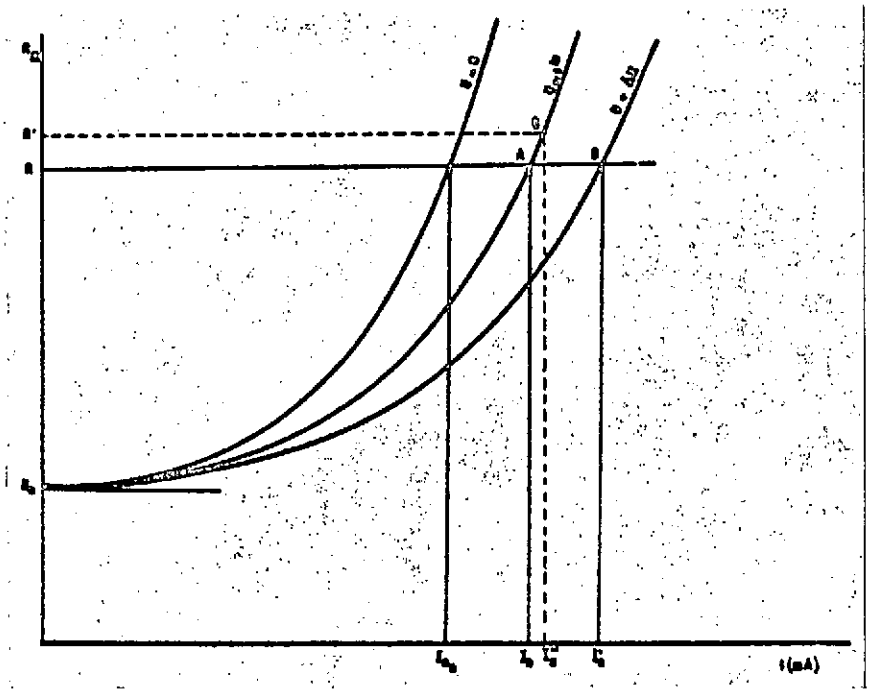

Figure 13. Principle of velocity fluctuation simulation

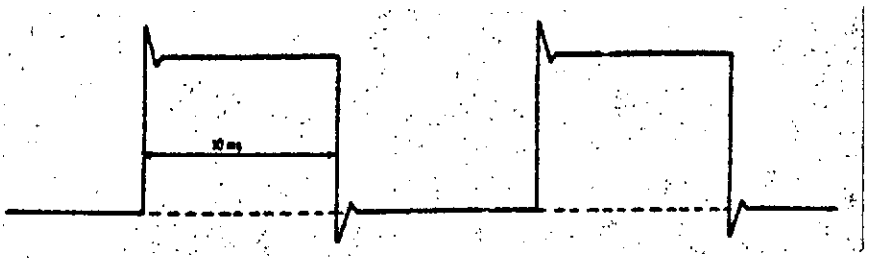

Figure 14. Servocontrol response to a fluctuation in velocity

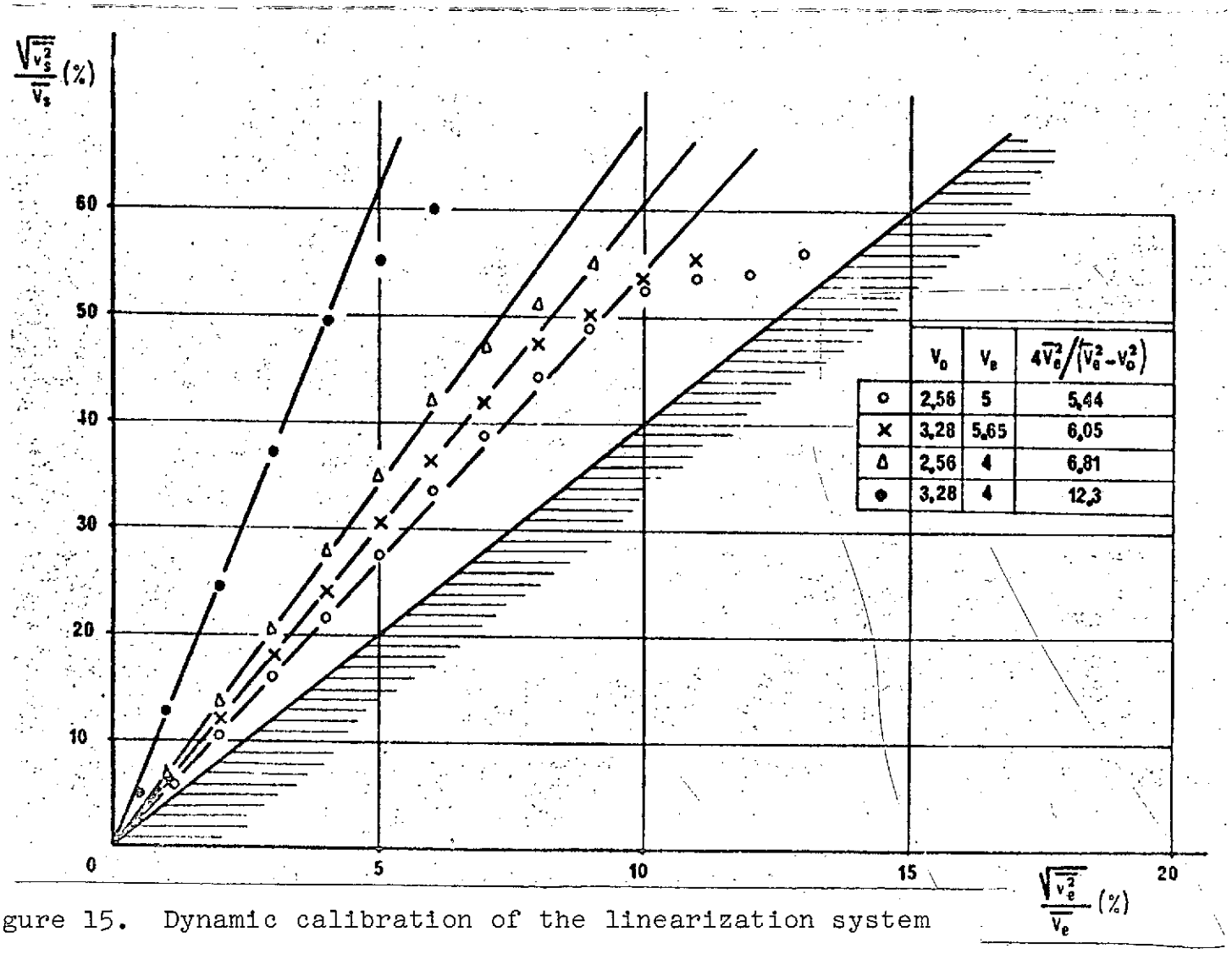

Figure 15. Dynamic calibration of the linearization system

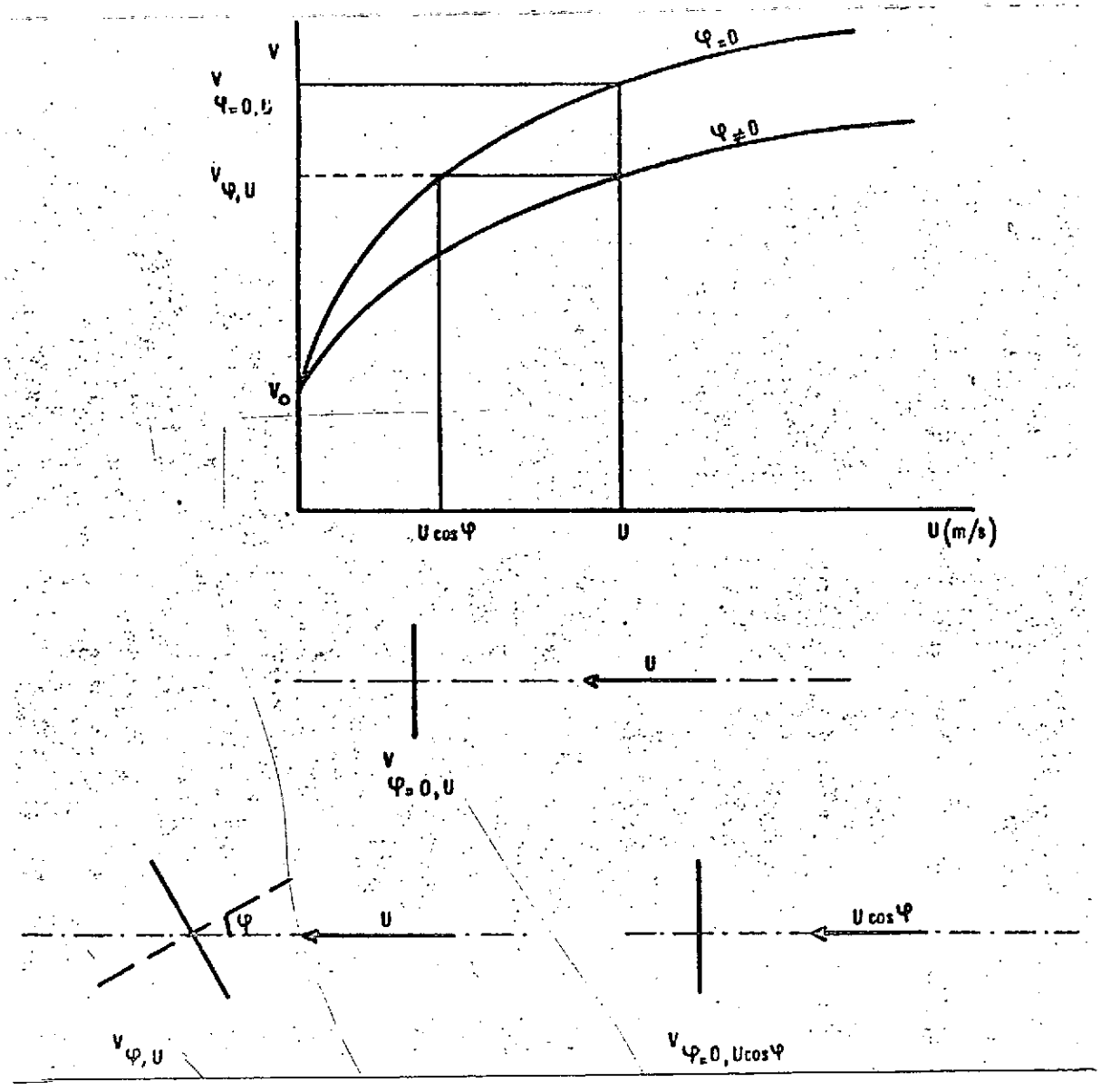

Figure 16.

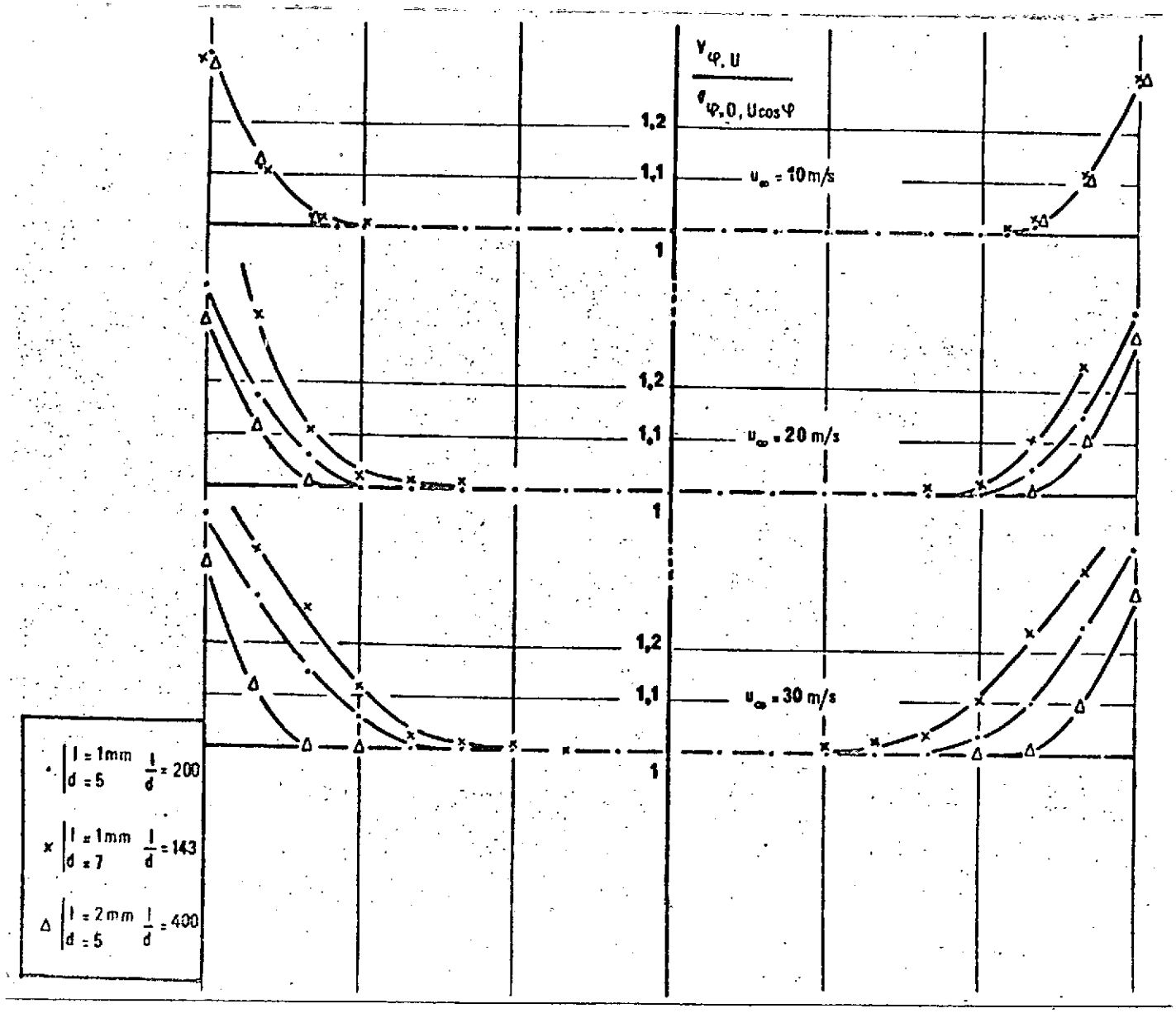
$\gamma_{\varphi,U}$
$\varphi_{\varphi,0,U\cos\varphi}$
1,2
1,1
1
u_∞ = 10 m/s
u_∞ = 20 m/s
u_∞ = 30 m/s
l = 1mm d = 5 l/d = 200
l = 1mm d = 7 l/d = 143
l = 2mm d = 5 l/d = 400

Figure 17. Characteristics of an inclined filament

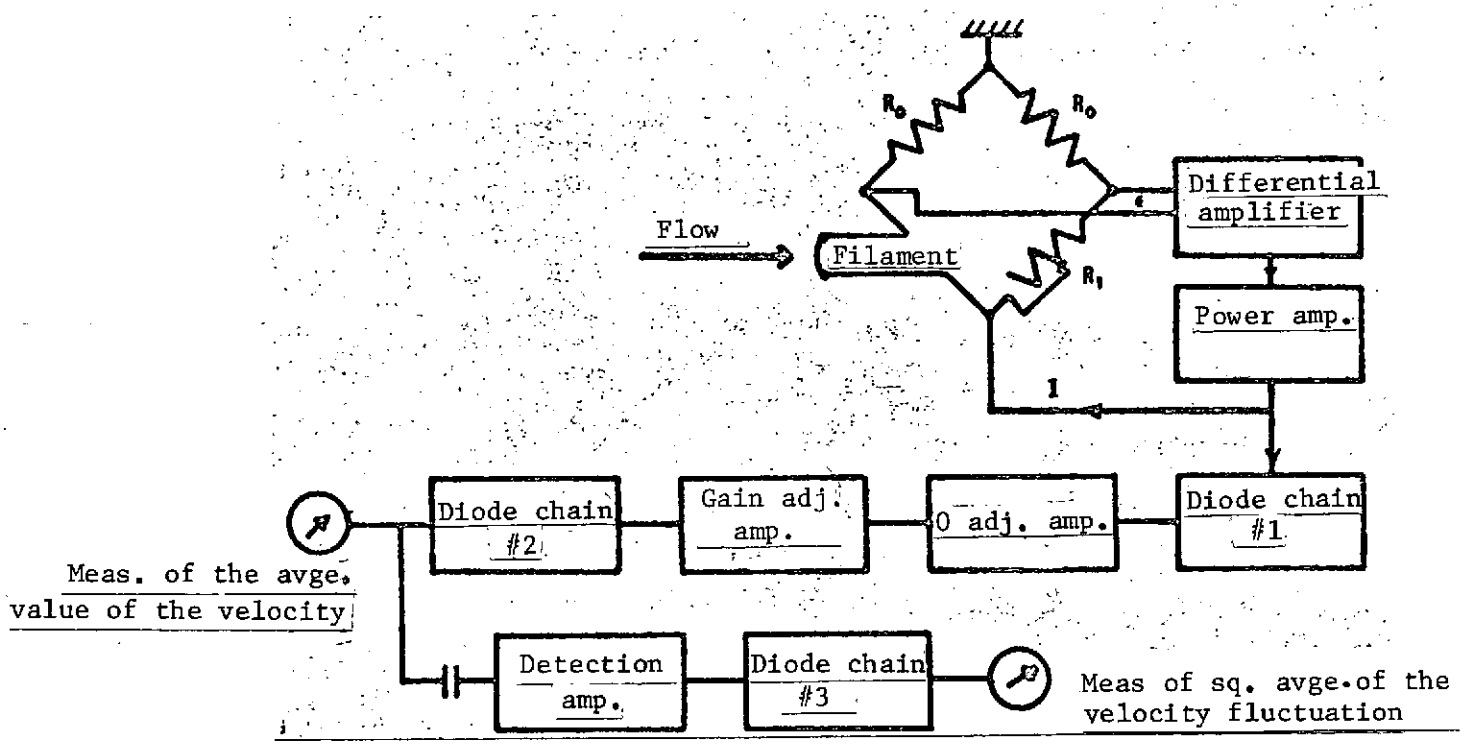

Figure 18. Synoptic schematic of the straight filament anemometer

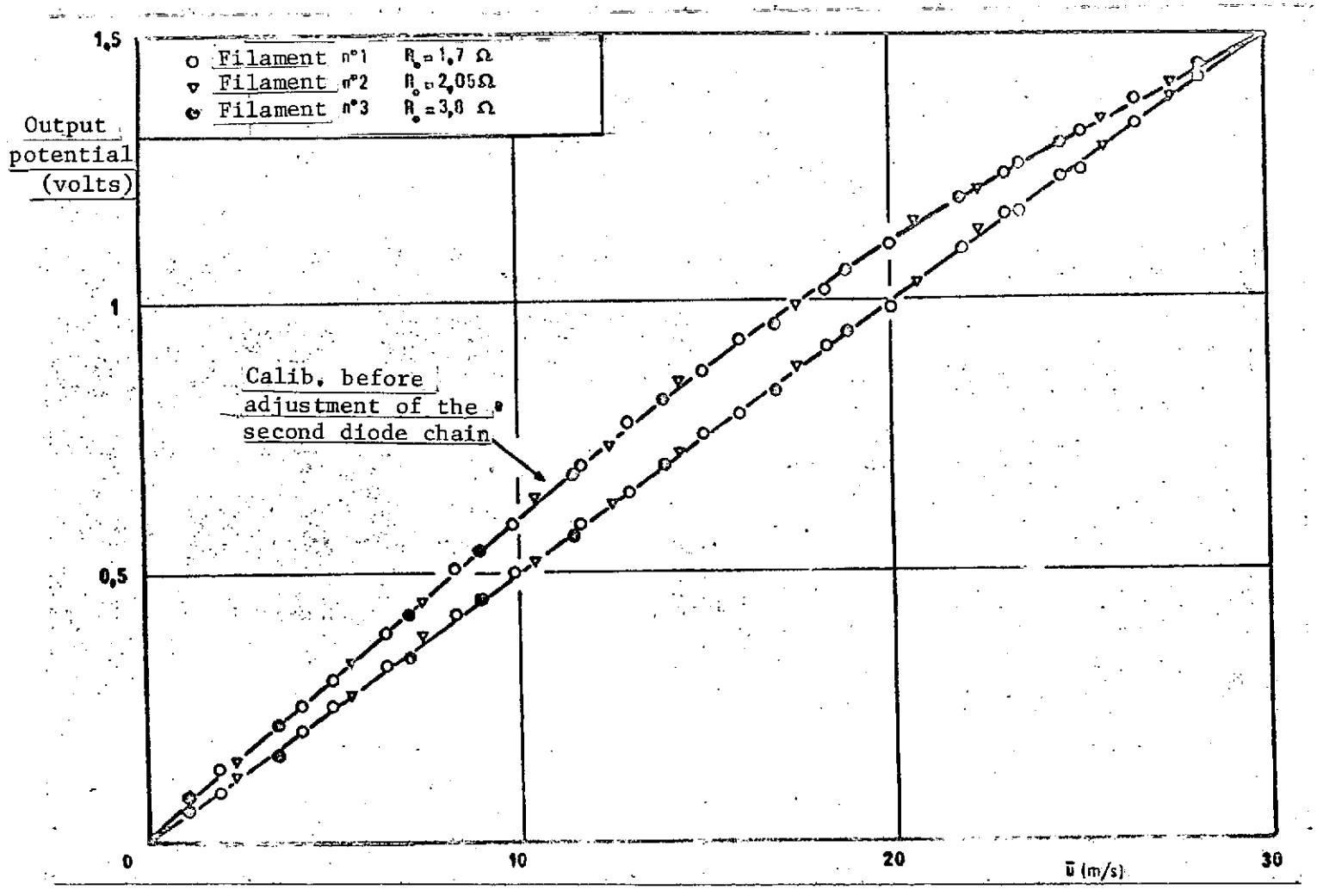

Figure 19. Linearization results

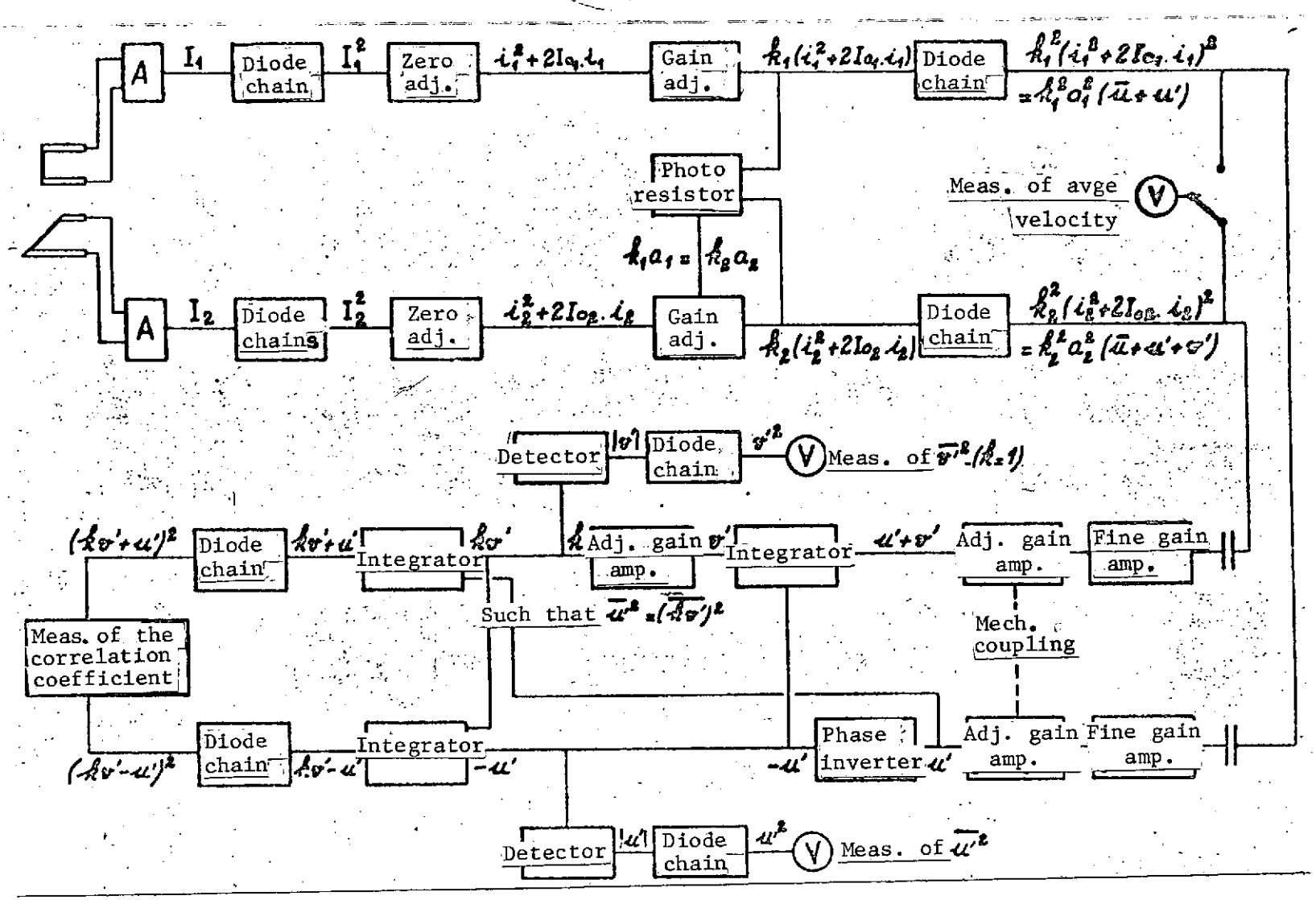
A
Diode chain
Zero adj.
Gain adj.
Diode chain
Photo resistor
Meas. of avge velocity
Diode chains
Detector
Meas. of
Adj. gain amp.
Integrator
Fine gain amp.
Such that
Meas. of the correlation coefficient
Mech. coupling
Phase inverter

Figure 20.

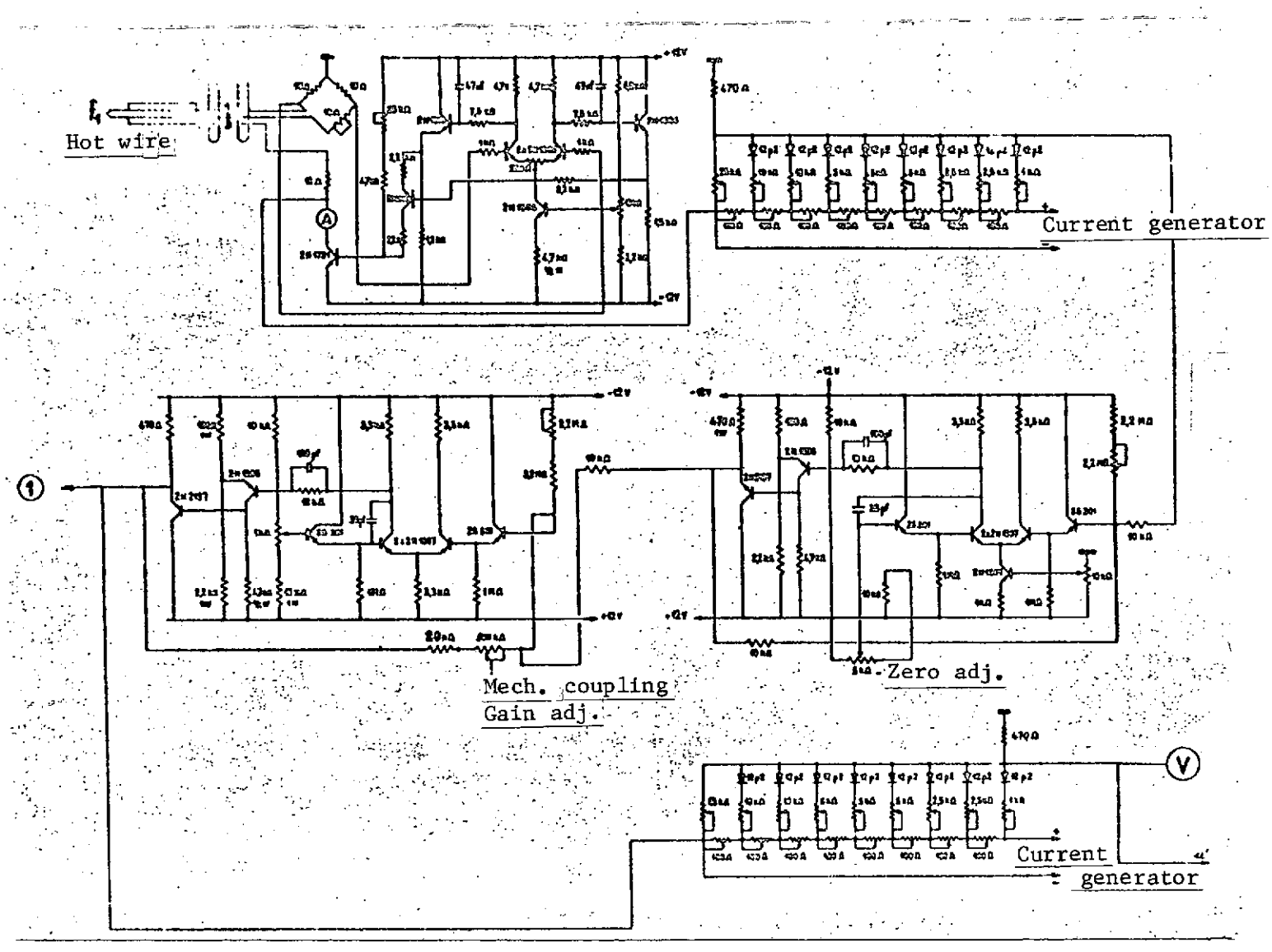
Hot wire
Current generator
Mech. coupling
Gain adj.
Zero adj.
Current
generator

Figure 21.

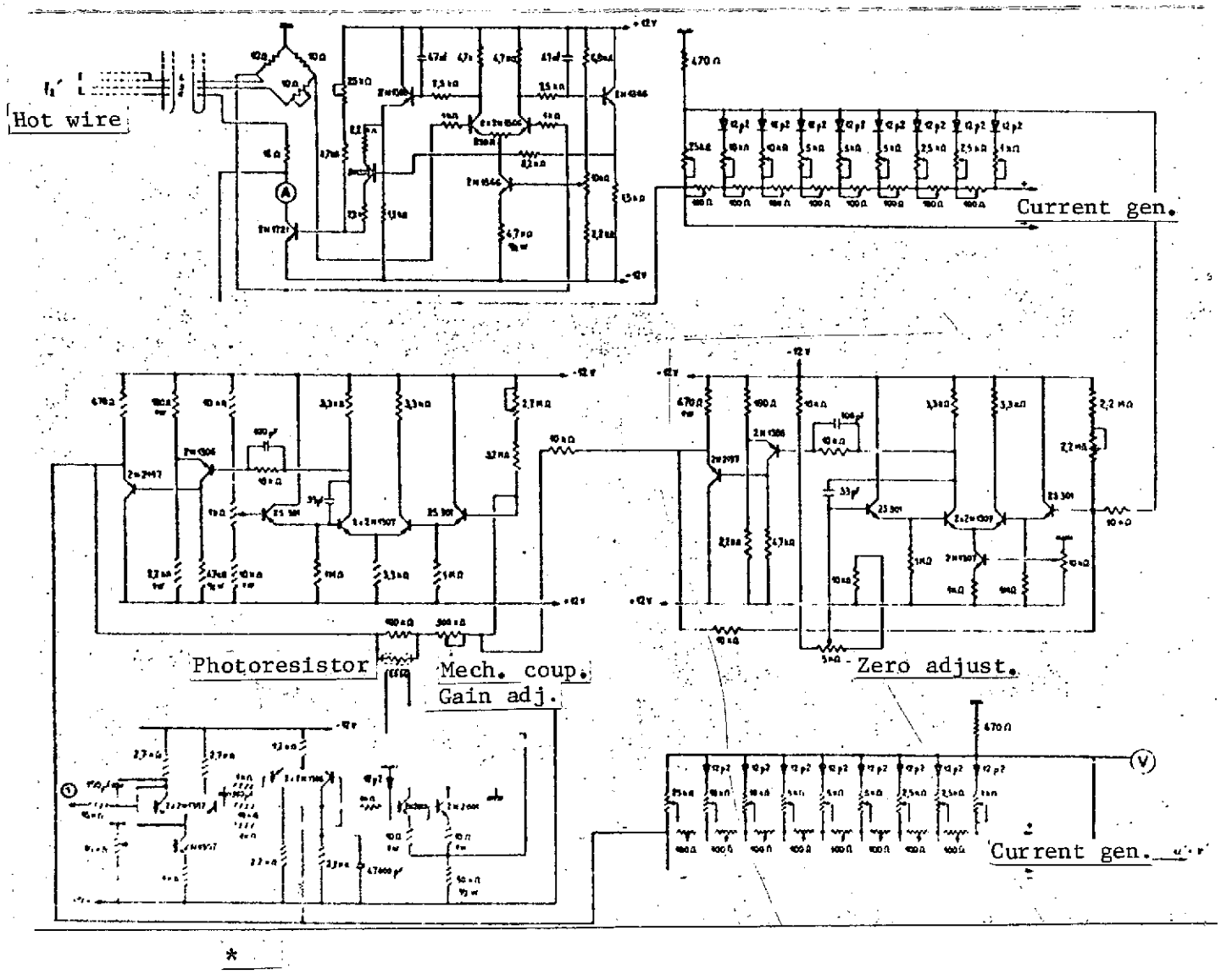

Figure 22.

* Translator's note: Illegible in foreign text.

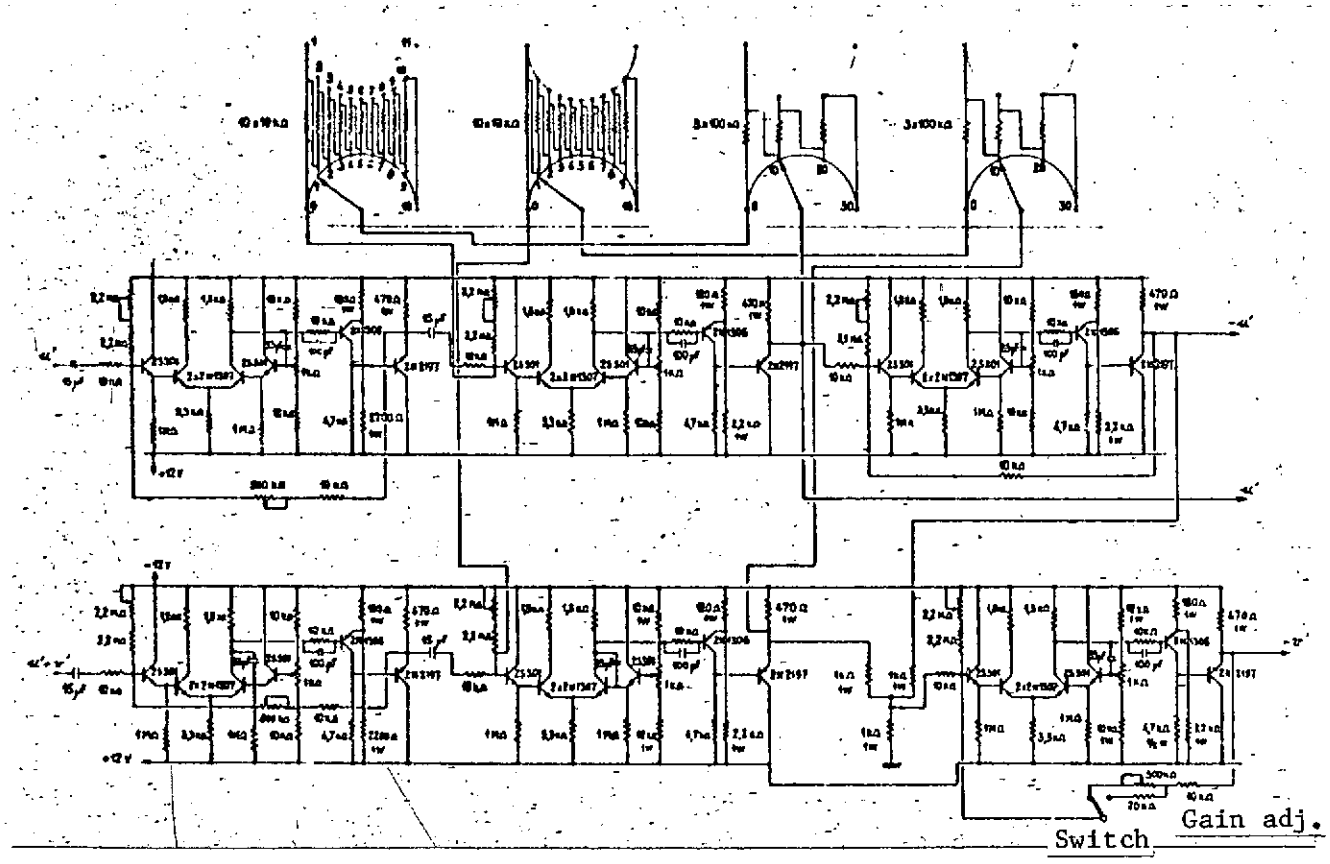

Figure 23. Amplifier chain for velocity fluctuations

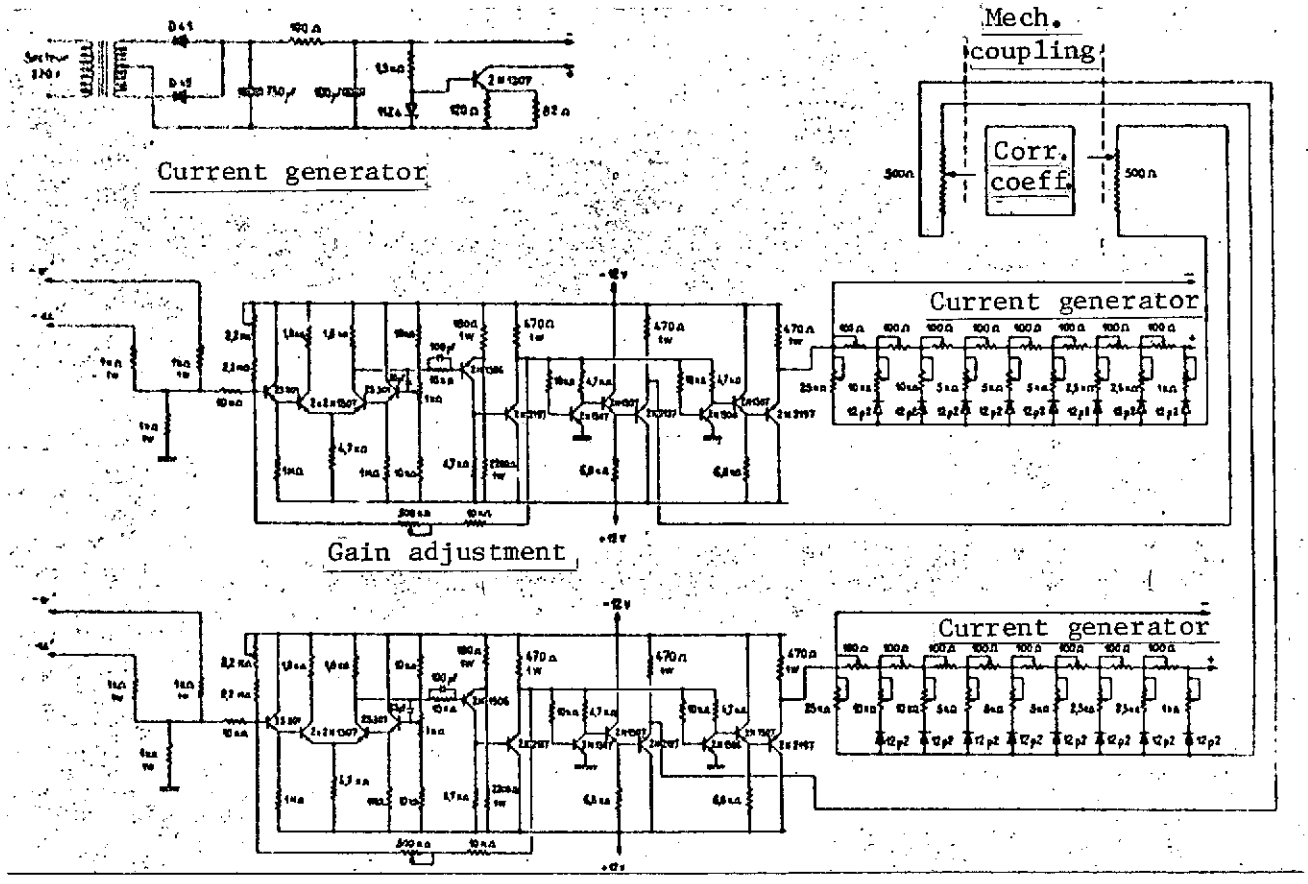

Figure 24. Correlation coefficient measurement

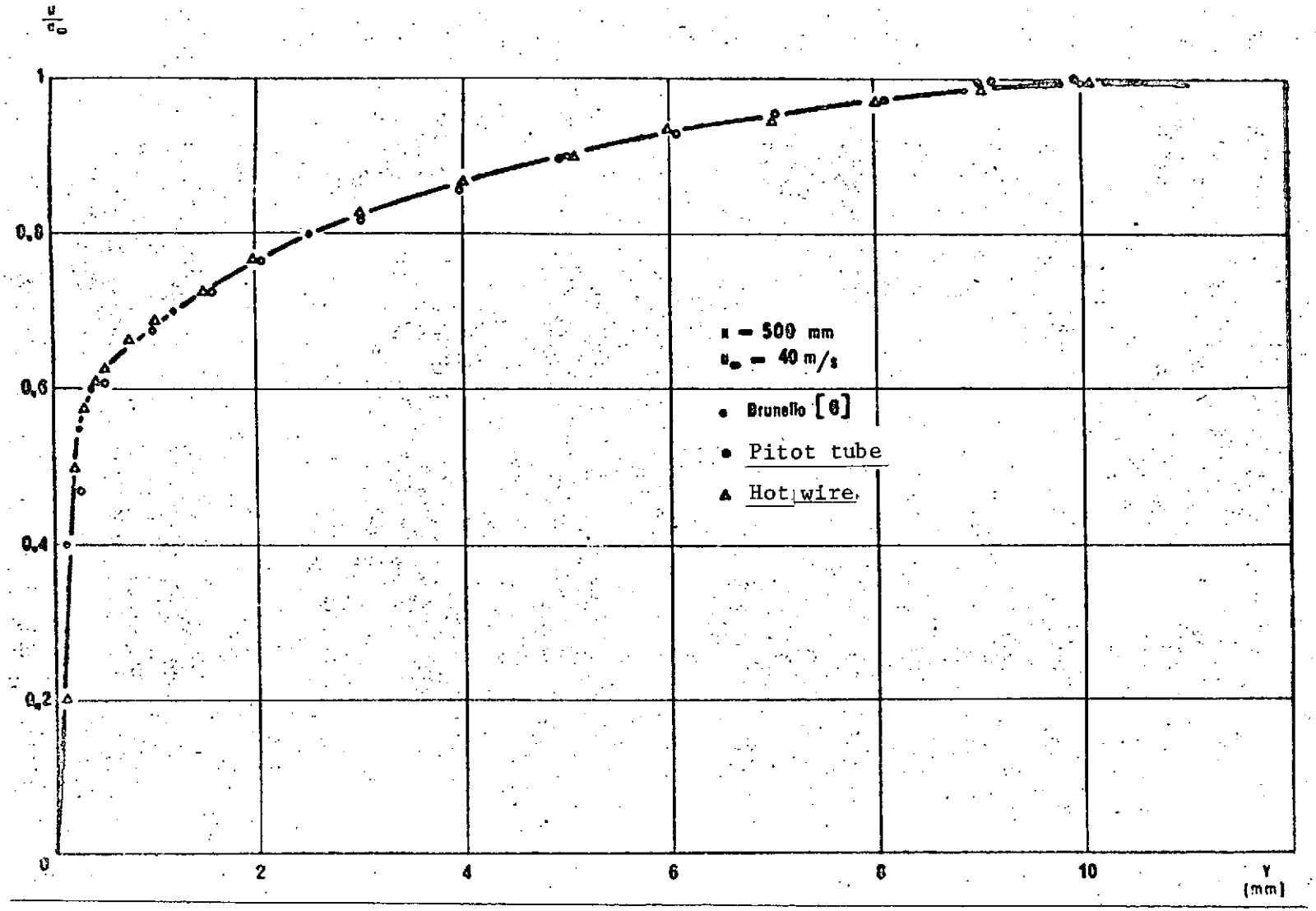

Figure 25. Velocity profile

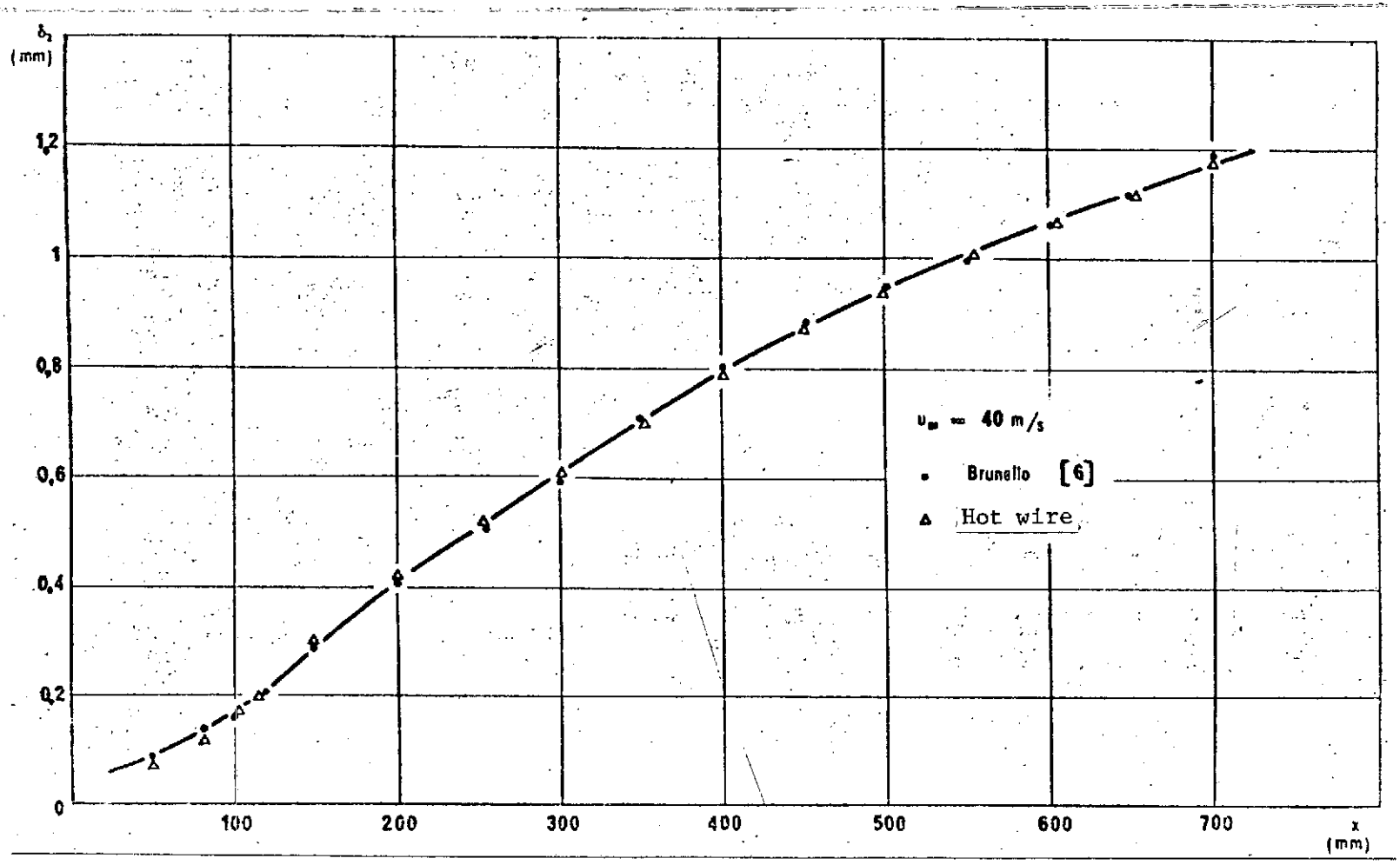

Figure 26. Momentum thickness

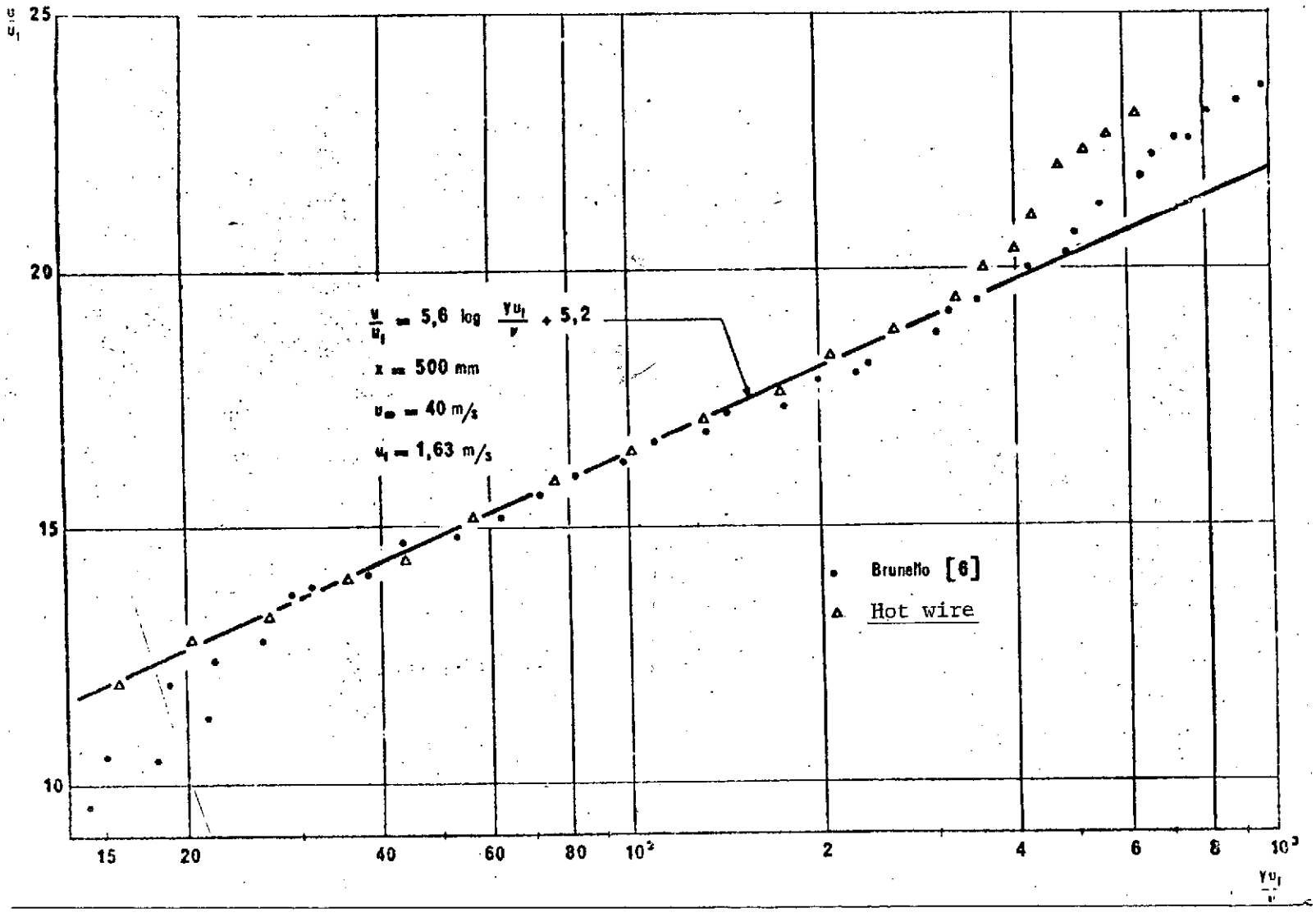

Figure 27. Semi-logarithmic *

* Translator's note: Illegible in foreign text.

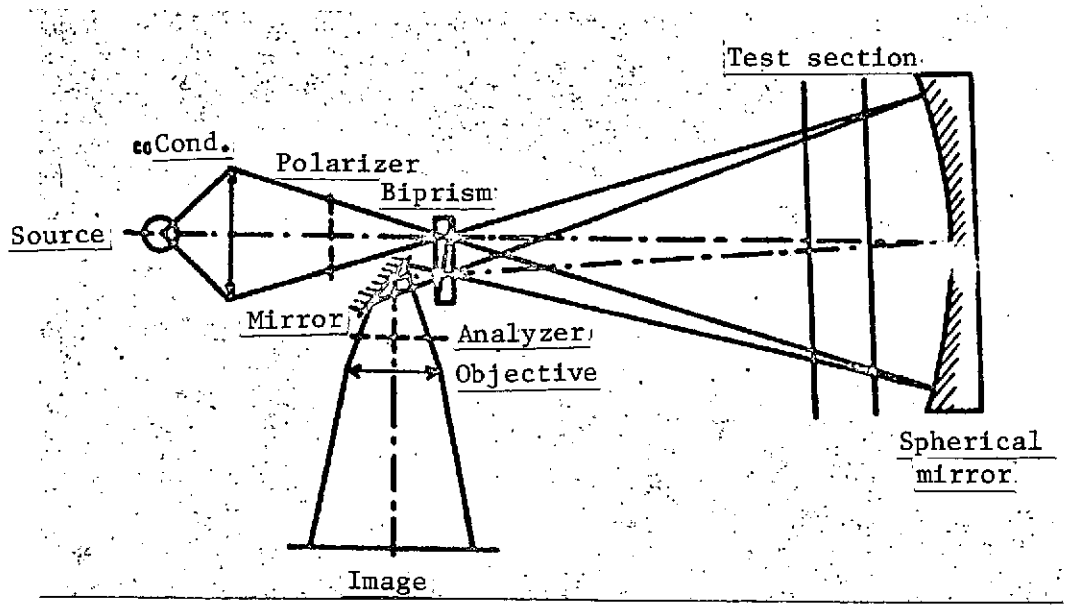

Figure 28. Schematic of the principle of a return strioscopic apparatus

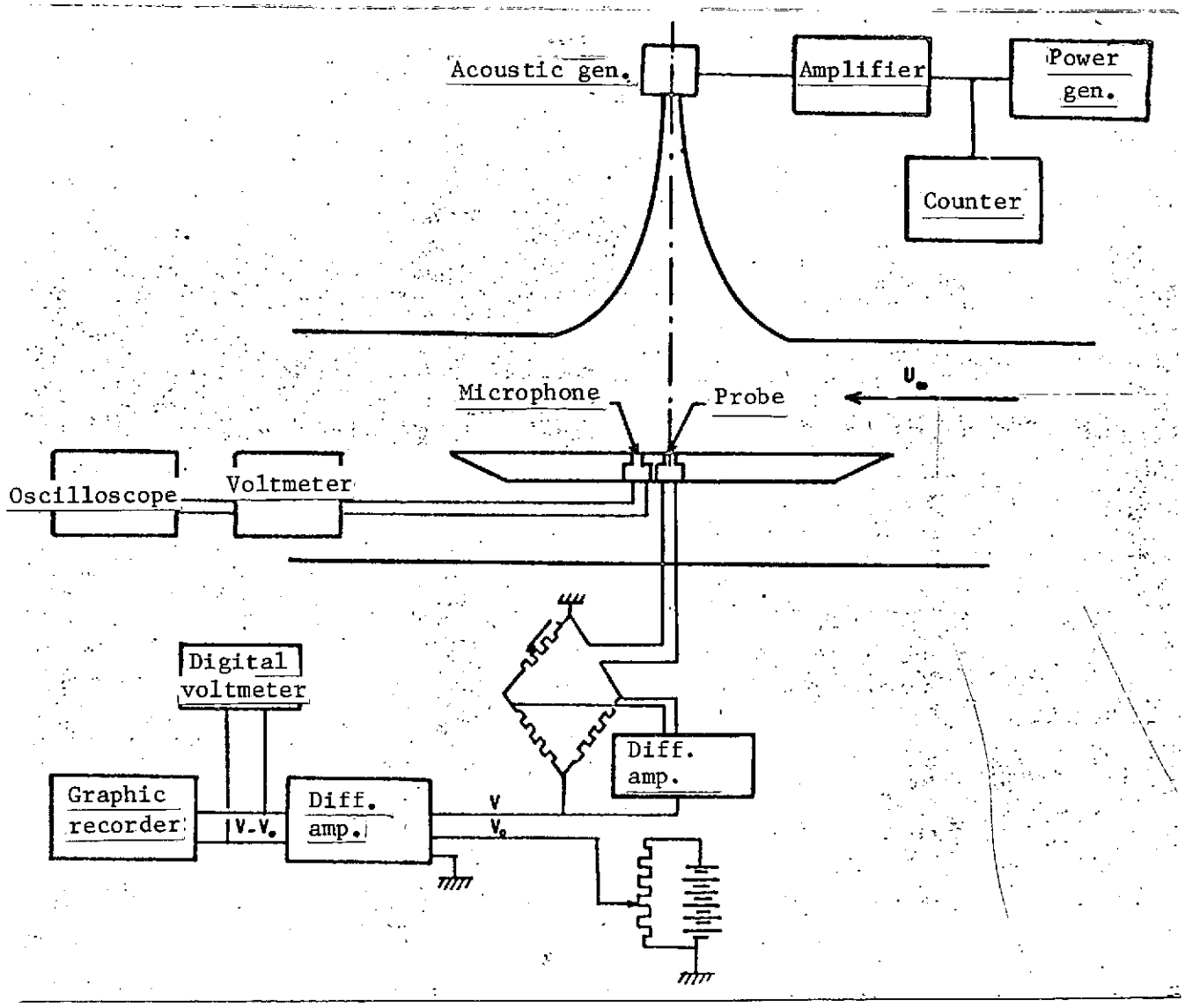

Figure 29. Experimental configuration

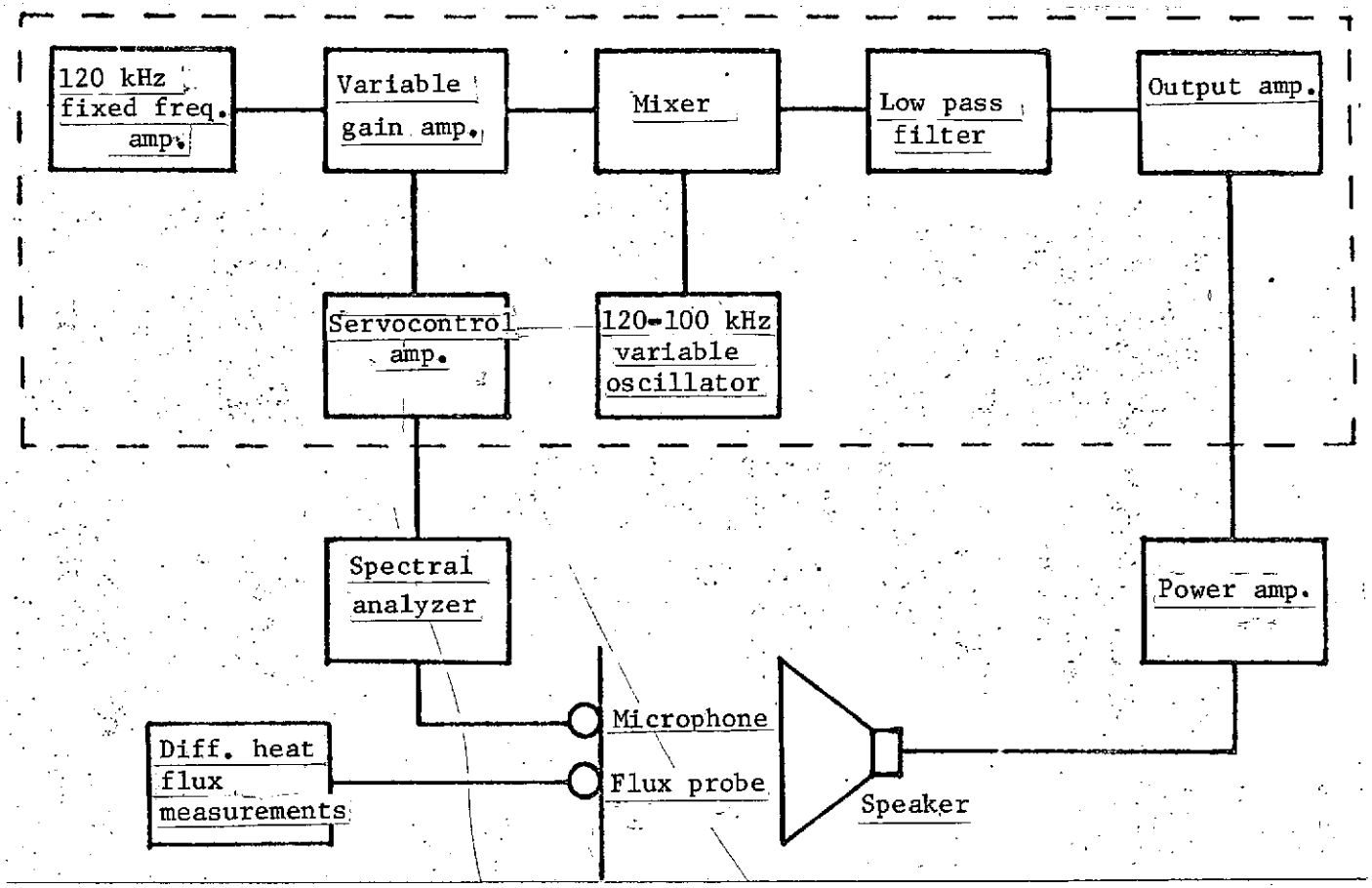
120 kHz fixed freq. amp.
Variable gain amp.
Mixer
Low pass filter
Output amp.
Servocontrol amp.
120-100 kHz variable oscillator
Spectral analyzer
Power amp.
Microphone
Flux probe
Speaker
Diff. heat flux measurements

Figure 30.

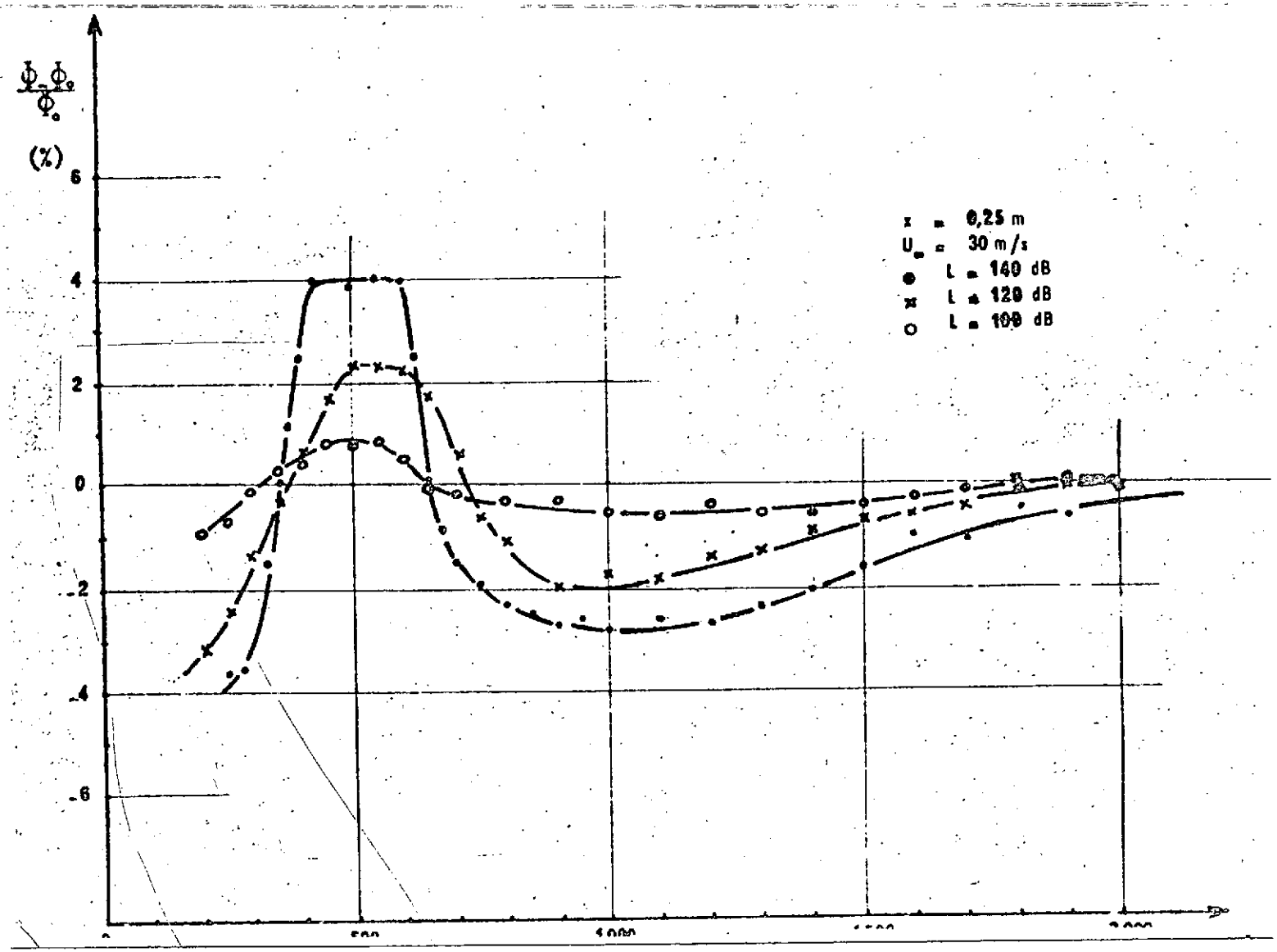
$\frac{\Phi - \Phi_0}{\Phi_0}$ (%)
6
4
2
0
-2
-4
-6
x = 0,25 m
U_∞ = 30 m/s
L = 140 dB
L = 120 dB
L = 100 dB

Figure 31.

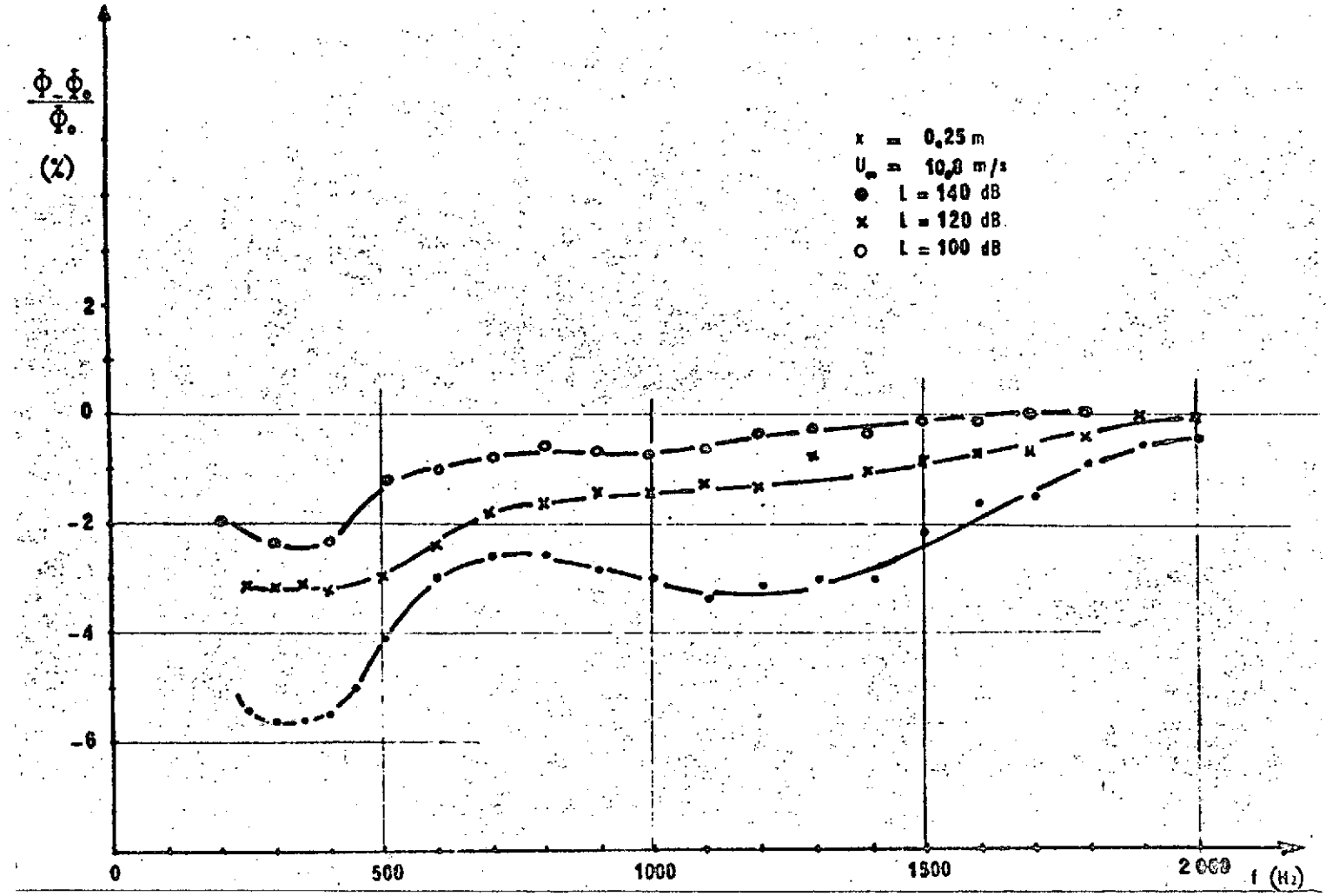
$\frac{\Phi - \Phi_0}{\Phi_0}$ (%)
x = 0,25 m
U_∞ = 10,8 m/s
L = 140 dB
L = 120 dB
L = 100 dB
2
0
-2
-4
-6
0
500
1000
1500
2 000
f (Hz)

Figure 32.

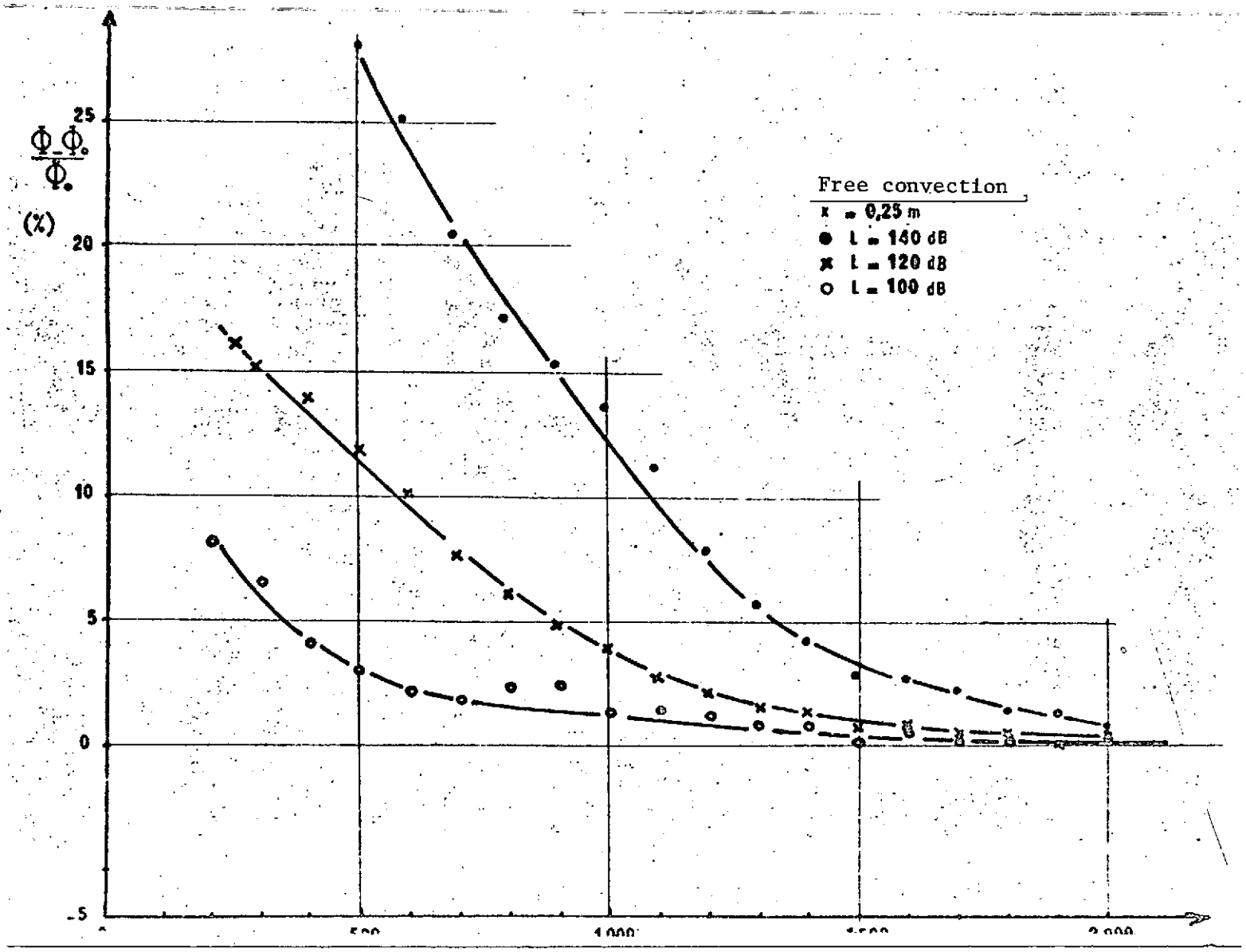
$\frac{\Phi - \Phi_0}{\Phi_0}$ (%)
25
20
15
10
5
0
-5
Free convection
x = 0,25 m
● L = 140 dB
✖ L = 120 dB
○ L = 100 dB

Figure 33.

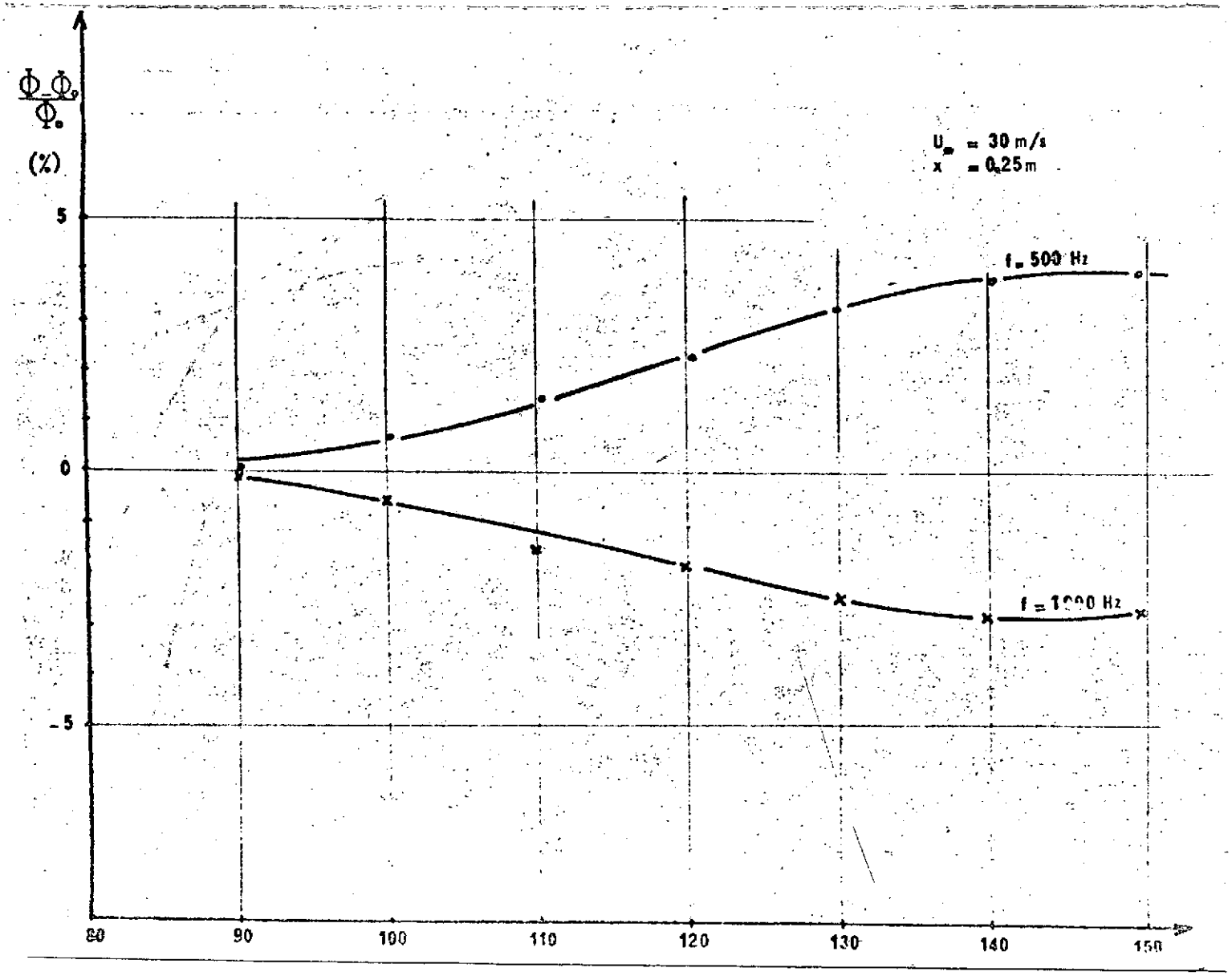
$\frac{\Phi - \Phi_0}{\Phi_0}$ (%)
U_∞ = 30 m/s
x = 0,25 m
f = 500 Hz
f = 1000 Hz
5
0
-5
80
90
100
110
120
130
140
150

Figure 34.

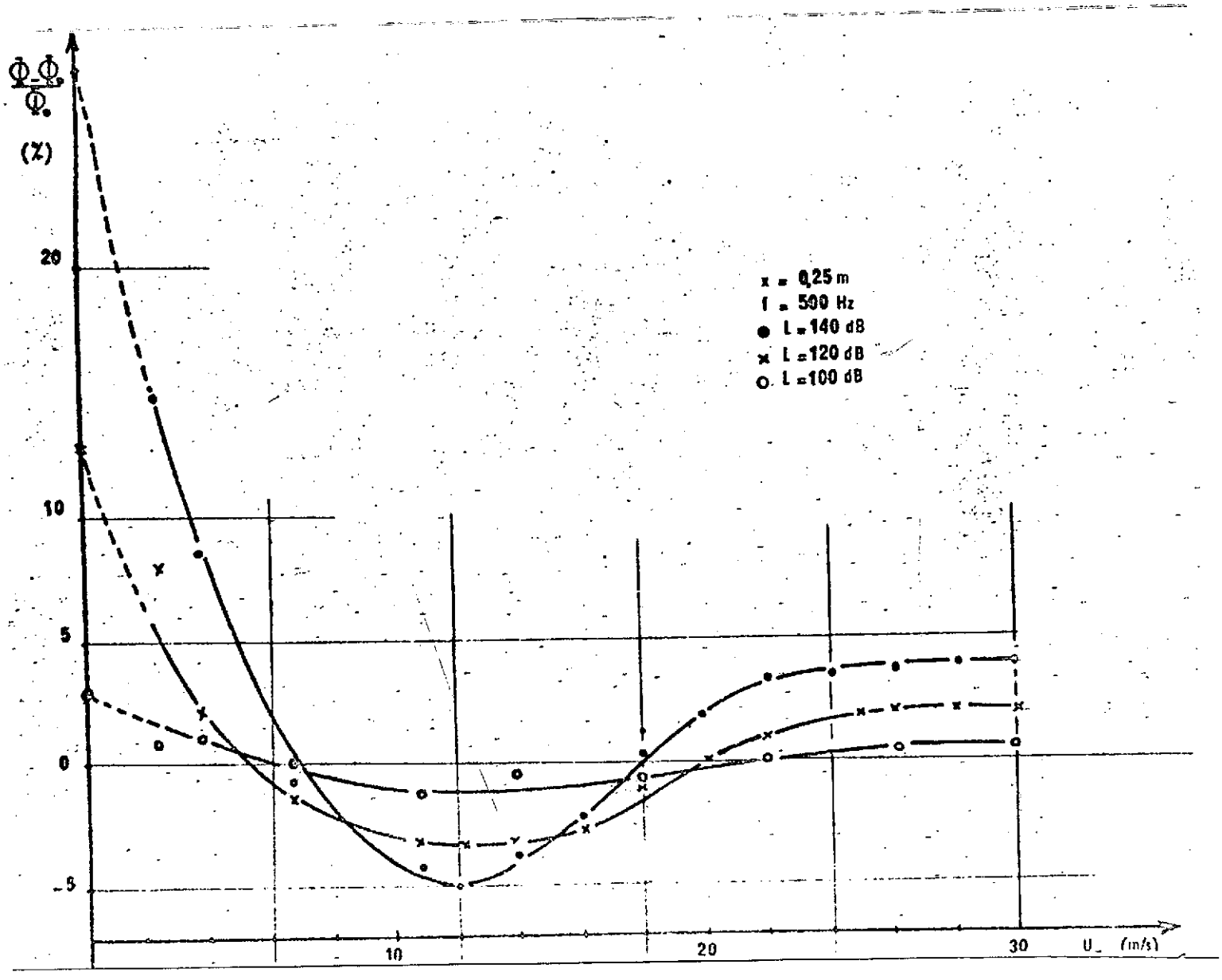

Figure 35.

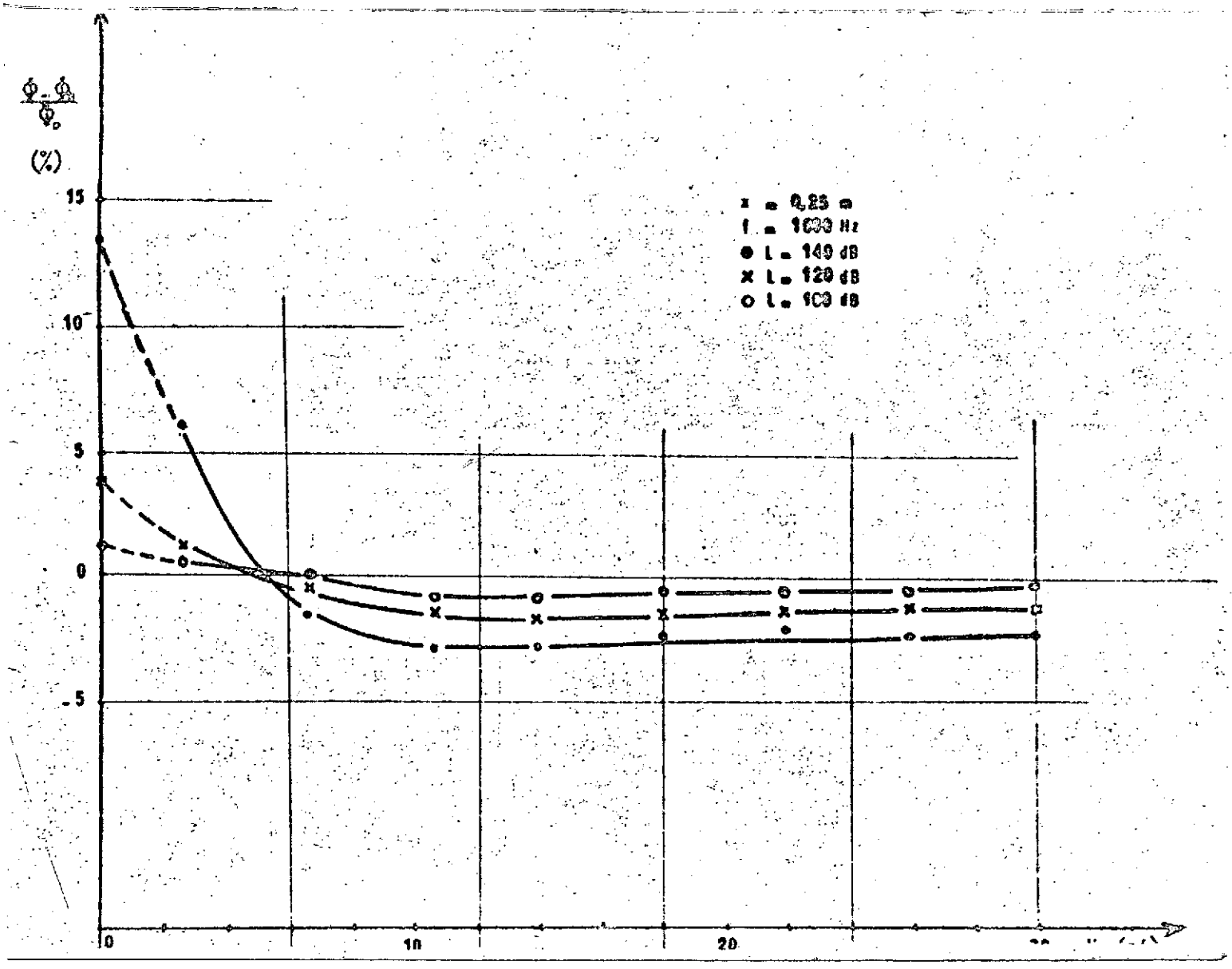
$\frac{\Phi - \Phi_0}{\Phi_0}$
(%)
15
10
5
0
-5
0
10
20
x = 0,25 m
f = 1000 Hz
● L = 140 dB
× L = 120 dB
○ L = 100 dB

Figure 36

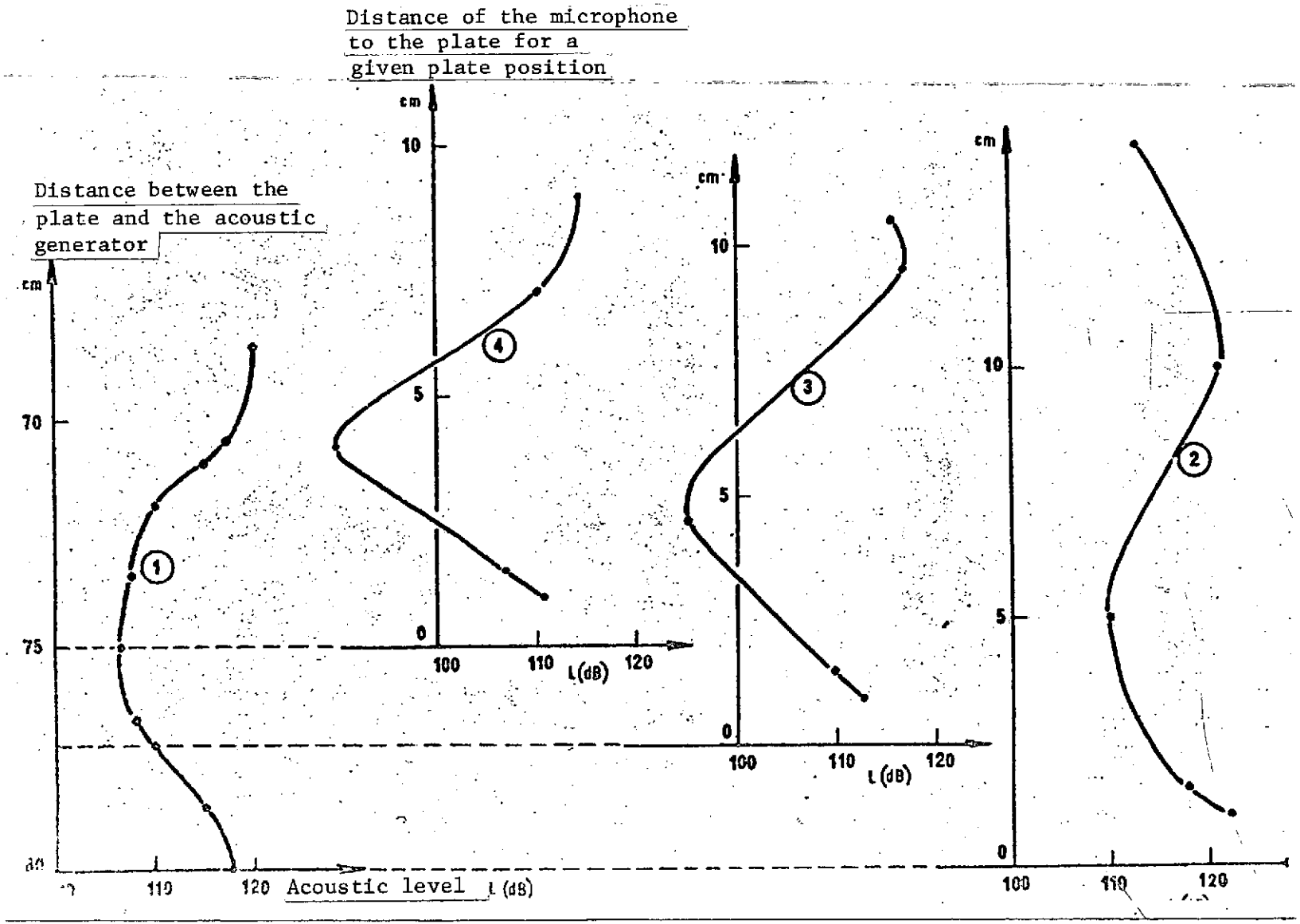
Distance of the microphone to the plate for a given plate position
Distance between the plate and the acoustic generator
cm
70
75
80
110
120
Acoustic level L (dB)
10
5
0
100
110
120
L (dB)
1
2
3
4

Figure 37.

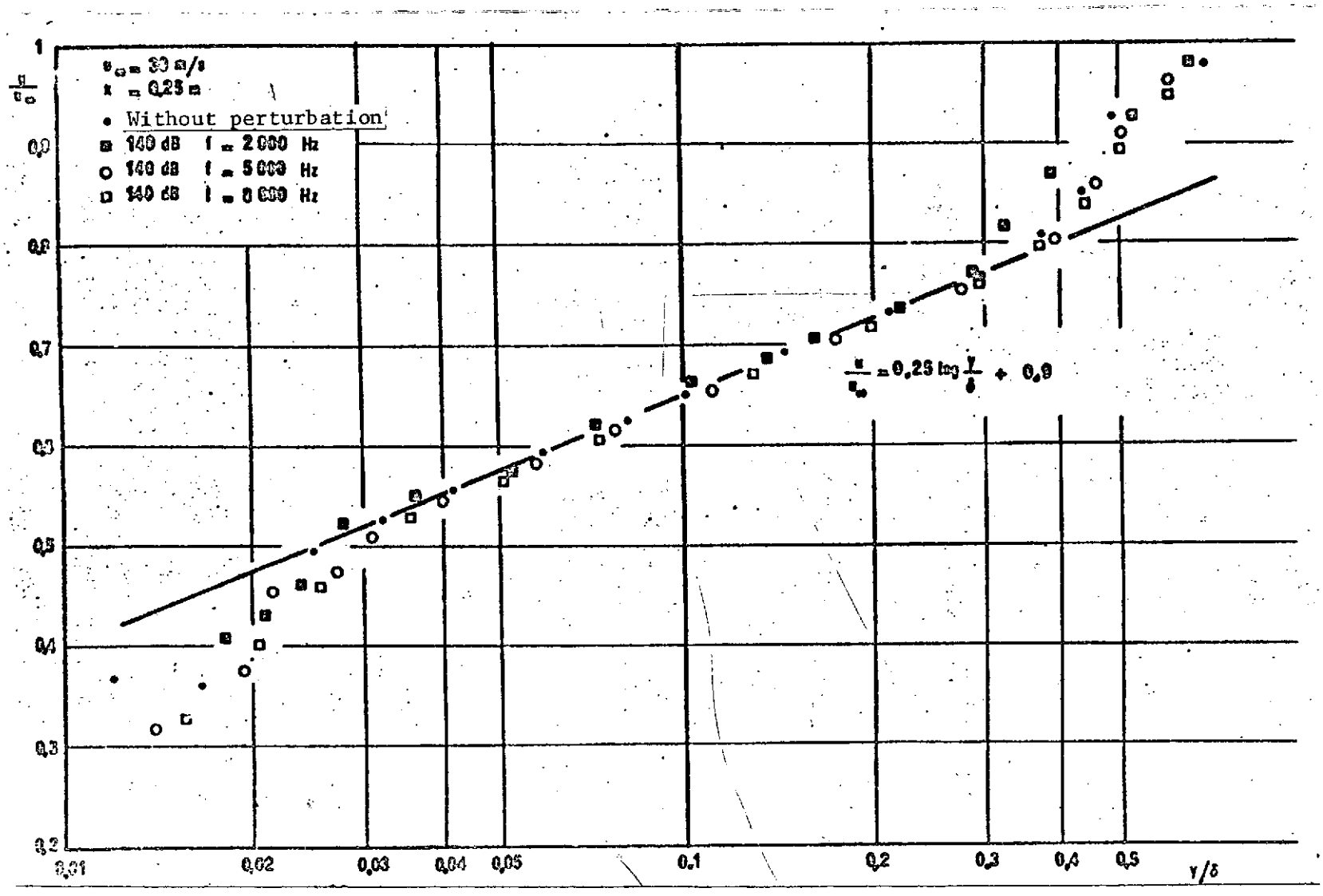
u_∞ = 30 m/s
x = 0,25 m
Without perturbation
140 dB f = 2 000 Hz
140 dB f = 5 000 Hz
140 dB f = 8 000 Hz
$\frac{u}{u_\infty} = 0{,}25 \log \frac{y}{\delta} + 0{,}8$
$\frac{u}{u_\infty}$
1
0,9
0,8
0,7
0,6
0,5
0,4
0,3
0,2
0,01
0,02
0,03
0,04
0,05
0,1
0,2
0,3
0,4
0,5
y/δ

Figure 38.

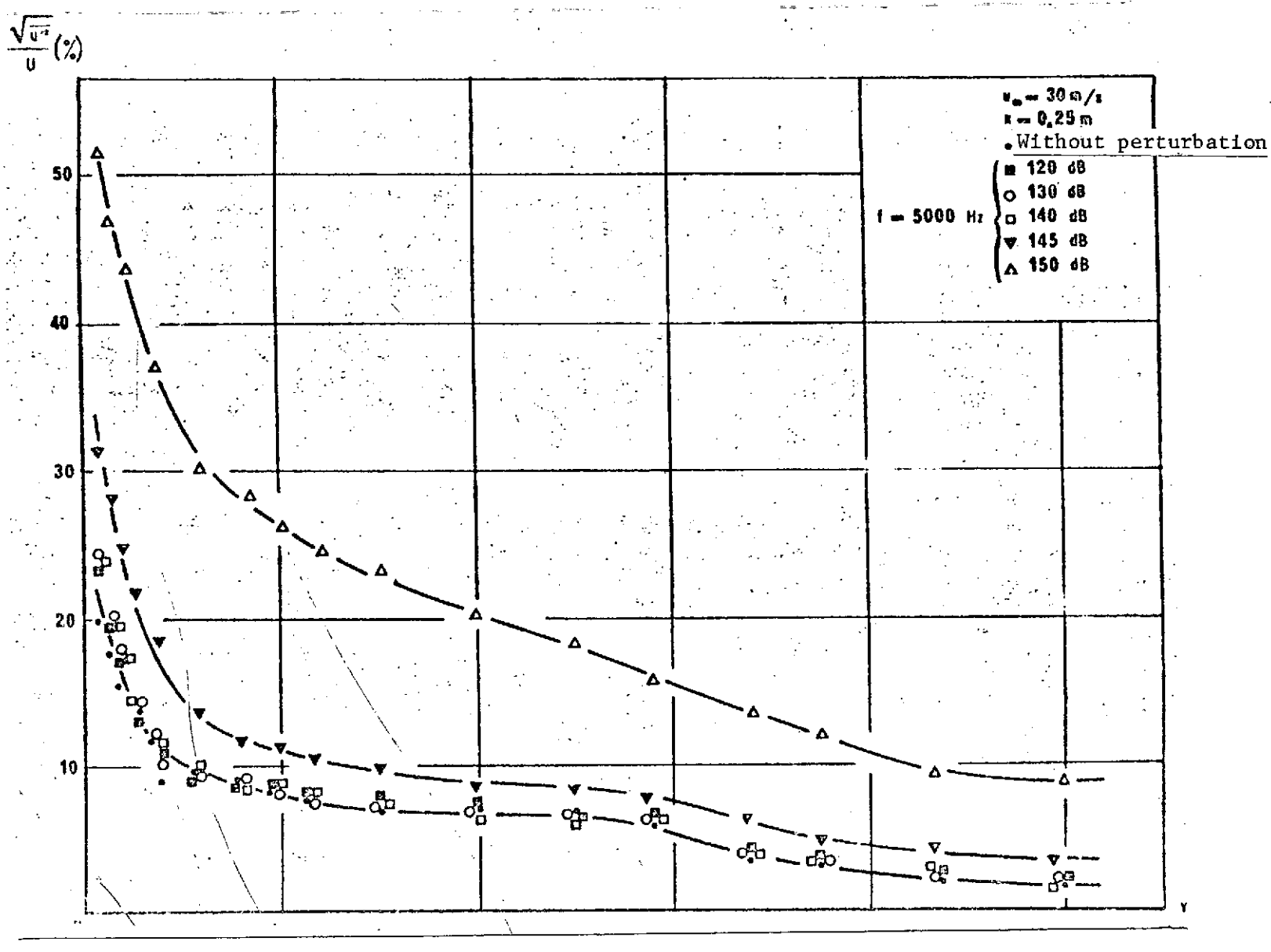
$\frac{\sqrt{u^2}}{U}$ (%)
50
40
30
20
10
u_∞ = 30 m/s
x = 0,25 m
• Without perturbation
f = 5000 Hz
120 dB
130 dB
140 dB
145 dB
150 dB
Y

Figure 39.

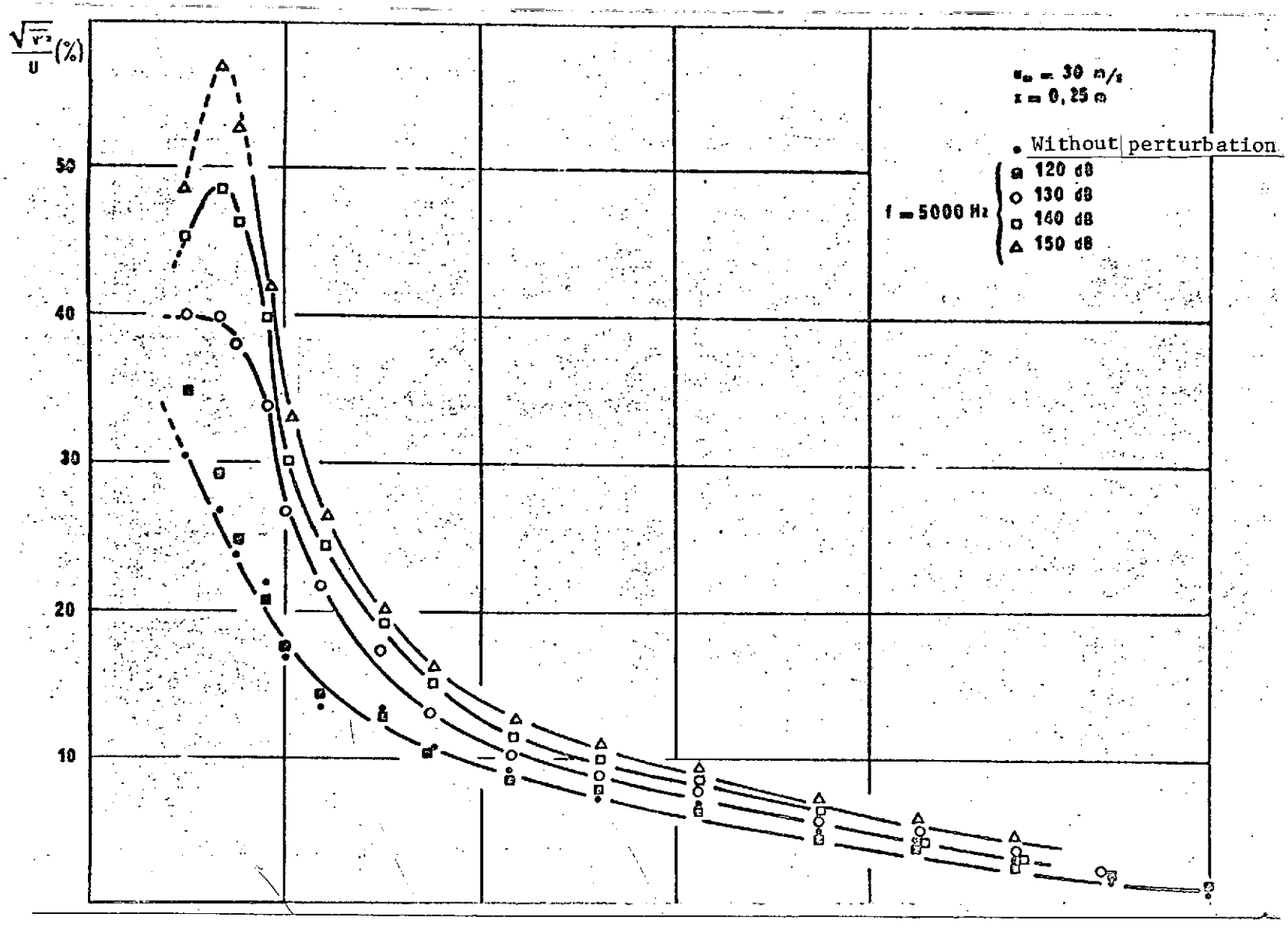
$\frac{\sqrt{v^2}}{U}$(%)
50
40
30
20
10
u_∞ = 30 m/s
x = 0,25 m
• Without perturbation
f = 5000 Hz
120 dB
130 dB
140 dB
150 dB

Figure 40.

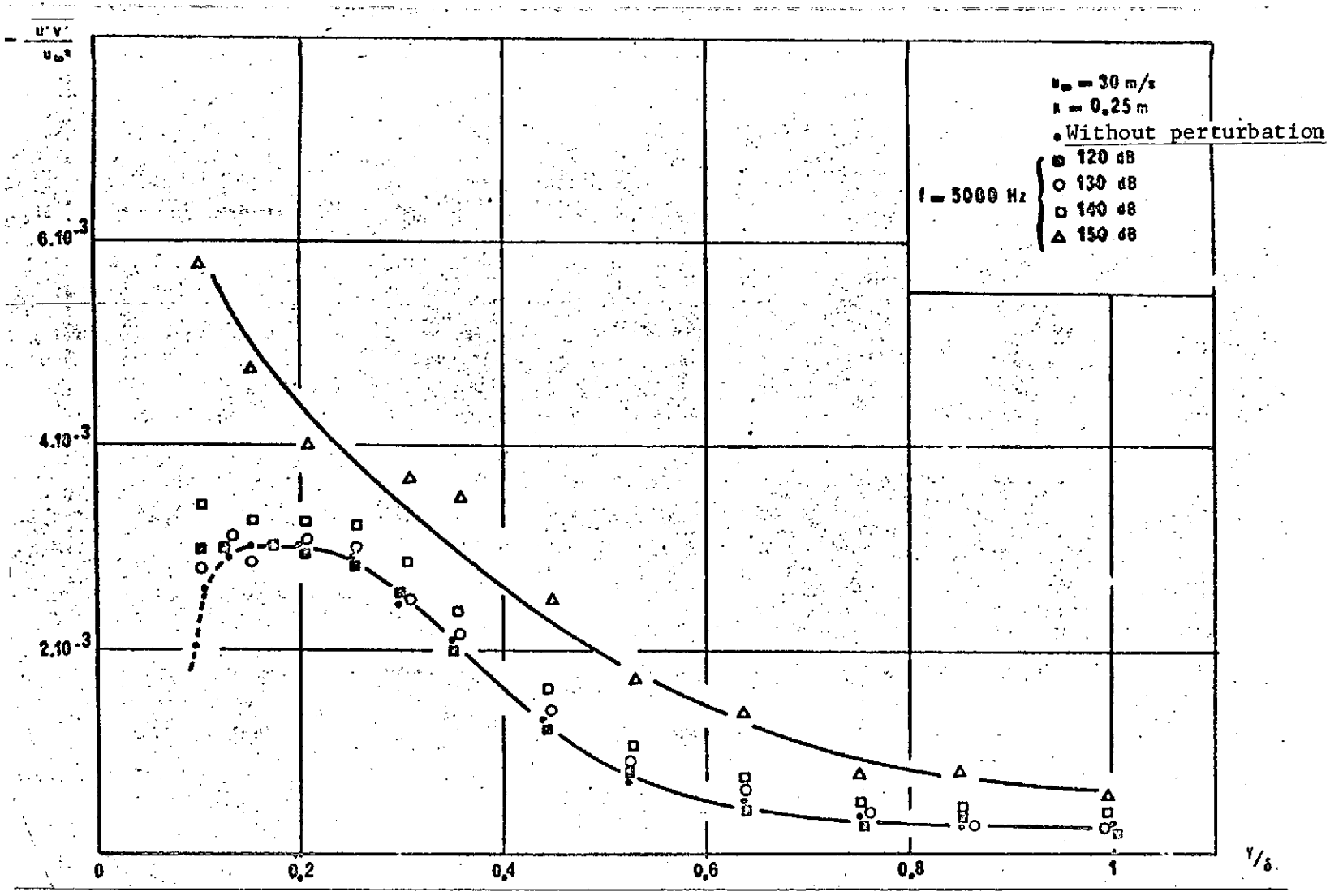
$\frac{\overline{u'v'}}{u_\infty^2}$
u_∞ = 30 m/s
x = 0,25 m
• Without perturbation
f = 5000 Hz
120 dB
130 dB
140 dB
150 dB
6.10⁻³
4.10⁻³
2.10⁻³
0
0,2
0,4
0,6
0,8
1
y/δ

Figure 41.

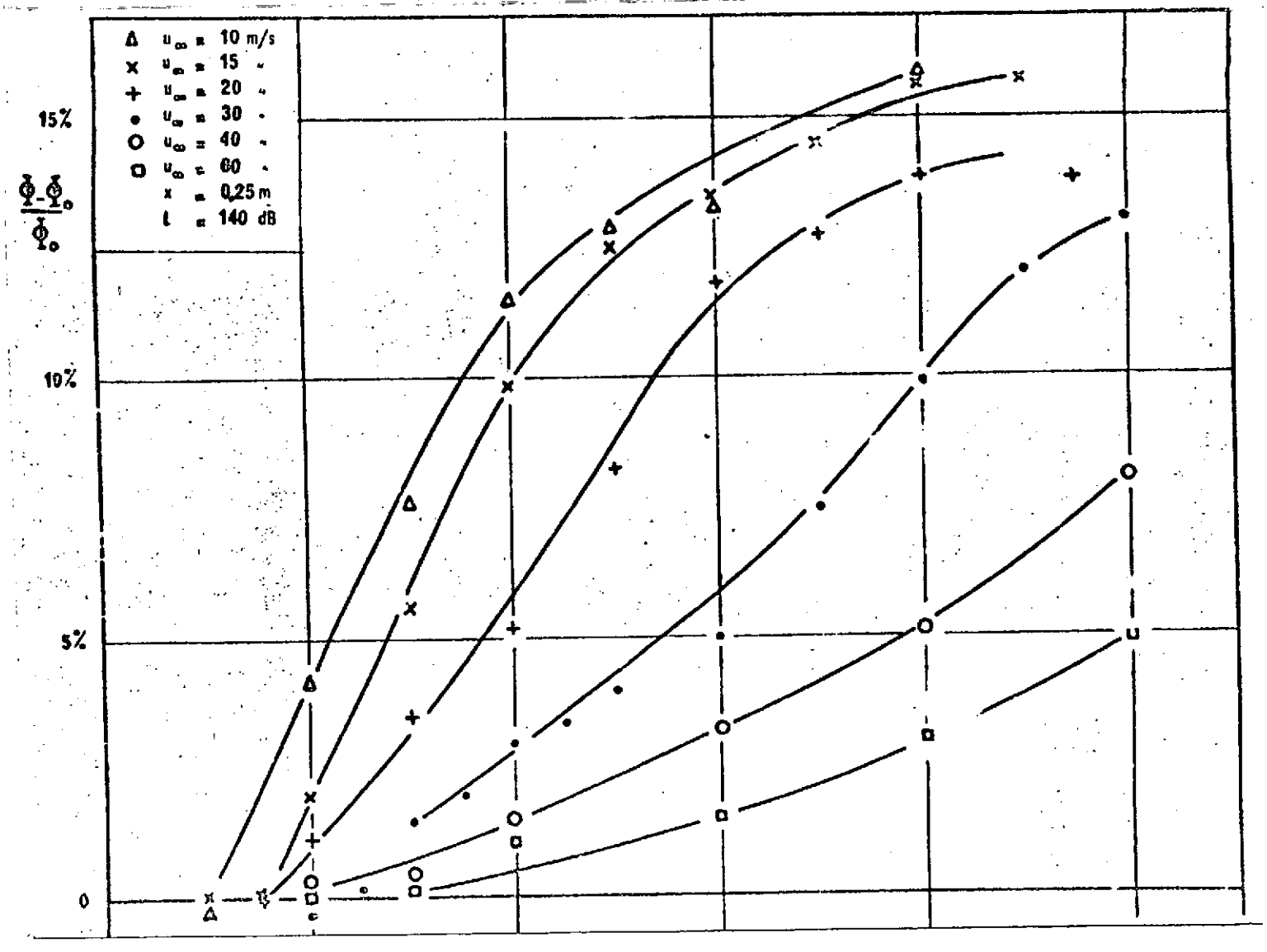
Δ u_∞ = 10 m/s
× u_∞ = 15 "
+ u_∞ = 20 "
• u_∞ = 30 "
○ u_∞ = 40 "
□ u_∞ = 60 "
x = 0,25 m
L = 140 dB
15%
10%
5%
0
$\frac{\Phi - \Phi_0}{\Phi_0}$

Figure 42.

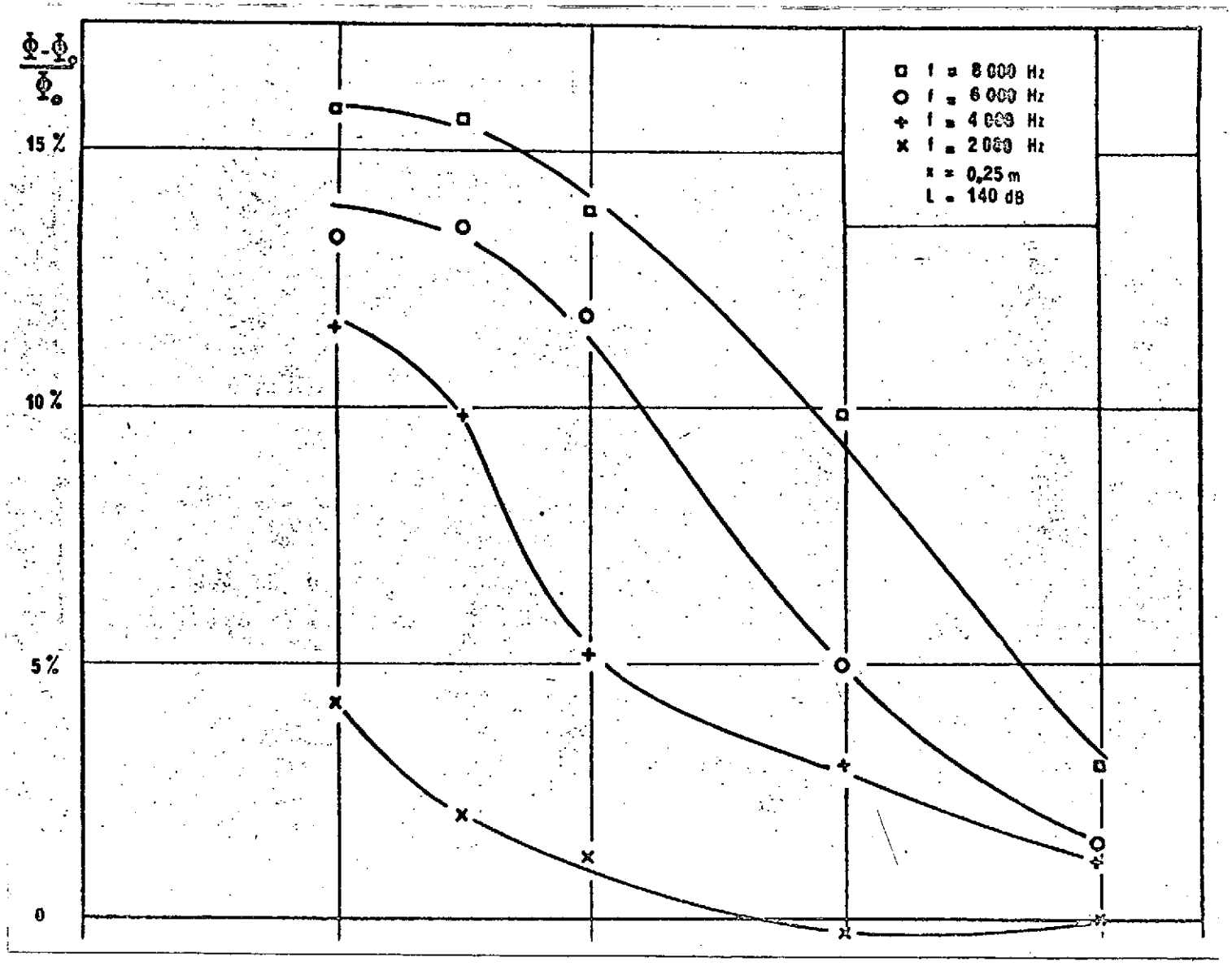
Φ-Φ₀ / Φ₀
15 %
10 %
5 %
0
f = 8 000 Hz
f = 6 000 Hz
f = 4 000 Hz
f = 2 000 Hz
x = 0,25 m
L = 140 dB

Figure 43.

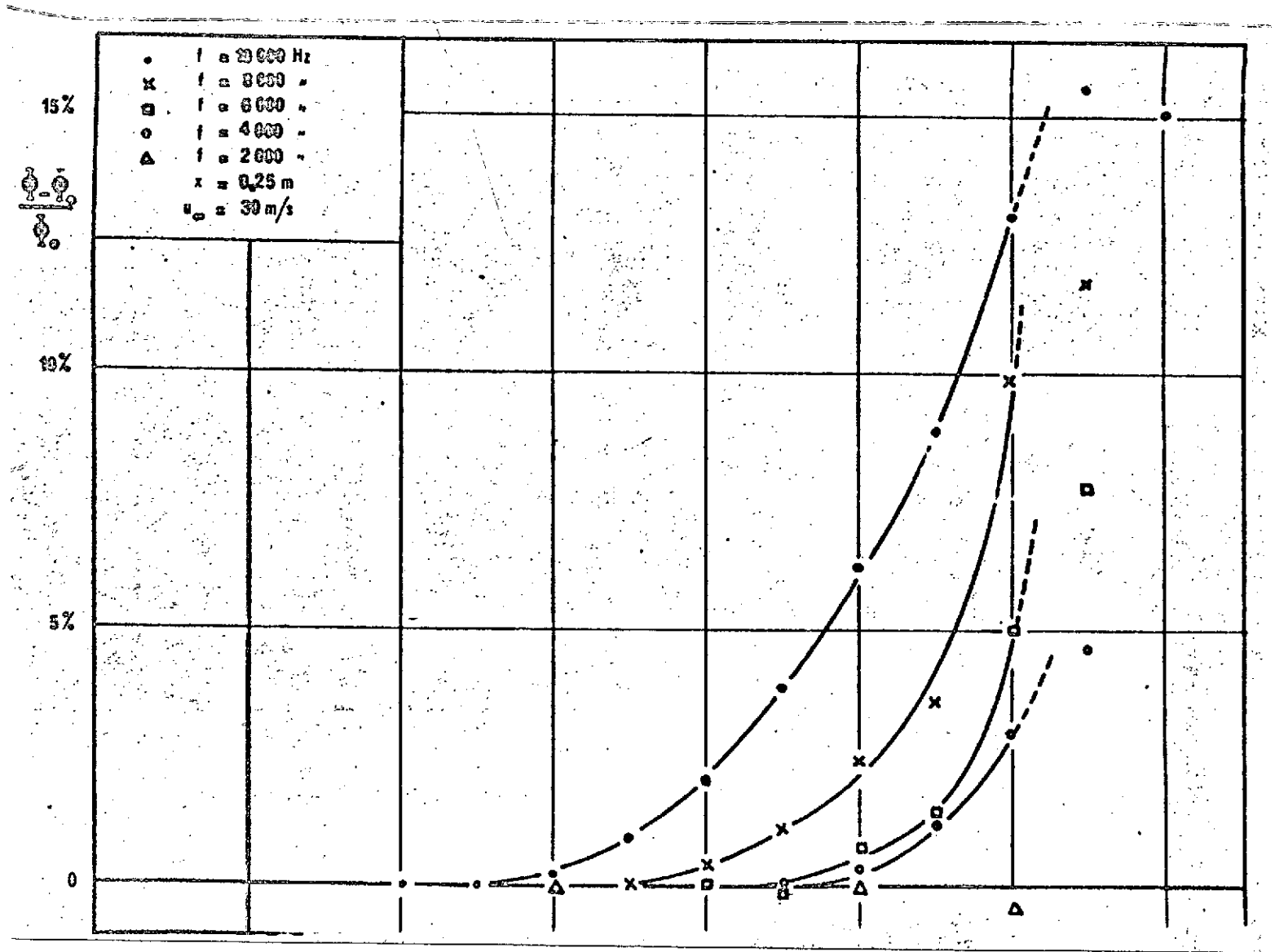

Figure 44.

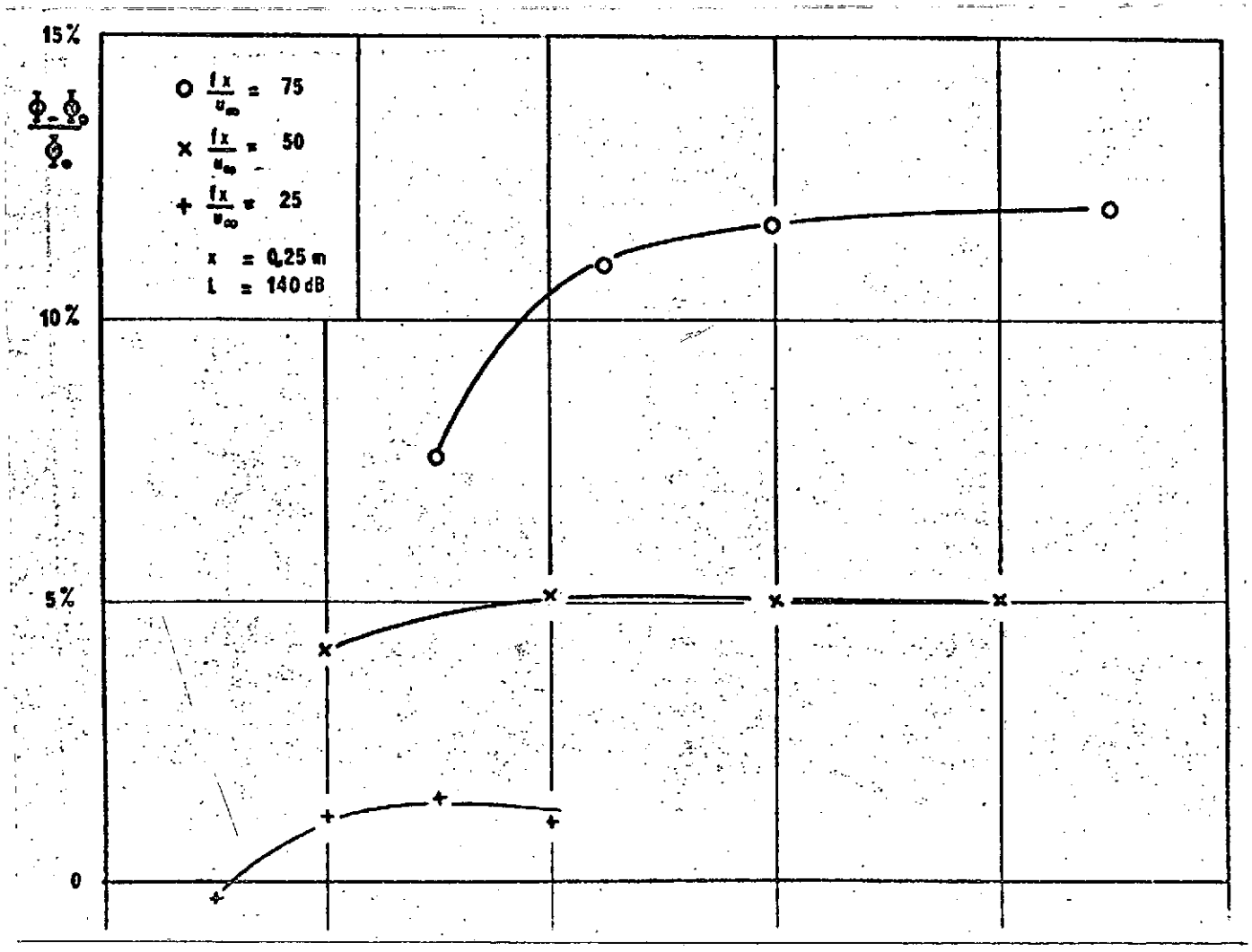
15%
10%
5%
0
$\frac{\Phi - \Phi_0}{\Phi_0}$
$\frac{fx}{u_\infty}$ = 75
$\frac{fx}{u_\infty}$ = 50
$\frac{fx}{u_\infty}$ = 25
x = 0,25 m
L = 140 dB

Figure 45.

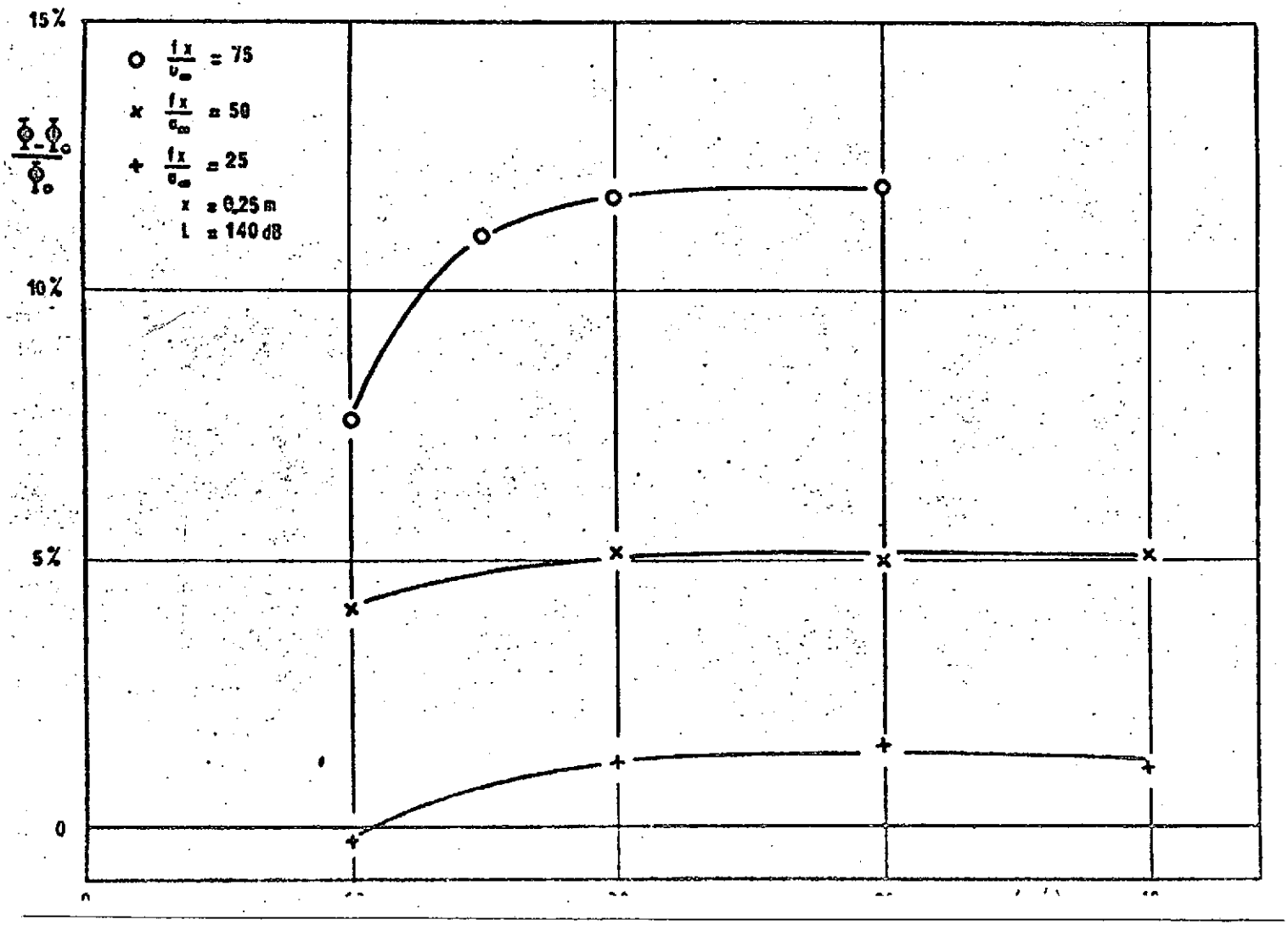
15%
10%
5%
0
$\frac{\Phi - \Phi_0}{\Phi_0}$
$\frac{fx}{c_\infty}$ = 75
$\frac{fx}{c_\infty}$ = 50
$\frac{fx}{c_\infty}$ = 25
x = 0,25 m
L = 140 dB

Figure 46

Translated for National Aeronautics and Space Administration
under contract No. NASw 2483, by SCITRAN, P. O. Box 5456,
Santa Barbara, California, 93108.